Tomas Bata University in Zlín
Faculty of Technology

Doctoral Thesis

Fully inkjet printed gas and humidity CuO sensor on flexible polymer substrate

Senzor plynů a vlhkosti na bázi CuO připravený výhradně inkoustovým tiskem na ohebném polymerním substrátu

Author:	**Ing. Petr Krčmář**
Study programme:	Chemistry and materials technology P2808
Study course:	Technology of macromolecular compounds 2808V006
Supervisor:	Assoc. Prof. Ing. et Ing. Ivo Kuřitka, Ph.D. et Ph.D.
Consultants:	Ing. Pavel Urbánek, Ph.D.

Zlín, April 2019

ACKNOWLEDGEMENT

CONTENT

ABSTRACT

The thesis is concerned with material printing methods, among which the greatest attention is paid to the inkjet printing. The main advantage of inkjet printing consists of the possibility of using wide range of printing liquids (solutions or dispersions) called inks, which however meet relatively limited range of requirements for suitable viscosity and surface tension. The work concentrates on preparation of inkjet ink based on copper oxide nanoparticles for material printing on polymer flexible substrates and its possible application as a sensor of humidity and volatile organic compounds at room temperature. The ink composition was developed on the basis of measurement of viscosity and surface tension which were optimized by addition of polymeric steric surfactants. The printing process was optimized with the help of dimensionless criteria and the aid of drop watch camera system integrated in used "Dimatix DMP 2800 series" printer which allows manipulation of the electronic pulses to the piezo jetting device for controlling of the drop characteristics as it is ejected from the nozzle. Polyethylene terephthalate (PET) film was selected as the most representative substrate used in polymer electronics. Silver nano-ink was used for printing of an interdigitated pattern which was overprinted by the copper oxide ink obtaining thus a flexible flat sensor for detecting alcohol vapours. Printed layers and motives on the substrate were characterized microscopically and the conductivity was evaluated by four-point probe method. Effectiveness of prepared sensor was demonstrated by measuring its response to the vapours of water and alcohols. A specific low temperature sensing mechanism was revealed. The applicability of prepared sensing devices was demonstrated by fabrication and testing of a sensor field integrating a 3 x 3 matrix of sensing elements on the PET substrate. Further investigation in this direction is envisaged and an overview of results achieved so far is included.

ABSTRAKT

Předložená práce se zabývá metodami tisku, z nichž byla největší pozornost věnována tisku inkoustovému. Hlavní výhoda inkoustového tisku spočívá v možnosti využití širokého spektra inkoustů (roztoky nebo disperze), které ovšem splňují poměrně úzký rozsah požadavků na vhodnou viskozitu a povrchové napětí. Práce se soustředí na přípravu inkoustu na bázi oxidu měďnatého pro materiálový tisk na flexibilní polymerní substráty a jeho možné aplikace. Inkoust byl vyvinut na základě měření viskozity a povrchového napětí a s použitím bezrozměrných kritérií. Vlastnosti inkoustu byly optimalizovány přidáním polymerních sterických povrchově aktivních látek. Proces tisku byl dále optimalizován pomocí drop-watch kamerového systému integrovaného v použité tiskárně „Dimatix DMP 2800 series", umožňující manipulaci piezo prvků na základě elektronických impulsů pro zajištění správného charakteru kapky i samotného procesu tisku. Substrát z polyetylen tereftalátu (PET) byl vybrán jako nejčastěji používaný substrát v polymerní elektronice. Tištěné vrstvy a motivy na substrátu byly charakterizovány mikroskopicky a vodivost byla hodnocena čtyřbodovou metodou. Pro přípravu flexibilního plochého sensoru pro detekci par alkoholu byl inkoustem z nanočástic stříbra vytištěn vzor hřebenových elektrod, a ten byl překryt sensorickou vrstvou s použitím inkoustu z nanočástic oxidu měďnatého. Účinnost připraveného sensoru byla prokázána měřením odezvy na přítomnost par vody a alkoholů. Byl prostudován a popsán nízkoteplotní mechanismus funkce senzoru. Aplikační potenciál připravených senzorů bylů demonstrován výrobou a testováním pole senzorů integrujícího 3x3 matici senzorickcýh prvků na PET substrátu. Teze dále předjímají budoucí výzkum v tomto směru a přináší přehled dosavadních výsledků.

KEYWORDS / KLÍČOVÁ SLOVA

English

Inkjet; print; interdigit; sensor; humidity; alcohol; vapour; copper oxide; nanostructured; dispersion; flexible; polymer substrate;

Česky

Inkjet; tisk; interdigit; senzor; vlhkost; alkohol; páry; oxid měďnatý; nanostrukturovaný; disperse; ohebný; polymerní substrát

1. INTRODUCTION

There are many technologies for deposition of thin polymer layers. Each method or technique has its specifics and one of the most widely using methods for the preparation of thin layers from solution is called material printing. Material print allows applying a defined amount of solution exactly to where it is intended by a defined rate. For highly viscous liquids (pastes), screen printing is applied. For less viscous liquids, inkjet printing is suitable. Besides bubble, piezoelectric printing is widely used. When an electric voltage is applied to the crystal in the piezoelectric head, the crystal is deformed which causes an increase of the pressure in the capillary hence a drop of ink is sprayed off the nozzle. Then the voltage is switched off, the crystal returns to its original shape, the head pressure drops, make up ink and the system is ready to generate another drop. Besides viscosity, surface tension plays crucial role in forming of the droplets. Mechanical ejecting of solution ink droplets operates largely independently of its chemical composition, which is one of the advantages of this technology. Piezo head works theoretically with any fluid that meets only the viscosity and surface tension processing window criteria. These properties are decisive in interaction of the deposited liquid volume with the substrate surface as well. However, the real printing process using a specific printing nozzle needs optimization of both the ink and process parameters. Good printability regime may be attained using dimensionless criteria involving whole material-tool-process parameter triade.

The material system of ink and substrate may be adjusted to large variety of purposes and functions. Therefore, the inkjet printing gets more and more to interest in the field of transparent electronics, sensors and solar cells. Among sensors, there is lack of cheap, flexible and low temperature operating devices suitable for volatile organic compounds detection. This work is focused on the preparation of flexible sensors based on CuO and on the study of its sensing mechanism at low tempreatures.

2. MATERIAL DEPOSITION METHODS

2.1 Coating techniques

The coating is used to describe a process by which a layer of ink is transferred to the substrate by essentially pouring, painting, spraying, casting or smearing it over the surface. The use of the word printing may also imply that a complex pattern is formed whereas coating generally does not infer this. Coating techniques include spin coating, casting, painting, doctor blading, spray coating, curtain coating, slide coating, slot-die coating and knife-over-edge coating. [1, 2]

2.1.1 Spin Coating

The spin coating is widespread method and highly reproducible coating technology of thin uniform layers of inorganic, organic and composite materials for flat substrates of large sizes (with diameters running into units or tens of centimeters). [3] Spin coating belong to the technology of deposition thin layers from liquid phase, because the coating material is pre-dissolved in a suitable solvent. The principle of is relatively simple (as shown in Figure 1) and consist in deposition a small amount (typically a drop or units of ml) of deposited material on the center of substrate. The material overspreads substrate and forms a thin layer surface. This process is caused by centrifugal force on the ground of rotation of substrate (up to thousands of revolution per minutes). Depending on many parameters such as acceleration rotation rate, rotation rate, the volatility of the solvent, the viscosity and concentration of the deposited material or surface tension can be prepared a layer with a thickness below 10 nm. [4-6]
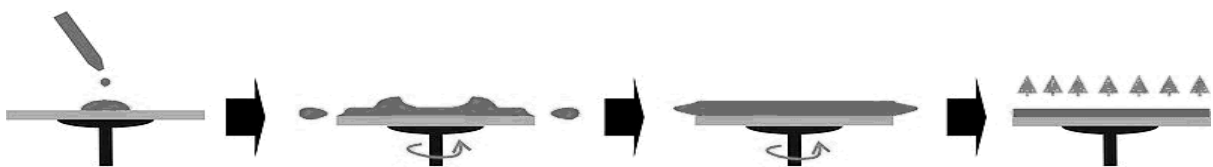
Figure 1 The spin coating process, adapted from [1].

2.1.2 Casting

This is probably the simplest film-forming technique available. The advantage is that no equipment is needed apart from a very horizontal work surface. The procedure is to simply cast a solution onto a substrate followed by drying. While it is possible to prepare films of good quality and also thick films the technique suffers from a lack of control over the film thickness and often picture framing effects are observed near the edges of the film or precipitation during drying. In cases where the surface tension of the liquid dominates the drying is inhomogeneous. Also there is a requirement that the material to be coated has a high solubility in the solvent used if crystallisation or precipitation is to be avoided. [1]

2.1.3 Doctor blading

Doctor blading is one of the simplest techniques. The doctor blading method can be applied on a wide range of ink viscosity ranging from low viscosity liquid up to a paste. As shown in Figure 2, a sharp blade is placed at a fixed distance from the surface of the substrate. Then the ink is dropped in front of the blade. A thin wet film can be uniformly deposited on the substrate by moving the blade across the substrate with a constant velocity. The thickness of the wet film depends on primarily on the distance of the blade from the substrate, however the surface energy of substrate, the surface tension of the ink, and the viscosity of the ink play important role in processing of the film and influence its thickness and other properties. The substrate may be heated during coating and following film setting using a hotplate with temperature control. [7]
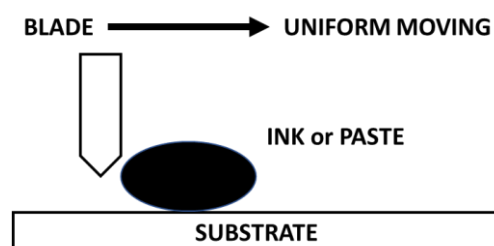
Figure 2 Schematic illustration of the doctor blading technique. Own source.

2.1.4 Spray coating

This technique involves forcing the printing ink through a nozzle whereby a fine aerosol is formed. A carrier gas and electrostatic charging may be involved to aid in directing the aerosol at the surface that is to be coated. The formation of the aerosol and evaporation of some of the solvent is complex and while spray coating in principle is roll-to-roll compatible, allows for patterning of the coated film with a reasonable detail (millimetre scale) it can be difficult to prepare films with a smooth surface. The aerosol droplets have to level once they have reached the substrate and this is not necessarily granted. The ease with which inks are prepared ranges from simple to complex and the range of viscosities that will work is wide. There is no simple relationship describing the wet film thickness while it is possible to prepare both thin and thick films. [8]

2.1.5 Slot die coating

Being a 1-dimensional coating technique slot-die coating allows for the coating of stripes of material which is well suited for making multilayer devices with stripes of different materials layered on top of each other. The alignment of the pattern is easy as the coating head is simply translated along the direction perpendicular to the direction of the web movement. The technique belongs to the premetered coating techniques where all the ink supplied to the coating head is coated with no loss. The slot-die technique is robust and simple in operation while the coating head is quite complex as compared to knife-over-edge coating. The most important part is the mask that defines the slots and the void in the coating head that disperse the ink through the individual slots. [9]

2.1.6 Knife-over-edge coating and slide coating

Knife-over-edge coating is a 0-dimensional coating technique and the coating is applied evenly over the surface of the substrate. In contrast to doctor blading, the knife is fixed and the substrate moves on rolls. The principle is illustrated in

Figure 3. While it is not suited for patterning, the barriers of the coating bath may be adjusted so as to limit the coating to a part of the knife width. The edge definition is, however, not sharp and depends on the gap between the knife and the substrate and the web speed. Slide coating allows for the simultaneous coating of a multilayer film (up to 18 layers may be deposited simultaneously). These techniques were developed originally for the photographic film industry where many layers were coated simultaneously on top of each other. This means that for the right combination of ink solutions all the layers in a device may in principle be printed in a single coating step. [1, 2]
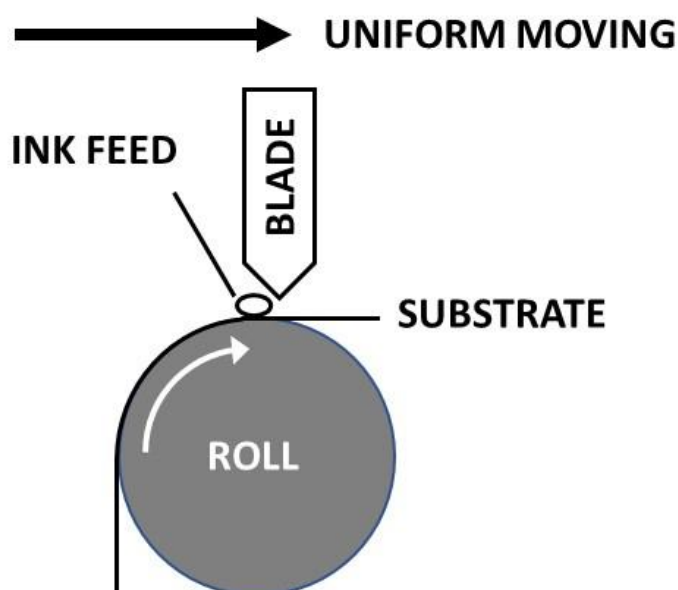
Figure 3 Schematic illustration of the knife-over-edge technique. Own source.

2.2 Printing methods

It is important to distinguish coating from printing in this context. Historically printing is a method by which a layer of ink is transferred from a stamp to a substrate. A good example is an office stamp that does just that. On the other hand, a coating is a process by which a layer of ink is transferred to the substrate by essentially painting, spraying, casting or smearing it over the surface. Printing methods include techniques such as inkjet printing, screen printing, pad printing, gravure printing, flexographic printing and offset printing. [1, 2]

2.2.1 Gravure printing

The gravure process has been used widely for printing magazines, tapes and packaging. [10] The primary advantage of roll-to-roll processing that is large areas of coated/printed films can be processed quickly at low manufacturing costs. A gravure roll-to-roll coater employs two rollers and a doctoring blade. An engraved roller is used to pick up fluid from a bath which passes through a flexible doctoring blade which meters off excess fluid. The engraved roller deposits the fluid from the cells onto the flexible substrate which is held in tension by another roller. In contrast to that, an offset gravure process has an intermediate roller between the engraved roller and the substrate. This intermediate roller receives the image formed by ink from the engraved roller and transfer it onto the substrate which is held in tension similarly as in simple gravure printing by an additional roller. This has been known for quite some time in traditional printing industries, but has now become of particular interest to the electronics industry who have begun to use an offset gravure printing mechanism to print electronic components. A simple non-roll-to-roll variant of such gravure-offset which resembles pad printing too because of using of a blanket for ink image transfer is shown   Figure 4. [9] In addition, a host of researchers have been investigating the adaptation of a number of water-based processing techniques like nanoimprint lithography and optical lithography techniques to web-based platforms. [11] Typical gravure cell sizes have a width ranging from 50 μm to several hundred microns and depths in similar ranges. [12, 13] A number of these cells are placed in an array on the engraved roller to print patterned arrays or coat films. During the gravure printing process, a liquid bridge is formed between the cell and the substrate that is being coated or printed on. This bridge plays an important role in the liquid transfer process from the cell on to the substrate. It is also strongly influenced by the surface properties of the cell and substrate, the limiting parameters being the contact angle between the liquid bridge and both the substrates and moving contact lines that are often pinned by the geometry of the cell. [14]
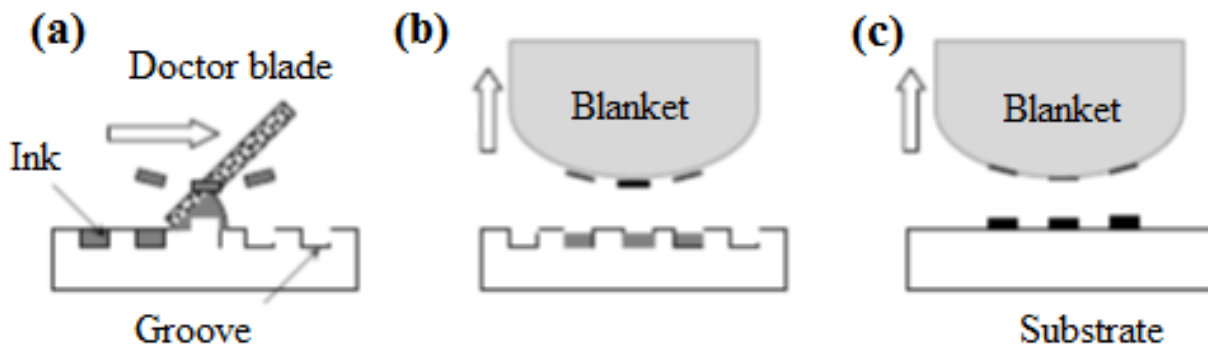
Figure 4 The schematic of gravure-offset printing process: (a) filling the grooves with ink; (b) picking up ink with a blanket; (c) the transfer of ink onto the substrate. [10]

2.2.2 Flexographic printing

Flexography is similar to gravure printing and among to techniques of relief printing. The printing points are stand up on the printing roller surface which is typically made from rubber. This method is very similar to pad printing and can be allowed for continuous pad printing where the image in formation is shaped into the pad.

The typical flexographic system is a four roller system, see Figure 5. The fountain roller is partially submerged in the ink tray. As the fountain roller turns, it draws ink from the tray and applies it to the anilox roller. The anilox roller contains thousands of precision engraved cells which receive the ink in measured quantities and a doctor blade which removes excess ink to ensure an even coating. The anilox roller then deposits a thin layer of ink onto the flexible plate where it is ready to be applied to the substrate. The process is simple and could be applicable to fabrication of polymer electronics. It may be an advantage with a closed ink chamber where by exposure of the ink to the atmosphere is limited to the surface on the Anilox roller and printing roller only. [15-17]
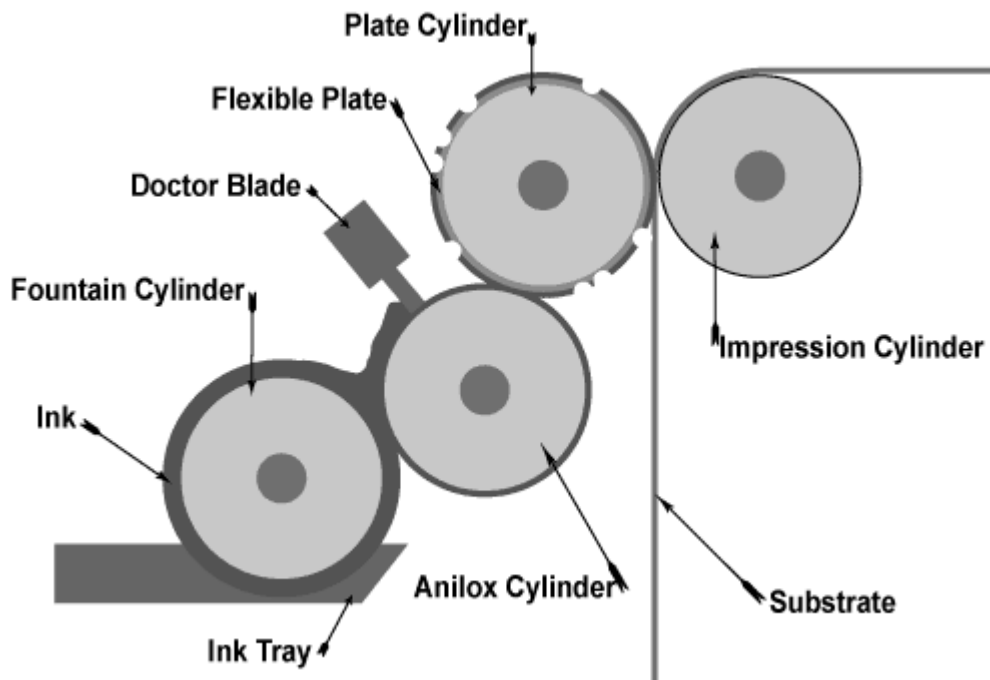
Figure 5 The flexographic printing process, adapted from [1].

2.2.3 Screen printing

Screen printing consists of three elements: the screen which is the image carrier; the squeegee; and ink. The principle is illustrated in Figure 6. The screen printing process uses a porous mesh stretched tightly over a frame made of wood or metal. [18] Proper tension is essential to accurate color registration. The mesh is made of porous fabric or stainless steel mesh. A stencil is produced on the screen either manually or photochemically. The stencil defines the image to be printed in other printing technologies this would be referred to as the image plate. Screen printing ink is applied to the substrate by placing the screen over the material. Ink with a paint-like consistency is placed onto the top of the screen. Ink is then forced through the fine mesh openings using a squeegee that is drawn across the screen, applying pressure thereby forcing the ink through the open areas of the screen. Ink will pass through only in areas where no stencil is applied, thus forming an image on the printing substrate. The diameter of the threads and the thread count of the mesh will determine how much ink is deposited onto the substrates.

Many factors such as composition, size and form, angle, pressure, and speed of the blade (squeegee) determine the quality of the impression made by the squeegee. At one time most blades were made from rubber which, however, is prone to wear and edge nicks and has a tendency to warp and distort. While blades continue to be made from rubbers such as neoprene, most are now made from polyurethane which can produce many impressions without significant degradation of the image. [1, 19]

If the item was printed on a manual or automatic screen press the printed product will be placed on a conveyor belt which carries the item into the drying oven or through the UV curing system. Rotary screen presses feed the material through the drying or curing system automatically. Air drying of certain inks, though rare in the industry, is still sometimes utilized. [20]
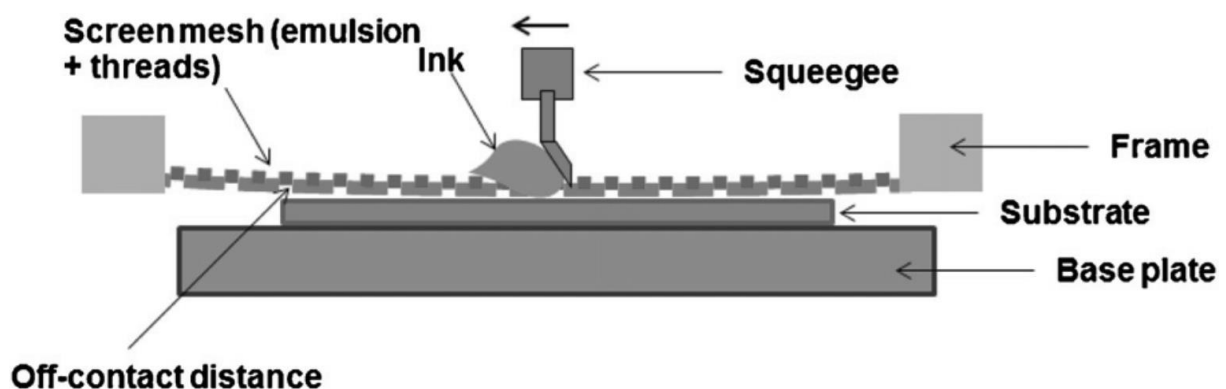
Figure 6 The scheme of screen printing process, adapted from [20]

2.2.4 Inkjet printing

The inkjet printing is only technique that could be placed in both categories. Fundamentally it is a coating technique but the possibility to reproduce a complex pattern and its association with office printing on paper makes it equally suited for being named as a printing technique. [1, 2]

The ink-jet is a non-impact device of generating images by directing small droplets or particles in quick succession on to the surface of a substrate under computer control. There are varied possible ways of generating and projecting

droplets but only the following two methods appear suited to real production applications. Inkjet printing is available in two technological variants, i.e. continuous printing and drop on demand printing.

Since the image is created by deposition of single droplets that form single dots on the substrate, the term resolution is important. Acronym dpi (dots per inch) tells us how many dots fit into one-inch lengths, i.e. 2.54 cm. In other words, it is a measure of the density of dot (e.g. ink droplet) placement by the printer or expression of drop spacing too, see Figure 7. Because there is considered only one ink and "monochrome" printing in material deposition, the term dot becomes equivalent to pixel. [21]

Increasing resolution [dpi]

Decreasing drop spacing
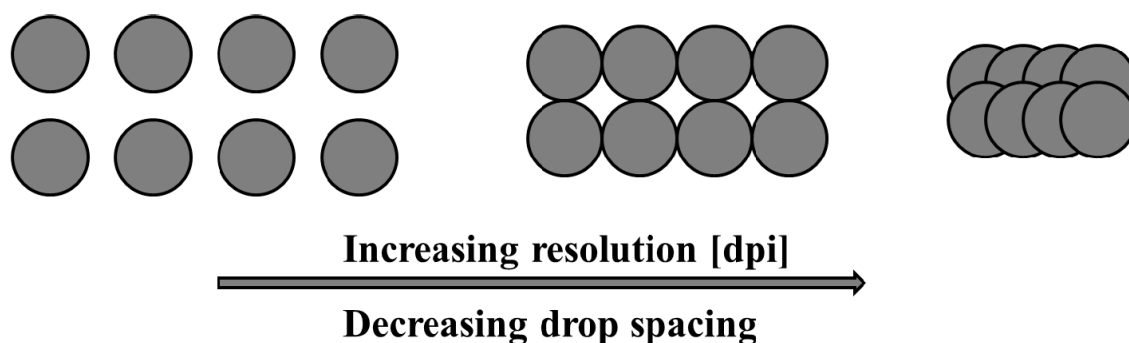
Figure 7 Scheme of the relationship between the resolution and drop spacing, courtesy Pavol Šuly, [22].

Continuous inkjet printing

Inkjet printing has proven to be a versatile, cost-efficient and easy-to-scale-up method for producing a large variety of microstructured materials used for organic transistors, photo-voltaics light emitting diodes, ceramics, and biopolymer arrays. [1] Continuous inkjet printing (CIJ) is primarily used for coding and marking of products and packages. In this technology, a pump directs fluid from a reservoir to one or more small nozzles, which eject a continuous stream of drops at high frequency (in the range of roughly 5 kHz to 100 kHz) using a vibrating

piezoelectric crystal (Figure 8). [23, 24] The drops pass through a set of electrodes which impart a charge onto each drop. The charged drops then pass a deflection plate which uses an electrostatic field to select drops that are to be printed and drops to be collected and returned for re-use. With multi-level CIJ, the printed drops are deflected into several positions onto the substrate, while with binary CIJ it is the un-deflected drops that are printed. [25] The high drop ejection frequency of CIJ gives a capability for very high speed inkjet printing, suitable for such applications as the date coding of beverage cans. An additional benefit of CIJ is the high drop velocity (of the order of 20 m/s), which allows for relatively large distances between the printhead and the substrate. [21, 26]
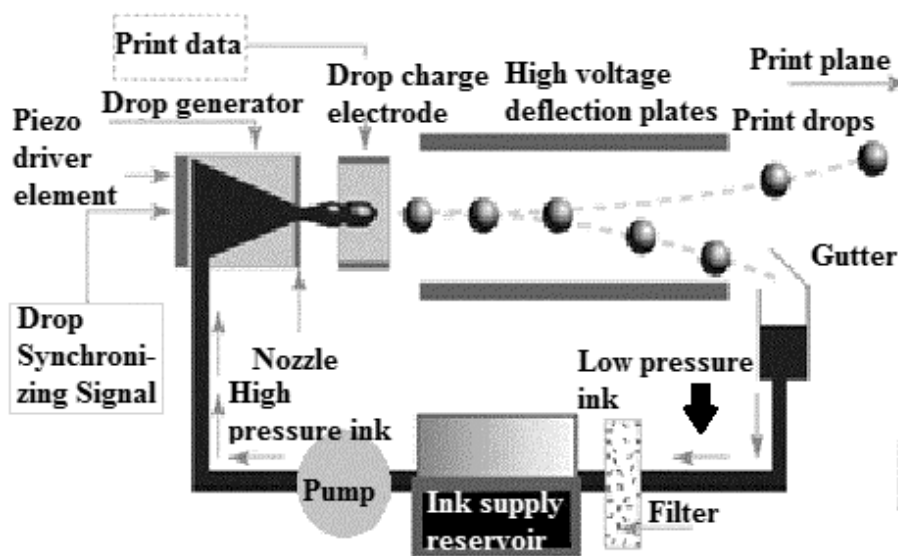
Figure 8 Continuous inkjet printhead, adapted from [21].

Historically, CIJ has enjoyed an advantage over other inkjet technologies in its ability to use inks based on volatile solvents, allowing for rapid drying and aiding adhesion on many substrates. The disadvantages of the technology include relatively low print resolution, very high maintenance requirements and a perception that CIJ is a dirty and environmentally unfriendly technology due to the use of large volumes of volatile solvent-based fluids. Additionally, the

requirement that the printed fluid be electrically chargeable limits the applicability of the technique. [26]

Drop on demand inkjet printing

The second major inkjet technology is termed 'drop-on-demand'(DOD). Drop-on-demand print heads usually have an array of nozzles, each of which ejects ink drops only when required to form the image. Figure 9 shows schematically how each nozzle works. An actuator of some kind creates a rapid change in the cavity volume and imparts some momentum to the ejected drop. This is a dynamic process, in which wave propagation in the ink and the geometry of the cavity behind the nozzle have significant effects. Although other methods have been explored, the two most common means to trigger the ejection are the creation of a vapour bubble within the ink using a heater pad ('bubble jet') or the distortion of a piezoelectric ceramic element. [27, 28]
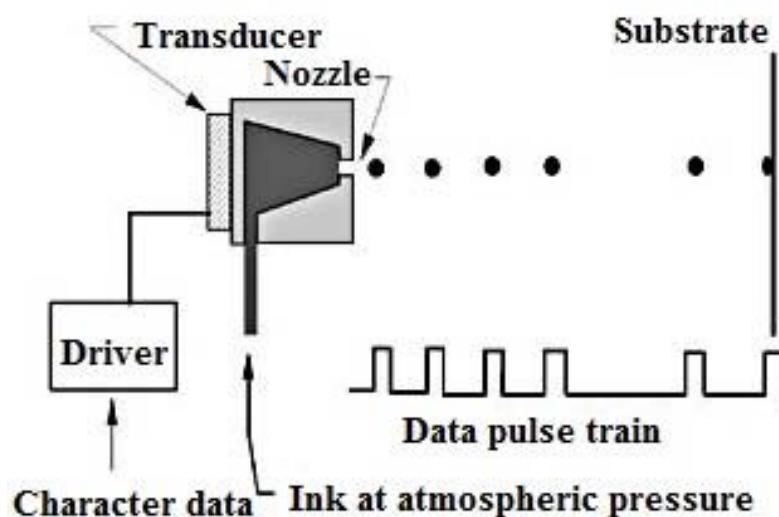
Figure 9 Drop on demand printhead, adapted from [21].

The principle of thermal inkjet technology (TIJ), sometimes called as 'bubble jet' or 'bubble printing' is ejection of a drop of ink from the nozzle driven by the pressure generated by an expanding bubble inside the nozzle chamber. The bubble is generated by rapid heating of a resistor integrated inside the nozzle chamber

wall. The vapour bubble collapses when its internal pressure reaches to the external atmospheric pressure. The whole process lasts several micro-seconds. It is obvious, that only such inks containing specific volatile solvents can be used. Moreover, the solid content of the ink may not be accumulated in the printing nozzle, hence only easily soluble or disperse-able compounds can be used and the ink formulation must be stable over used temperature range. [29]

Piezoelectric inkjet (PIJ) printing does not suffer from above mentioned disadvantages and it's the widest DOD technology in the world. The only limitation is that the inks for PIJ must not contain the compounds vaporisable (forming bubbles) at printing conditions. Moreover, the printing heads have longer life because of omission of heating element. On the other hand, the construction of printing heads and the associated hardware is more complicated. [30] In the case of PIJ, the driving element integrated in the nozzle chamber is a piezoelectric element. The piezoelectric effect can be observed in two manifestations. First, as a direct effect, when the material generates electric field in a response to applied mechanical strain. On the other hand, mechanical displacement or deformation of the material occurs when external electric field is applied which is called indirect piezoelectric effect. [31] All piezoelectric inkjet printers use the indirect effect as the mechanism of drop generation. The fluid is ejected from the nozzle as a result of distortion of the piezoelectric element (PZE). The mechanical deformation generates pressure which pushes the fluid out of the printing nozzle orifice. There are many geometrical configurations and constructions of the printing element. Usually, many nozzles are integrated into one printing head and the nozzles must operate simultaneously or synchronically. On the other hand, they are individually tuneable and programmable in order to achieve regularity and homogeneity of printing by individual control of all nozzles. [32]

The deformation of piezoelectric element is defined by applied voltage. Thus the drop ejection is controlled by so called pulse waveform, see Figure 10. The

waveform can be divided into several segments representing a sequence of programmed voltage steps resulting in a sequence of events. A typical waveform exemplified for a single piezoelectric element nozzle consist of following stages. The standby position of PZE corresponds to the 'START' phase on the waveform. Note, that non-zero voltage is applied and the PZE is kept at certain state of deformation. In the Phase 1, the voltage drops to zero which results into returning of PZE to its off-position (i.e. most relaxed position) which causes increase of the nozzle chamber volume. This has two effects, first the chamber is filled by the ink from the ink reservoir and next the ink is pulled out from the nozzle orificium or meniscus. At the end of this stage, the camber is filled by maximum amount of ink and the system is ready for the next step. The Phase 2 starts by steep increase of voltage followed by short holding period. The deformation of PZE leads to a compression of the nozzle chamber volume and ejection of the ink due to generated pressure. Then the deflected PZE is slightly returned back to enhance and precisely define the pinch-off of the ejected liquid thread from the nozzle in Phase 3. Finally, the voltage decreases to the initial level and the cycle may be started again. If the droplet is not requested, no waveform packed is send to the PZE and the system rests in standby position. The duration of the waveform cycle limits the maximum achievable repetition rate of drop generation in PIJ. [33]
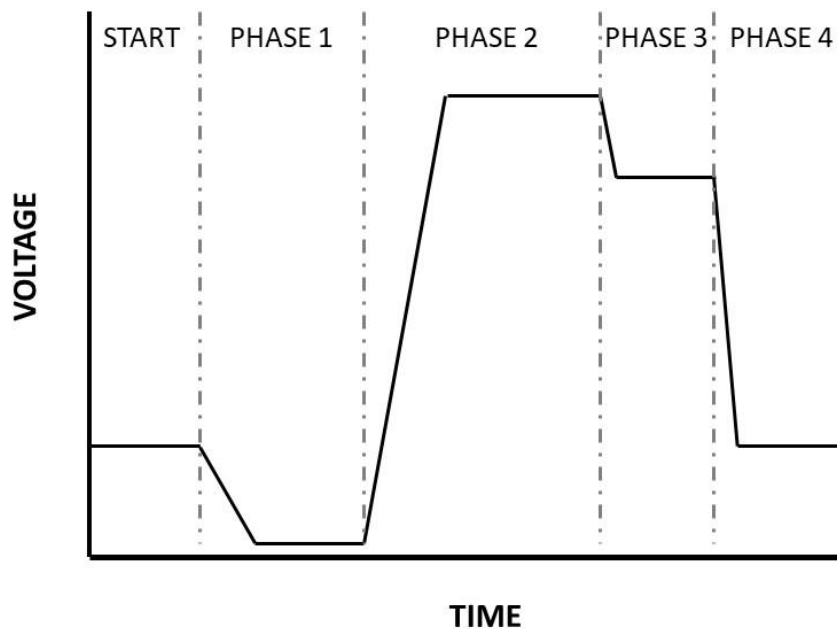
Figure 10 Segments of a voltage pulse waveform (a general example, for description see text). According to [33].

As the droplet of ink is ejected it first emerges as a jet, followed by a ligament or tail which is still connected to the ink in the nozzle. The event of its separation from the nozzle orificium called pinch-off can be finely tuned by the adjustment of the voltage drop in the phases 3 and 4 in the waveform. At the pinch-off stage the ligament parts: some ink returns to the nozzle and the rest of the tail joins the drop, or possibly breaks up into smaller satellite drops. Generation of a single drop in this manner can be considered as 'good printability' regime. Drop-on-demand technology is in some ways simpler than continuous as it does not require the external drop selection and recovery system; however, the techniques needed to make the print head, particularly with many fine nozzles, are very demanding. One issue confronting any drop-on-demand system is the need for the ink to dry or solidify on the printed surface, but not to dry in or clog the nozzle. This can be addressed at the print head, by appropriate cleaning and capping for example, and at the substrate by using low volatility inks and absorbing substrates, heaters, dryers or UV-curable inks. [28, 34-36]

3. INKJET PRINTING MATERIALS AND PRINTABILITY

It is necessary to distinguish between material that is printed and the material on which is something printed. The material which is printed usually is called printing inks are colored liquids or pastes, formulated to transfer and reproduce an image from a printing surface. [21] The materials on which is printed are called substrates such as paper, glass, ceramics or transparent polymer sheets.

3.1 Printing inks

At the present time there are four main types of inkjet inks available: water-based, phase-change, solvent-based and UV curable. Other types exist, but are less common, such as sparingly used liquid and oil-based toner. [30] Printing inks consist of dispersions of insoluble colorants or solutions of dyes which will distribute and transfer on the printing substrate. Important ink parameters are viscosity, surface tension, nature and molecular structure of colorants. Table 1 shows typical parameters of various type of inkjet inks and relevant inkjet printing techniques. [21, 37]

Table 1 Typical viscosity, surface tension and technique of inkjet printing for various types of inks.[21, 37]

Ink	Viscosity (Pa.s)	Surface tension (Nm^{-1})	Technique*
Water-based	$(1-5)x10^{-3}$	$(20-50)x10^{-3}$	PIJ
Phase-change	$(10-40)x10^{-3}$	$(20-40)x10^{-3}$	TIJ
Solvent-based	$(2-10)x10^{-3}$	$(20-35)x10^{-3}$	DOD PIJ and CIJ
UV curable	$(8-12)x10^{-3}$	$(20-30)x10^{-3}$	DOD PIJ

*PIJ - piezoelectric inkjet printing

DOD - drop on demand inkjet printing

CIJ - continuous inkjet printing

3.1.1 Water-based inks

Water-based or aqueous inks are primarily distributed to home printers. Water-based inkjet inks usually have a very low viscosity, low surface tension, an anionic character, and they are therefore not usually suitable for standard commodity grade non-porous substrates. These inks require porous substrates or substrates with specially prepared surface. Their advantage is their suitability for biological and food applications. [38]

3.1.2 Phase-change inks

In general, phase change materials or inks (sometimes referred to as "hot melt inks") are in the solid phase at ambient temperature, but exist in the liquid phase at the elevated operating temperature of an ink jet printing device. At the operating temperature, droplets of liquid ink are ejected from the printing device and, when the ink droplets contact the surface of the printing media, they quickly solidify to form predetermined pattern of solidified ink drops. [39] The advantages of phase change inks that they are very fast solidifying, environmentally friendly and have good opacity. [30] On the other hand their primary disadvantages are the lack of durability and poor abrasion resistance. [40]

3.1.3 Solvent-based inks

Solvent inks, based on organic volatile compounds, are an ink family which presents a particular challenge with respect to nozzle. Solvent inks which have fast drying characteristics and compatibility with low or nonporous substrates are used in the industrial printing space. They are generally considered as low cost. The disadvantages lie in some of these inks in rapid evaporation of solvents, which can cause clogging of the print head nozzles. For example, solvent based inks are often used in a segment of the industrial printing called product coding. In this segment the finished or nearly finished packaged products receive a printed code for tracking purposes. [30, 41, 42]

3.1.4 UV curable inks

Ultra violet Curable screen printing ink is a 100% solid system: that is, it essentially does not contain solvent that must evaporate during the curing phase. The cure takes place through the interaction of the ink ingredients and a strong UV (ultra violet) light source in a dryer, or more accurately, a reactor. The printing industry embraced UV-curing inks and coatings because they give out little to no volatile organic compound (VOC) solvents, do not dry during print process before curing, but will dry almost instantly when cured, and the curing equipment occupies much less space than the conventional thermal conveyer dryers. [30, 43-45]

3.2 Printability of inks

Viscosity and surface tension (surface energy) are considered as the main properties of inks for DOD PIJ. Indeed, producers of inkjet printers (specifically printing heads) define processing window for the use of their products in terms of viscosity and surface tension ranges applicable at specific fluid ejection (drop) velocities. Besides that, there are also other concerns, among them critical size of particles in case of dispersions used as inks and volatility of used solvents etc. Thus, development of a new ink formulation focuses to reach these criteria starting from the first guess followed by the trial and error method of subsequent optimization by testing the formulations on the real printing head under variable adjustment of processing parameters. A lot of effort has been spent to find general rules governing the DOD inkjet printing process and define rationally the conditions of successful printing achievement. This work continues this line. [46]

3.2.1 Viscosity

Newtonian fluids are defined to be those fluids exhibiting a direct proportionality between shear stress and shear rate in laminar flow as defined by Newton's Law:

$$\tau = \eta \cdot \dot{\gamma} \qquad (3.1)$$

where τ is the shear stress, η is the shear viscosity and $\dot{\gamma}$ is the shear rate. The viscosity is independent on the shear rate although it might be dependent (and in real cases it is) on other physical parameters as temperature and pressure. All other fluids which do not obey this law due to non-linearity or due to an initial yield stress are classified as non-Newtonian. All fluids can be classified as belonging to one of the three groups: time independent, viscoelastic and time dependent. However, these classification shows some overlaps for real cases. Those fluids which shows combination of properties characteristic for more than one of these groups are said to be complex fluids. [47]

Characteristic behaviour time-independent fluids in shear flow is demonstrated in Figure 11. Principally, shear thinning, shear-thickening and shear-independent fluids can be recognized each with and without yield-stress. The simplest case is the Newtonian fluid represented by the straight line A. Among all models describing time independent fluids, Herschel-Bulkley model can be used for their classification.

$$\tau = \tau_0 + \eta \cdot \dot{\gamma}^n \qquad (3.2)$$

where τ is the shear stress; τ_0 is the yield stress; η is the shear viscosity; $\dot{\gamma}$ is the shear rate; and n is the flow behaviour index. [48]

A typical non-Newtonian time independent fluid appears to be Newtonian at low shear rates. After this so called initial Newtonian plateau the viscosity is found to vary with increasing shear rate. The fluid is described as shear-thinning or pseudoplastic if the viscosity decreases (curve B in Figure 11, $\tau_0 = 0$ Pa $n < 1$), and shear-thickening or dilatant if the viscosity increases (curve C in Figure 11, $\tau_0 = 0$ Pa, $n > 1$) on increasing shear rate. After this shear-dependent regime, the viscosity reaches a limiting constant value at high shear rate. This region is described as the upper Newtonian plateau. If the fluid sustains initial stress without flowing, it is called a yield-stress fluid. The curve D in Figure 11 ($\tau_0 > 0$

Pa, $n = 1$) represents Bingham plastic fluid, curves E and F represent shear thinning fluid with yield stress ($\tau_0 > 0$ Pa, $n < 1$) and shear-thickening fluid with yield stress ($\tau_0 > 0$ Pa, $n > 1$), respectively.
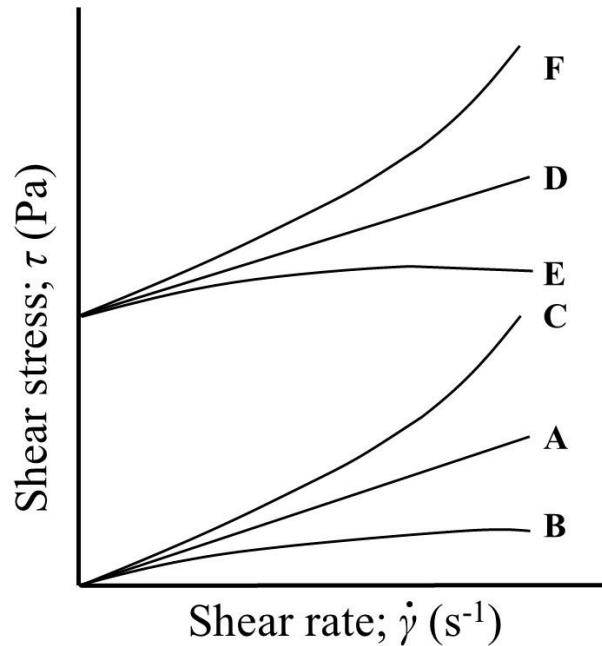
Figure 11 Flow curves for various time-independent materials. A represents Newtonian fluid; B, a pseudo-plastic fluid; C, a dilatant fluid; D, a Bingham fluid; E, a pseudo-plastic fluid with yield stress; and F, a dilatant fluid with yield stress. According to [47].

Viscoelastic fluids show partial elastic recovery upon the removal of a deforming stress. These materials combine properties of both viscous fluids and elastic solids. Maxwell, Kelvin (or Voigt) and Tucket (four elements) models can be considered as the most prominent ones describing their behaviour. [49]

The time dependent fluids (third class of fluids) consist of fluids that exhibit time-dependent behaviour at constant shear rate and constant temperature. When the fluid experiences a shear flow and its shear stress increases with time (shear hardening) the fluids is classified as rheopectic. On the other hand, the fluid is classified as thixotropic if the shear stress of the fluid decreases with time under constant shear rate flow (shear softening). [47]

Viscosity of fluids increases with pressure, however, the changes are quite small for pressures differing from atmospheric pressure by about one bar. Therefore, pressure dependence of viscosity may be neglected in this work. On the other hand, viscosity of fluids decreases significantly with increase of temperature and temperature is a factor, that is normally under control in printing process. The temperature dependence of the viscosity is most easily expressed according to the Arrhenius relationship.

$$\eta = Ae^{\frac{E_a}{RT}} \tag{3.3}$$

Where A is the preexponential factor having the dimension of mPa·s, E_a is the activation energy, T is the thermodynamic temperature, and R is the universal gas constant. [49, 50]

Dependence of viscosity on the composition of the fluid is a highly intriguing issue and no general models are available. Specific cases are described well, e.g. viscosity of polymer solutions is most studied, namely dilute solutions are covered by theories. [49] However, flow behaviour of a dispersion of particles in polymer solution in a co-solvent systems as an example of a typical real ink case is far from being analysed by simple models. Such ink formulations are mostly close to what is called complex fluids (though this term may be used for non-Newtonian fluids in general also). Nevertheless, there are many controversies in literature and specifically developed models available which are relevant to certain material systems. The majority of these models are basically empirical in nature and arise from curve-fitting exercises. [47, 51]

Rather than detailed analysis and modelling, real multicomponent ink samples are experimentally studied. High shear rates above 10^5 s^{-1} can be expected for the flow of liquid ejected from the printing nozzle [52]. Only instruments based on the flow of the liquid through a microchannel can be used for direct rheological measurements of inkjet inks at such high shear rates. However, low-shear rate viscometers are still used for basic characterization of inkjet inks in inkjet printing

industry as well as in academia due to low availability of microfluidic slit rheometers. The data obtained by ordinary viscometers can be considered relevant for characterization of prepared inks with the full awareness of their rough character. This radical simplification of complex fluid behaviour to the Newtonian-like one is based of the assumption that the investigated ink is ejected in laminar flow regime although the shear rate is so extremely large. It will be shown in further sections, that these ink flows are characterized by very small Reynolds numbers. Moreover, the apparent viscosity (the shear stress applied to a fluid divided by the shear rate) of inks that have to pass through the printing nozzle and its ink feeding channel is quite low (ranging from 1 mPa·s up to at most a few tens mPa·s), and the common ink formulations are only slightly or at most moderately deviated from the Newtonian model.

3.2.2 Surface tension

Surface tension (SFT) is the second crucial parameter of inkjet inks. Surface tension is defined as a reversible work necessary for creation of a unit surface area in a liquid substance. Sometimes it is also called the surface energy which generalises the concept to solids as well. [49] All liquids are made up of molecules close to one another and exerting attractive forces. In other words, SFT is a measure of the cohesion of the liquid too. The molecule in the bulk of liquid senses the same attractive forces in all directions, whereas these attractions are lacking from outer side for the molecules at the surface. Every liquid has its specific SFT value. Unlike viscosity that spans over several orders of magnitude, values of SFT for almost all common liquids (solutions and dispersions) ranges within several tens mN/m. Liquid with higher SFT (for example water) demonstrates a high intramolecular attraction and a strong tendency to form a drop, ideally a sphere. On the other hand, liquids with lower SFT have a weaker tendency toward sphere formation that is overcome by countering external forces which results into more pronounced deviation of their shape from ideal sphere. [50, 51]

Since free surfaces of liquid inks appear only at the atmospheric pressure in the PIJ technology, the dependence of SFT on pressure can be ignored. The dependence of SFT on temperature plays certain role, however, SFT decreases only gradually with increasing temperature. Typically, a decrease of SFT value about few mN/m is experienced when the temperature is increased by about ten centigrades. Surface tension is sensitive to composition in case of mixtures. It was found, that SFT of a mixture deviates negatively from a linear function of mole fraction of its components. This behaviour is usually explained qualitatively by the fact that the surface layer of the liquid is enriched in the component of lower surface tension, thereby minimizing the Helmholtz free energy of the mixture. However, in case of strong interactions between components, larger deviations of SFT from proportional contribution of components might be found. As an extreme case, surface active compounds (surfactants, tensides) can be given. The surfactants are effective even at very low concentrations as they are specifically adsorbed on the liquid-gas interface, thus SFT of the solution decreases steeply with increasing amount of the surfactant in solution up to a specific concentration beyond which, no prominent decrease in surface tension can be observed. This specific concentration represents the critical micelle concentration point (CMC) above which the surfactant molecules preffer to associate into micelles and do not further increase their mole fraction in surface layer of the liquid. This behaviour is typical for amphiphilic non-ionic molecules and ionic compounds, as well as for block copolymers, polymers with polar or ionic side groups etc. Surface active compounds have other roles in ink dispersions also, e.g. as stabilizers of dispersion, humectants and viscosity modifiers, hence their final effect on SFT of prepared ink composition cannot be predicted in trivial way. [30, 50, 53-55]

Surface tension and interfacial energy play important role in wetting of the surface of the substrate after impact of the ink drop. Final shape of dried material dot as well as the adhesion of the material is influenced by the matching of ink's SFT and surface energy of the substrate. Better wettability could be obtained

26

either by decreasing the surface tension of the ink or by increasing the surface energy of the surface. [50, 55]

3.2.3 Drop generation and dimensionless criteria

The development of an ink formulation starts normally with a set of compositions that try to match processing window criteria and map the dependencies of viscosity and surface tension on the ink composition. However, the key step in inkjet printing process is ejection of the defined amount of the liquid ink and formation of a spherical drop without existence of smaller drops known as 'satellite drops'. A definition of good printability as 'conditions of the printing process assuring that a single drop is formed either directly without second pinch-off or the satellite drop merges with the main drop within its travel distance forming thus a single drop safely before hitting the substrate creating thus a single dot' can be adapted from Kim & Baek's work. [56]

The drop generation in DOD PIJ printing process is a repeated cycle process. Each cycle can be described as a sequence of five phases: (1) ejection and stretching of liquid, (2) pinch-off of liquid thread from nozzle exit, (3) contraction of liquid thread, (4) break up of liquid thread into primary drop and satellites, and (5) recombination of primary and satellite drops. Ideally, no break up appears and spherical drop formation and its travel represent the fourth and last stage. [56, 57] Besides viscosity and surface tension of the ink, inertia and eventually viscoelasticity must be taken in consideration as they influence the final shape and form of the drops too. [58] However, since the breakup of boundary free Newtonian fluid jets is known very well and is most clearly described historically [59], the analysis of drop generation may be reduced to Newtonian fluid-like model for weakly viscoelastic fluids with still acceptable level of approximation [56]. Then, the Rayleigh type of axisymmetric varicose instabilities represents adequate model for drop generation in the inkjet printing process of viscous fluids.

[56] The jet break up theory by Rayleigh estimates the time constant for drop formation. [60]

$$\tau_d = \left(\frac{r_{jet}^3 \cdot \rho}{\sigma} \right)^{1/2} \tag{3.4}$$

The formation of a single drop either directly without break up or by the merge of the satellite drop(s) with the main drop defines the minimum stand-off distance (MSD) which must be kept in the printing process. Stand-off about 1-2 mm is generally used in digital printing. The effect of gravity is negligible on such distances, hence viscosity, SFT, density of the ink, liquid ejection velocity (i.e. drop velocity) and equivalent diameter of the printing nozzle orificium as characteristic length represent physical variables sufficient for 'global' description of the real printing process. [61]

These material, tool and process parameters can be analysed in a scale independent general manner by a number of their dimensionless groupings – dimensionless numbers, namely by the Reynolds (*Re*), the Weber (*We*), and the Ohnesorge (*Oh*) number. The reciprocal value of the Ohnesorge number is known as the number *Z*. The number Oh^{-2} is known as the Laplace number (*La*) or the Suratman number (*Su*). [27, 61-63]

$$Re = \frac{v \cdot \rho \cdot A}{\eta} \tag{3.5}$$

$$We = \frac{v^2 \cdot \rho \cdot A}{\sigma} \tag{3.6}$$

$$Oh = \frac{\sqrt{We}}{Re} = \frac{\eta}{\sqrt{\sigma \cdot \rho \cdot A}} = Z^{-1} \tag{3.7}$$

$$La = Oh^{-2} = \frac{Re}{Ca} = \frac{\rho \cdot \sigma \cdot A}{\eta^2} \tag{3.8}$$

where η, ρ and σ are the dynamic viscosity, the density, and the surface tension of an ink respectively, v is the drop velocity and A is the characteristic length corresponding to the inner equivalent diameter of the nozzle orificium.

Single dimensionless number based approaches were introduced historically first for printability assessment to the field of DOD inkjet printing. The number Z was implemented by Fromm who suggested that stable drop generation occurred for $Z > 2$ and that for a given pressure pulse the drop volume increases with an increasing value of Z as well. [64] Reis & Derby found that stable drop formation occurred for Z values between 1 and 10. [65] According to them, too small Z value impedes drop ejection due to viscous dissipation, whereas the primary drops are accompanied by satellite drops if generated at too high values of the number Z. [27] Jang et al. reinvestigated the Reis & Derby's printable range for various liquids based on water, ethylene glycol and diethylene glycol and found good printability characterized by Z values falling into the interval $4 < Z < 14$. [61]

Although the Z number is widely used for the printability assessment, other dimensionless criteria have to be considered because velocity "v" terms describing dynamic effects are cancelled in the Z formula (equation 3.7) and only material constants and characteristic length is actually taken into account. [46, 66]

Plotting Oh against a dimensionless number which includes the velocity to construct a graph showing the field of parameter values for stable operation of DOD inkjet printing was the idea of McKinley & Renardy [67] who redrew the schematic diagram originally constructed by Derby [27] using logarithmic coordinate system. Their diagram in Figure 12 shows a quadrangle field, in which a fluid is printable and single drop formation may be achieved. Any printable fluid must not be too viscous, i.e. the value of the Ohnesorge number mustn't be higher than 1. On the other hand, if its value is lower than 0.1 satellite drops are formed and the printing process gets progressively worse. This range is actually the same as Z values between 1 and 10 (see the paragraph above). The fluid must have sufficient energy for drop formation also which defines the left-lower diagonal borderline from 3 (for $Oh = 1$) to 30 (for $Oh = 0.1$) in Reynolds number space. The right-upper diagonal borderline indicates the splashing onset region from $Re = 20$ (for $Oh = 1$) to $Re = 130$ (for $Oh = 0.1$).
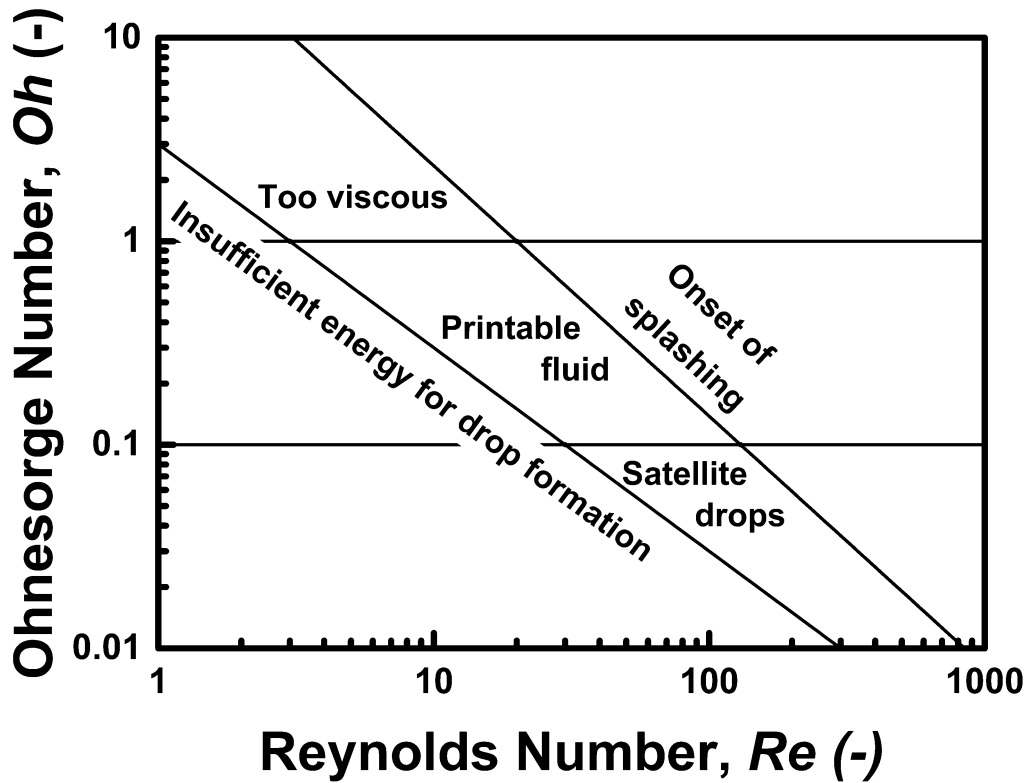
Figure 12 McKinley & Renardy logarithmic coordinate system, redrawn according to [67].

The opportunity to revive McKinley-Renardy graph recently published in [68] is used in this dissertation, since it covers all material-tool-process parameters also and it offers large ranges of parameters on both axes due to the use of logarithmic scales. Moreover, each value of the Weber number can be represented by a diagonal line with the slope -1 and position according to ist square root because:

$$\log Oh = \log \sqrt{We} - \log Re \qquad (3.9)$$

While the printing head nozzle is constant, effect of the fluid velocity may be predicted instantaneously with the help of McKinley-Renardy graph. Similarly, it may serve for in initial guess of parameters as well as intended viscosity, surface tension and/or density modification steps in development of a new functional ink.

Another approach was developed by Kim&Baek [56]. They identified conditions for change of drop generation mode, satellite drop formation, satellite recombination with the main drop, and other instabilities or failures in printing. They used the capillary number (*Ca*) which takes the drop velocity during printing

into account although the characteristic length and density are not included and the Weber number which does not contain viscosity.

$$Ca = \frac{We}{Re} = \frac{v \cdot \eta}{\sigma}$$

(3.10)

Within these *Ca-We* coordinates, Kim&Baek mapped various printing regimes including good printability window. The graph is shown in Figure 13. The white area I represents the good printability processing window. The area II covers a field of parameters where one or more satellite drops are generated, but they will not recombine with the main drop. The area III indicates field of long threads generation which result into fine satellite droplets generation and generally threading due to a simultaneous combination of large *Ca* and large *We*. The area IV at large *Ca* and small *We* shows the field where the viscosity effects prevail over inertial forces and the ejection of fluid fails. The area V at small *Ca* and small *We* represents the filed where surface tension dominates both viscous and inertial forces thus the fluid cannot be ejected too. [56]
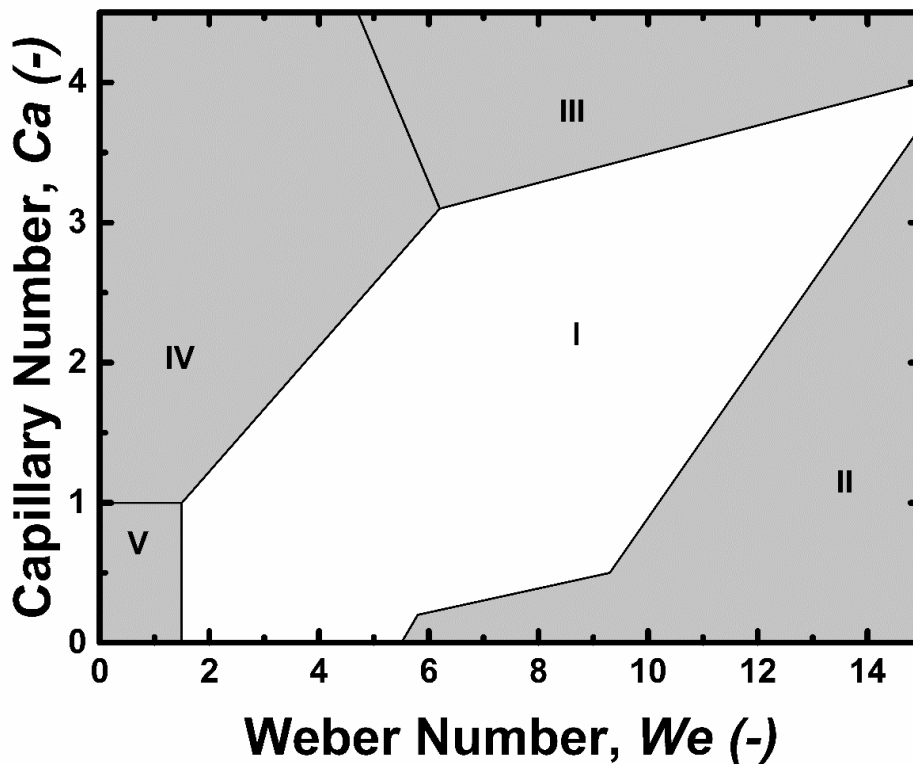

Figure 13 Kim and Baeks Capillary-Weber diagram, redrawn according to [56].

On the other hand, the map in Figure 13 does not include inviscid flows as well as the ink dripping, when the liquid leaks from the nozzles due to week surface tension and low viscosity. Moreover, the range of the x-axis is to small to include printability parameters expressed as *We* which are advised by the producer of the printer Dimatix used in this study. Pavol Šuly [46] replotted this graph in *Re-Ca* space and obtained a suitable map covering all possible reagimes and failures of inkjet printing. His graph is shown in Figure 14. The influence of printing fluid velocity is best analysed with the help of the Laplace number isolines. Generally, an increase of the velocity causes shifts of any operating point in the direction from the origin along the constant Oh^{-2} line and any velocity decrease causes shift of the operating point towards the origin of the graph – i.e. closer to the point [0,0]. The weber number is included in hyperbolic iso-*We*-lines. [46]
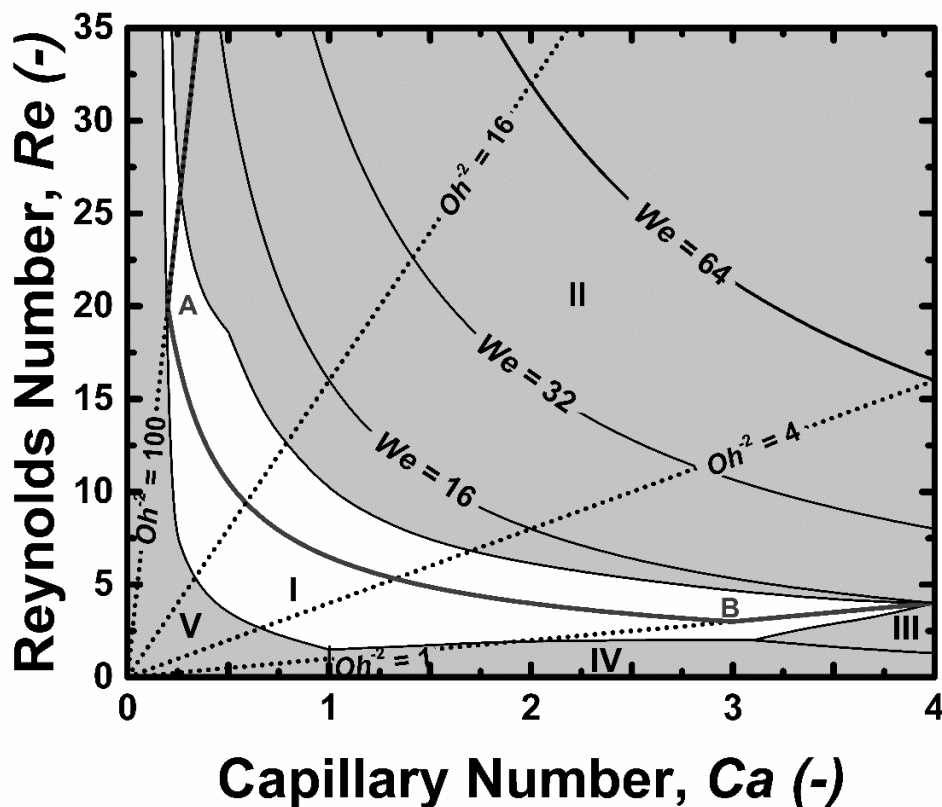

Figure 14 Reynolds-Capillary number diagram, courtesy Pavol Šuly, [46].

3.3 Inks on substrates

State-of-the-art printing inkjet technology for classical image printing comprises highly sophisticated solutions of the ink vs substrate problem with respect to the production of high quality resolution pictures. Material printing introduced nowadays requires more general approaches and the substrate development process starts from less specialized but multipurpose substrates that can be upgraded towards different expected functions.

3.3.1 Special substrates in classical image inkjet printing

The inkjet substrates must demonstrate several unique properties to produce high quality images with inkjet inks. Inkjet substrates typically contain a special thin layer coating on top of substrates enabling high print quality. Once the ink droplet is deposited on the substrate, the ink must adhere without running or smudging and spread uniformly in all lateral directions to generate sharp edges. The substrate should also have adequate smoothness to promote high print densities. The substrate is coated with a thin, highly absorptive layer to absorb the ink droplets being ejected from the print head. The principle of the technology is presented in Figure 15. [30]
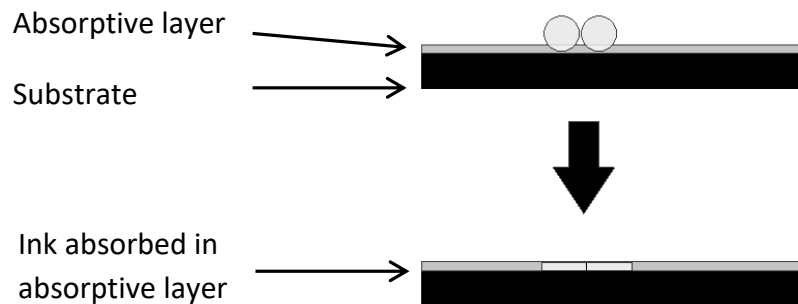

Figure 15 Tailored substrates for image inkjet printing.

3.3.2 Generalization of substrate requirements for material printing

The initial level of innovation in any universal material is quite low and may look like a downgrade in comparison with the specialized materials described in the above section. However, this is due to the extremely large variability of the material printing technology. The choice of substrate is related to ink selection through maximum processing temperature, spreading, wetting and adhesion interactions, and the requirement for physical flexibility. Possible substrates include almost any solid material and the most common substrates used in printable conductive applications are summarized in Table 2. [30, 69]

Table 2 Typical substrate materials [69]

Substrate	Flexible	Common uses
Paper	Yes	RFID, greeting cards
Glass	Very thin	Displays
Metals	Thin	Display backpanels
Ceramics	No	Multilayer ceramics capacitors
Thermoset composites	No	Printed circuit boards (PCB)
Polymers	Usually	PCB, flexible electronics and RFID
Textiles	Yes	Clothing

Very important step is to achieve matching of the ink surface tension to the surface energy of the substrate. However, the exact match of the surface tension of the inks and substrate means that a particular set of inks will be suitable for printing on narrow span of substrates - only the substrates matching the surface tension of the inks. Different substrates will require development of a different set of inks. Common polymer substrates for flexible electronics are PTFE, PI (Kapton®), PET usually with surface modification. Other functionality can be achieved by the deposition of an ITO thin layer on PET substrate for making a transparent yet conductive electrode. Table 3 shows most used substrates for various types of inks. [30]

Table 3 The most used substrates for various types of inks[30]

Ink	Substrate
Water-based	Paper, PVC, PS, PC, PES
Phase-change	Paper, porous material
Solvent-based	Metal, plastics, glass
UV curable	Paper, textile, PVC, PP, PE, PC, ceramics

3.4 Polymer-nanoparticles composites for inkjet printing

In recent years, polymer–nanoparticle composite materials have come into focus many researchers, due to their synergistic and hybrid properties derived from several components. Either in solution or in bulk, these materials provide unique electrical, optical, mechanical and thermal properties. Such improvements are produced by the physical occurrence of the nanoparticle and by the interaction of the polymer with the particle and the state of dispersion. One big advantage of nanoparticles, as polymer additives in comparison with conventional additives consist in loading requirements, which are quite low. Micro-sized particles used as auxiliary or dopant agents scatter light, then reducing light transmittance and optical clarity. In contrast to that, efficient nanoparticle dispersion combined with good polymer–particle interfacial adhesion eliminates scattering and allows the exciting possibility of developing strong yet transparent films, coatings and membranes. [70]

With respect to the inkjet printing, the use of nanoparticle dispersions is limited by the size of the nanoparticles which must not seal the capillary and nozzle during printing. As a rule of thumb, the diameter of particles shall not be bigger than 1/10 of the diameter of the capillary through which it is to be passed. [33] Obviously, the use of nanoparticles is limited by their influence on general ink properties like viscosity and surface tension too.

4. SENSORS

The sensors are defined as the devices which reply to a signal or stimulus and respond with an electrical signal. The signal may be in the form of current, voltage or charge. These stimuli are generally referred to as measurands. The term sensor should be distinguished from transducer. A transducer is an electronic device that converts energy from one form to another. A sensor is composed of two major components: a sensitive element and a transducer. Figure 16 shows a scheme of a sensor, which incorporate two transducers and direct sensor producing electrical output. The sensitive element has the capability to interact with stimuli and produce a change in the operation of the transducer. Affected by this change, the transducer produces a signal, which is further transformed by the second transducer to that form of energy that can be operated by the direct sensor. That sensor makes a direct energy conversion into a generation or modulation of an electrical signal that can be processed to data which are recordable by a data acquisition system. In other words, a direct sensor converts a stimulus into an electrical signal whereas a complex sensor needs one or more transducers of energy before a direct sensor can be employed to generate an electrical output. From sensor specification are very important factors accuracy, sensitivity and selectivity. A sensor does not function by itself, it is always a part of larger system that may incorporate many other detectors, signal conditioners, signal processors, memory devices, data recorders and actuators. [71-74]
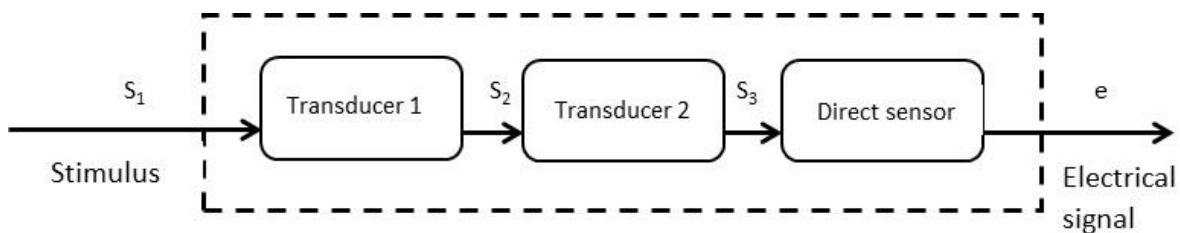

Figure 16 A sensor with two transducers and direct sensor producing electrical output e. [71]

4.1 Sensors characteristics

The sensors characteristics are usually classified into two groups: static and dynamic. Both groups exactly describe the input and output of a system.

4.1.1 Static characteristics

Accuracy is one of the static characteristics refers to how close (highest deviation) a measurement is to an actual ("true") value of a stimulus at its input. For example, a temperature sensor which shows 25.1°C is more accurate than sensor which shows 26°C when real temperature is 25°C. [73]

Precision describes the reproducibility of the measurement. For example, measure a steady state signal many times. In this case if the values are close together then it has a high degree of precision or repeatability. The values do not have to be the true values just grouped together. For instance, a temperature sensing system is precise, if when the ambient temperature is 25.0°C and it shows 26°C, 26.1°C or 25.9°C in three different consecutive measurements. It is not considered precise, if it shows 25.5°C, 25.0°C and 24.5°C although the measured values are closer to the actual temperature.[71-73]

This is the ability of a sensor to repeat a measurement when put back in the same environment. It is often directly related to accuracy, but a sensor can be inaccurate, yet be repeatable in making observations. For a temperature sensing system, when ambient temperature remains constant at 25.0°C, if the system shows 25°C, 25.1°C and 25°C in 1 min intervals, and shows 26.0°C, 26.1°C and 26.2°C after 1 h, in similar 1 min intervals, the system has a good short-term and poor long-term repeatability. [71-73]

Stability is a sensor's ability to provide reproducible results for a certain period time. [71-73]

The transfer function represents the relation between stimulus s and response electrical signal S produced by the sensor. This relation can be written as $S = f(s)$. Normally, stimulus s is unknown while the output signal S is measured. An

inverse $f^{-1}(S)$ of the transfer function is required to compute the stimulus from the sensor's response S. The value of S that becomes known during the measurement is just a number (voltage, current, digital count, etc.) that represent the value of stimulus s. In reality, any sensor is attached to a measuring system. [71]

Sensitivity of a sensor is defined as the change in output of the sensor per unit change in the parameter being measured. In other words the sensitivity is an absolute quantity, the smallest absolute amount of change that can be detected by a measurement. For nonlinear transfer function, sensitivity B is not fixed number, as would be the case in a linear transfer function. A nonlinear transfer function exhibits different sensitivities at different points in intervals of stimuli. In case of nonlinear transfer functions, the sensitivity is defined as a first derivative of the transfer function (equation 4.1):

$$b_i(s_i) = \frac{dS(s_i)}{ds} \approx \frac{\Delta S_i}{\Delta s_i}$$
(4.1)

where traditionally Δs_i is a small increment of the output stimulus and ΔS_i is the correspoding change in the output S of the transfer function.[71-73]

Selectivity is the ability of a sensor to measure only one parameter, in the case of a chemical sensor, to measure only one chemical species. For example, an oxygen gas sensor that does not show any response to other gas species, such as carbon dioxide or nitrogen oxide, is considered a very selective sensor. [71-73]

4.1.2 Dynamic characteristics

Under static conditions (a very slowly changing input stimulus) a sensor is fully described by its transfer function, span, etc. However, when an input stimulus varies with an appreciable rate, a sensor response generally does not follow with perfect fidelity. The reason is that both the sensor and its coupling with the source of stimulus cannot always respond instantly. In other words, a sensor may be characterized with a time-dependent characteristic, which is called a dynamic

characteristic. If a sensor does not respond instantly, it may represent the stimulus as somewhat different from the real, that is, the sensor responds with a dynamic error. A difference between a static and dynamic error is that the latter is always time-dependent. If a sensor is part of a control system, which has its own dynamic characteristics, the combination may cause at best a delay in representing a true value of a stimulus or at worst cause spurious oscillations.[71-73]

4.2 Chemical sensors

Chemical sensors consist of a recognition element that is sensitive to stimuli produced by various chemical compounds (analyte) and a transduction element that generates a signal whose magnitude is functionally related to the concentration of the analyte. Chemical sensors also include a special branch referred to as biosensors for the recognition of biochemicals and bio-reactions. The use of biological elements such as organisms, enzymes, antibodies, tissues, and cells as receptors differentiates biosensors from conventional chemical sensors. In general, the chemical sensors are broadly classified into gas, liquid, and solid particulate sensors based on the phases of the analyte. They are further categorized as optical, electrochemical, thermometric, and gravimetric (mass sensitive) sensors according to the operating principle of the transducer. Chemical sensors have become an indispensable part of our technology- driven society and can be found in chemical process, pharmaceutical, food, biomedical, environmental, security, industrial safety, clinical, and indoor monitoring applications. [71, 73]

Manifestation of such technological changes can be seen in the all-out effort of miniaturized, reduction of cost, portable of sensors, and mass fabrication of chemical sensors able to static and continuous measurements even in remote environments. Moreover, research on nanomaterials in the field of sensors enables application of sensors as electronic nose (e-nose) systems. An electronic nose consists of a mechanism for chemical detection, such as an array of electronic

sensors in order to mimic the olfaction capabilities of mammals. These types of sensor are usually used for breath analyser to test for blood alcohol levels. Breakthroughs over the last decade have pushed chemical sensors into new markets, as well as new applications within existing markets. [72, 75-80]

4.3 Sensor for VOC and gases

Detection of various gases and volatile organic compounds and subsequent evaluation of their concentration is an important task in monitoring various manufacturing processes. The detection of such substances is very important in the human environment. Very cheap resistive sensors are popular for such applications, e.g. humidity sensing [81]. They have already introduced many methods of manufacture and methods of measurement that would improve their selectivity and sensitivity under different measurement conditions. But still there are methods that could be obtained directly, easily and quickly authoritative information about the detected gas. Some methods are based on gain of information from a series of sensors, which are then processed using various detection algorithms. Neural networks with self-learning capabilities are good example of this. At present, the development focuses on new methods that would ensure low energy consumption of sensors while maintaining their high sensitivity and selectivity even at low operation temperatures. Another direction of development should be effective gas detection, without sophisticated processing of signals. [38, 39]

4.4 Sensors based on a change in conductivity

Sensors based on a change in electrical conductivity can be understood as sensors based on changes in electrical resistance also because the electrical conductivity can be expressed as the reciprocal electrical resistance value, see Equation 4.3. The electrical resistance can be calculated from Ohm's law (Equation 4.2), but this law applies only for direct current. Changes of external

physical, chemical or mechanical properties will change the electrical conductivity (electrical resistance) of the sensor.

The sensor should be understood as part of the electrical circuit, in particular as a resistor whose electrical conductivity (electrical resistance) varies due to the aforementioned measured characteristics.

$$R = \frac{U}{I} \tag{4.2}$$

$$G = \frac{1}{R} \tag{4.3}$$

where R is the electrical resistance $[\Omega]$, G is the electrical conductivity $[S] = [\Omega^{-1}]$, U is the voltage $[V]$, and I is the electrical current $[A]$.

Sensors based on the change of electrical conductivity or electrical resistance are one of the most widely used class of sensors in general. These sensors are often used, for temperature measurement, detection of chemical substances or gases and volatile organic compounds, humidity, deformation etc.

4.4.1 Resistance measurement

The electrical resistances can be divided according to their size and relevant measurement methods into three categories. A small resistance is a category for $R \leq 1\Omega$, the resistances in the range $1\Omega \leq R \leq 1M\Omega$ are classified as moderate ones, and resistance higher than $1M\Omega$ is regarded as large.

Measurement of the electrical resistance should be carried out using direct current, since the use of an alternating current could cause a manifestation of inductance and capacitance on the measurement result. Measurements of electrical resistance can be divided into two categories of methods. The first category are the direct methods which directly obtained by the value of the electrical resistance. Measuring bridges are a good example using comparation of the measured resistance with a known resistance. The second category are indirect methods, in which numerical values of the quantities voltage and current are

obtained by measurements and the following computational processing according to the given equations allows obtaining the value of the electrical resistance. This concept is simple to integrate into common multimeters. [4, 5, 40]

4.5 Printed sensors

Currently, the printed sensors begin to be manufactured and applied. The reason is primarily to minimize the dimensions of the sensors and measuring devices. There are other motivations for printing sensors too, such as simple and productive manufacturing process, lower costs, fabrication of disposable devices, integration with flexible electronics, product weigth reduction, to name a few. Printed sensor is normally a thin device which is easier applicable wherever the thick sensors could not be used due to their size. Printed sensors are typically fabricated using appropriate printing or lithographic method on a suitable substrate [82]. Typical examples of commonly used flat sensors are a temperature sensor, humidity, pressure, strain and chemical sensors, acoustic sensors, electrical sensors, sensors of magnetic and electromagnetic fields, various small antennas and so on. [71, 83]

The simplest part of the circuit may be formed by just two elctrodes contacting an area covered by sensing material layer. (See Figure 17, left side.) In connection with the printed sensors, the term 'interdigit' is often found in literature. This term refers to most commonly used finger-like electrode pattern, which is formed in a plane two interlocking comb-shaped parallel periodically repeating conductive tracks. These electrodes are in touch or penetrate into the material of the sensitive layer. Such structure then forms a sensor having at least two electrodes (two poles). The resistance of the sensitive layer depends on the external stimulus effect so the sensor and transducer function is integrated within one active material layer. From another point of view, such structure may be perceived and used (measured) as a capacitor also having two electrodes and a dielectric there between. Such configuration would be beneficial in case of high resistances or for

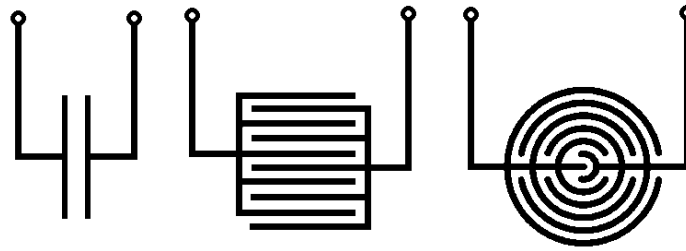imopedance (capacitance) measurements. [71] Figure 17 shows examples of these patterns of an own design.

Figure 17 Simplest possible resistance motif – left side. Example of interdigit patterns – the middle and right schematics. [own source]

5. NANOSTRUCTURED CuO FOR SENSORS

Cupric oxide (CuO) has been a hot topic among the studies on transition metal oxide (MO) because of its interesting properties as a p-type semiconductor with a narrow band gap (1.2 eV in bulk) and as the basis of several high-temperature superconductors and giant magneto resistance materials. [84-92] CuO nanostructures with large surface areas and potential size effects possess superior physical and chemical properties that remarkably differ from those of their micro or bulk counterparts. These nanostructures have been extensively investigated because of their promising applications in various fields. CuO nanostructures are also considered as electrode materials for the next-generation rechargeable lithium-ion batteries (LIBs) because of their high theoretical capacity, safety, and environmental friendliness [93]. They are also promising materials for the fabrication of solar cells because of their high solar absorbance, low thermal emittance, relatively good electrical properties, and high carrier concentration [94]. Furthermore, CuO nanostructures are extensively used in various other applications, including gas sensors [95], bio-sensors [93], nanofluid [96], photodetectors [97], energetic materials (EMs), field emissions, supercapacitors, removal of inorganic pollutants, photocatalysis, and magnetic storage media[98-104]. Recent studies have demonstrated that nanoscale CuO can be used to prepare various organic–inorganic nanocomposites with high thermal conductivity, high electrical conductivity, high mechanical strength, high-temperature durability, and so on [105]. Moreover, the nanoscale CuO is an effective catalyst for CO and NO oxidation as well as in the oxidation of volatile organic chemicals such as methanol [106-108].

5.1 Synthesis of CuO nanostructures

The development of synthetic methods has been widely accepted as an area of fundamental importance to the understanding and application of nanoscale

materials. It allows scientists to modulate different parameters such as morphology, particle size, size distributions, and composition. Numerous methods have been recently developed to synthesize various CuO nanostructures with diverse morphologies, sizes, and dimensions using various chemical and physical strategies. The most common synthetic strategies and associated mechanisms for tuning the morphology, size, and structure of the CuO nanostructures are presented along with the studies of the effects of these parameters on the chemical and physical properties of the synthesized nanostructures. [84]

5.1.1   Solution-based methods

Solution-based synthetic methods are very common and effective ways to prepare various MO nanostructures with good control of shape, composition, and reproducibility. They usually have relatively low reaction temperature and are flexible and suitable for large-scale production. Moreover, the synthesis parameters can be rationally tailored throughout the entire process, which is beneficial for more precise control of compositions, sizes, and dimensions of the resulting materials. Among a variety of solution-based synthetic methods, hydrothermal and chemical precipitation techniques have been widely used to synthesize CuO nanostructures. [90, 109-112]

5.1.2   Hydrothermal synthetic method

Hydrothermal synthetic method, in which the reactions are conducted in water in a pressurized sealed container and reaction temperature usually rises significantly over the boiling point (eventually over the critical point) of a solution, has been widely used to generate different nanomaterials. The pressure in the raction systems grows as well which supports condensation reactions. Moreover, products of such reaction system are usually easily collected with convenient post treatment. [84, 90, 113].

5.1.3 Solution-based chemical precipitation methods

Chemical precipitation synthesis is similar to the hydrothermal method with a reaction also occurring in the solution, but the chemical reactions can be conducted in an open container with a relatively low reaction temperature (normally below 100 °C). This process can be simply defined as the chemical reaction between the precursors to produce monomers that subsequently aggregate into final resulting materials [113].

5.1.4 Solid-state thermal conversion of precursors

Various CuO nanostructures can be generated through the thermal conversion of the precursors, and the morphological features of the precursors can be well-preserved in the final products given that heat treatment is appropriately performed. $Cu(OH)_2$ and basic Cu salts have become favourable precursor candidates to exploit the interesting morphologies of CuO because of their unique and well-known layered structure. The process usually starts with the synthesis of the Cu precursors via the reaction of cupric salt (normally nitrate or chloride) with alkaline compounds (normally NaOH). The obtained cupric precursors are then centrifuged and washed with distilled water and absolute ethanol. Finally, these cupric precursors are calcined in solid state to obtain the final CuO nanostructures. Moreover, the corresponding $Cu(OH)_2$ particles are formed and precipitated in H_2O by adding a basic solution (usually NaOH) to the obtained cupric precursors solution. Thebresulting nitrate or chloride salts are then washed away, and the corresponding $Cu(OH)_2$ particles are thermally dehydrated after filtration and washed to obtain the final CuO nanostructures [114].

5.2 Properties of CuO nanoparticles

CuO is a narrow-bandgap p-type transition metal oxide (MO) semiconductor. The electronic bandgap of CuO corresponds to the difference between the energy levels of the top of the valence band (VB) derived from the Cu 3d orbital and the

bottom of the conduction band (CB) derived from the Cu 3d orbital [115]. The electronic structure of CuO was theoretically investigated using cluster model calculations [84] and other ab initio calculations based on the local spin-density approximation (LSDA) [8, 116, 117]. However, these calculations normally fail to predict the semi-conducting ground state because of the strong electron–electron interactions of CuO that have not been considered in the calculations. For a p-type MO semiconductor, the charge carriers based on a considerable concentration of the free holes existing in their VBs are widely accepted. The concentration of the free holes in these materials is mainly determined by the metal deficit concentration (or excess oxygen) within the crystallite sites of the materials [85, 118, 119]. This phenomenon is attributed to the deviation from the stoichiometric composition of the components, which can be induced by regulating the preparation condition of the material [119]. Given that oxide crystals usually cannot accommodate a large oxide ion, the nonstoichiometry of p-type CuO is expected to be cation deficient. [84]

Copper (II+) oxide, CuO, is a compound with limited stability in environment of low oxygen partial pressure. Meyer et al. [120], who obtained Cu oxides with different stoichiometries, particularly the three crystalline phases, namely, Cu_2O, Cu_4O_3, and CuO, when they varied the oxygen flow during synthesis. The resistivity of the obtained CuO films changed from high to low by two orders of magnitude with increasing oxygen flow. Moreover, the lowest carrier densities of CuO are $\sim 10^{17}$ cm^{-3}, which also reach 10^{20} cm^{-3} with increasing oxygen flow. Moreover, nonstoichiometric phases can be found. The change of redox state of copper ions which can be formally Cu (I+) or Cu (II+) is not that disambiguous due to the character of 3d orbitals involved in bounding which leads to various structural arrangements of its solid compounds with chalcogenides. Therefore, this class of materials may be considered as suitable candidate for application as the active layer in a direct sensing device. [84]

For example, resistivity decreases significantly and carrier concentration increases rapidly with an increase in oxygen concentration when the oxygen concentration is more than 1.2% (note that Cu_2O is the major phase when the oxygen concentration is below 1.2%) [121]. Changing the synthesis parameters, thickness, and roughness of samples can also vary the resistivity of the prepared CuO samples. Resistivity reportedly increases along with thickness and deposition temperature of CuO sample because of the irregular grains (or aggregates) that contributes to more trapping and scattering of free charge carriers [122-124]. Moreover, carrier mobilities tend to significantly decrease when going from single crystals to polycrystalline and nanocrystalline materials by the scattering at grain boundaries and energy barriers at these boundaries [125]. Other factors, such as lattice strain and crystal distortions, can also affect the charge movement, resulting in an increase in the resistivity and a decrease in conductivity. [84, 124]

5.3 Application in gas sensors

Semiconducting MO gas sensors were firstly introduced in the 1950s when their gas sensitivity at elevated temperature was discovered [126]. Since that time, gas sensors based on these MOs for detection of hazardous, flammable, and toxic gases has been increasingly developed because of their small dimension, low cost, and high compatibility with microelectronic processing. These materials allow fabrication of direct sensors because the response to changing gaseous analyte concentration is change of the material´s resistivity modulating thus directly the electrical signal. However, these sensors need to be operated at high temperatures usually at least above 200°C to achieve reasonable sensitivity and signal baseline stability. Increased temperature helps also to maintain the active surface free of adsorbed humidity or other condensates [127, 128].

Development of the nanotechnologies and nanomaterials opened new approcheas toward design of these gas sensors. The physical and chemical

properties of nanostructured materials are strongly influenced by their large specific surface area, morphology and dimensional constraints for electronic properties namely when approaching size comparable with the Debye length. Therefore, gas sensors based on nanostructured MOs can be expected to have better performance than their bulk or micro analogues. Metal oxides can be prepared in many nanostructured morphologies such as nanowires and nanobelts, nanorods, nanoplates or nanosheets, multipodes, stars, urchins and flower-like nanoparticles. These basic shapes may be assembled into hierarchically organised multiscales structures combining functions of corresponding hierarchical levels. Such diversity of material design has attracted considerable attention for their utilization as active materials for fabrications of gas sensors. [129-131]

Among various MOs, CuO has the unique property of being intrinsically p-type and is advantageous because of its low cost, high stability, nontoxicity, and capability for electron transfer [131]. Therefore, CuO nanostructures have been extensively investigated as good candidates for sensing applications. Gas sensors based on CuO nanostructures were operated by measuring the resistance changes when they are exposed to reducing or oxidizing gases. A suitable operation temperature is crucial to the gas sensing capability of CuO because it enhances the sensitivity and reduces the response and recovery time. Coating of noble metal catalysts, such as Ag, Au, Pd, and Pt, on the surface of CuO nanostructures will enhance their sensing properties because they can act as adsorption sites for analytes or as surface catalyst [132]. The sensing mechanism of gas sensors based on p-type CuO differs from that typical for n-type MOs [129, 131, 132]. In the air, oxygen molecules are adsorbed onto the CuO surface forming oxygen ions (O^-, O_2^-, O^{2-}), charging it negatively. If a reducing species, such as NH_3 is present, it oxidizes and releases a negative charge (electron). In this regard, the electron transfer from oxygen ions (O^-, O_2^-, O^{-2}) to CuO results in decreased hole density and thus decreased conductance. Meanwhile, the number of oxygen ions (O^-, O_2^-, O^{2-}) absorbed on the surface of CuO is also reduced, which leads to the decrease

in the magnitude of the negative quasi-gate resulting in further decrease in conductivity. Exposure to oxidizing gas, such as NO_2, likely results in the occurrence of charge transfer from the CuO to the NO_2 as governed by $NO_2 + e^-$ $\rightarrow NO_2^-$. The electron transfer from the CuO to the NO_2 results in the lowering of the quasi-Fermi level and thus increases free hole density and enhances conductance. Additionally, the negatively charged chemisorbed NO_2 molecule at the CuO surface may act as a negative gate bias and increase CuO conductance. [84]

Based on the above described physical principle of CuO sensing property it can be reasonable expected that this sensing material has conductivity decrease response upon exposure to electron donating (nucleofilic) molecules. Indeed, a number of studies have focused on the development of novel CuO nanostructures for the detection of a wide range of gases, such as organic gases [132], hydrogen sulfide (H_2S), CO, NO_2, ethanol gas, NH_3, HCN and humidity [133].

According to the state of the art described one may consider the field of CuO based sensors being quite well described and only specific production and application details remaining open questions. Nevertheless, it pertains fabrication of high temperature operated sensors only. Preparation of CuO based sensors operating at room temperature is still challenging issue namely in form of flexible polymer surface devices which require low temperature fabrication process also.

6. AIM OF WORK AND OUTLINE OF THE THESIS

The main aim of this Thesis was defined according to literature review and already gathered experience in our laboratories. The work presented here serves to address specific issues of gas and humidity sensor prepared by inkjet printing on polymer (PET) substrate which requires low temperature fabrication process and operation of the sensor itself at low temperature as well. In concrete terms, *the aim is to develop and fabricate a novel fully inkjet printed CuO sensor for sensing of alcohol vapours and humidity*. The work shall be done at least to the stage of a proof of concept. It requires material design of CuO nanostructured particles, formulation of inorganic ink based on nano-CuO for material printing and preparation of a sensor for the detection of alcohol vapours by material ink-jet printing method. The sensor was tested and sensing principle of the active material was investigated to identify specific effects connected with the low temperature preparation and operation of the device.

According to the aim, the objectives of this dissertation are specified as follows:

- Synthesis and characterization of CuO nanostructured particles.
- Preparation and characterization of inorganic ink based on nanostructured CuO particles.
- Sensor design and optimization printing process for prepared ink-jet ink on material printer (FUJIFILM Dimatix materials Printer DMP-2800 series) and printing of sensors on selected substrate.
- Characterization of morphology, physical and other properties of printed thin layers as well as the properties of complete device.
- Testing of prepared sensors for detection of alcoholic vapours and its response to other external conditions and investigation of the sensing mechanism.
- Preparation of a sensor field to demonstrate capability of printing process.

6. EXPERIMENTAL

- **Materials**

Aqueous dispersion of Ag nanoparticles (Metalon JS-B25HV, 25 wt%) was delivered by Novacentrix, US. As substrates, PET foils (product name: Novele^{TM} IJ-220 with surface energy 49 mNm^{-1}, thickness 0.15 mm, Bekk smoothness >1000 Sec) were used for material printing and supplied by Novacentrix, US too. Finally, both dispersant and stabiliser BYK® 348 and DISPERBYK® 190 were supplied by BYK Additives & Instruments, a member of ALTANA, Germany.

- **Room or laboratory temperature**

Wherever used in this thesis, the room or laboratory temperature means (24 ± 2) °C unless given more precisely. There is air conditioning in the laboratory.

- **Synthesis and characterization of CuO nanoparticles**

CuO nanoparticles were prepared via simple water-ethyleneglycol (water-EG) solvothermal microwave assisted method. The method was adopted from [134] and enhanced by utilization of microwaves [135]. Cupric chloride dihydrate ($CuCl_2 \cdot 2H_2O$) was used as a precursor. Potassium hydroxide (KOH) was used as a starting agent in the absence of any surfactant or template. All chemicals were of analytical purity and used as received from Sigma-Aldrich s.r.o. Typical experimental procedure was carried out this way: 1 g of $CuCl_2 \cdot 2H_2O$ was dissolved in 54 mL of distilled water. Then, 6 mL of EG and 3 g KOH was added in turns. The as-prepared solution was poured into the Teflon vessel proper to use in microwave oven (MARS 5, CEM Corporation). Vessels with solution were sealed to ensure appropriate pressure inside. The reaction was maintained at 100 °C under 110 kPa for 30 minutes. After reaction, the product was washed by distilled water and absolute ethanol for several times to remove eventual impurities. Prepared powder was dried for 20 hours at 60 °C.

Prepared powder was characterized by Scanning electron microscope Nova NanoSEM 450 and by powder X-ray diffraction (XRD) using X'Pert PRO X-ray diffractometer (PANalytical, The Netherlands) with Cu Kα radiation of $\lambda = 0.15406$ nm. The size of nanocrystallite domains was estimated with the help of Scherer equation from the diffraction lines broadening.

- **Ink formulation and its preparation**

The series of inkjet inks was prepared from copper (II) oxide nanoparticles by dispersing them in the mixture of a surfactant and a dispersant in various ratios and constant volume of water. The dispersion process was agitated by an ultrasound apparatus working in 50:50 duty cycle with the full power and 5 minutes (GM 20170, BANDELIN electronic, sonopuls Rosette cell) The concentration of CuO varied in the range of 3-10 wt% and the amount of polymeric dispersant and surfactant was set in the range 5-35 wt%. Five ink compositions were prepared. The viscosity, density and surface tension were measured at 25 °C. Prepared ink compositions and their properties are summarized in Table 4.

- **Determination of crucial ink parameters**

The surface tension measurements were carried out using force tenziometer Krüss K100. The Wilhelmy plate method was used in all cases of determination of surface tension of solutions. The viscosity of dispersions was measured by microviscometer Lovis 2000 M/ME at 25 °C. The diameter of used capillary tube was 1.8 mm and 1.5 mm for the gold ball. The density was measured by density meter DMA 5000M at 25 °C.

- **Deposition method**

All obtained dispersions were tested for deposition by FUJIFILM Dimatix materials Printer DMP-2800 series. A single square of the size 2 cm x 2 cm was used as the testing motive printed on the PET substrate to evaluate preliminary the conductivity (by four point probe) of inks and silver films. The Ink 4 was found

as the best performing for printing and most stable dispersion. Therefore, it was used for fabrication of sensor devices intended for further testing. The device was fabricated by the same material printer. Interdigitated silver electrode pattern from the commercially available Metalon dispersion was printed on the flexible PET substrate. Printed electrode motives were dried in the vacuum oven at 80 °C for 20 minutes. To achieve good quality of electrodes, the first layer was trapped by another one under the same conditions. After that, continuous thin CuO film discs were printed on the top of this patterned substrate to form the set of sensing devices. A sheet with printed devices was dried once again under the same conditions as the electrodes. This process was repeated five times to obtain films of sufficient coverage, thickness and quality. Finally, single devices were cut from the printout sheet. Similarly, the sensor field of the 3×3 dimension was manufactured with the use of same procedure but using more complex design of printed motif integrating 9 single sensors onto one larger PET sheet.

- **Analysis of printed patterns**

The surfaces of printed patterns were analysed by optical microscope LEICA DVM25000 Digital Camera, Atomic Force Microscopy Dimension ICON in ScanAsyst mode, Scanning electron microscope Nova NanoSEM 450 and optical profilometer Bruker ContourGT.

- **Electrical and sensing properties**

Measurements of printed film conductivity were performed by van der Pauw four-point probe method. The apparatus comprises a Keithley ammeter 6517B, Keithley source 2410, and Keithley switch 7002. The probe contacts were golden coated and square geometry of the samples with contacs joined at the corners was used.

The electrical resistance of the single sensors was measured with using multimeter UNI-T HC-UT71D. Figure 18 shows a scheme of prepared gas sensor connected to the resistance meter. The holder with the sensor was quickly

transferred into an airtight conical flask full of saturated vapours of the alcohol or water. After 5 min adsorption, the sensor was promptly removed from the flask and for the next 5 min the sample was measured in the mode of desorption on the ambient air atmosphere. Humidity in the laboratory ambient atmosphere was not under control, so it varied naturally over the range of common values and can be a source of baseline drift in records of sensor responses for alcoholic vapours. In case of humidity sensing, the sensor responses actually to the change between ambient humidity and 100 % RH in saturated vapours. The resistance measurement of each sensor was performed always for three such adsorption – desorption cycles. All measurements were conducted at atmospheric pressure and temperature 25 °C.
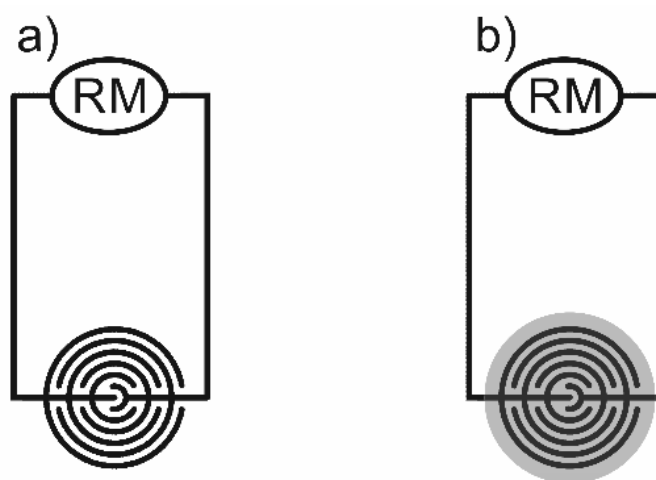
Figure 18 Schematics of the sensor and its connection in the circuit. RM – resistance meter, a) without sensitive CuO layer and b) with sensitive CuO layer – the grey disk. [136]

Recording of I-V characteristics was performed with the aid of home build setup of a multimeter HP 34401A (Hewlett Packard, USA) utilized for current measurement and a power supply HP 6038A (Hewlett Packard, USA) operated in the regime of voltage control. Both apparatuses were controlled by a PC using Labview application.

Above described experimental details were also published in [136]

The 3 x 3 sensor field (matrix) has one common (ground) conductive path in shape of the most outer loop around the matrix field and 9 measuring channels i.e. one channel for each single device. These are arranged into a flat row of connectors that can be plugged into a female plug a FFC/FPC connector (DS1020-04-22BRT1, CONNFLY). Then, the ground is connected to the 0 th and 10th pin of the connector and the measuring channels are connected to the pins inbetween. This connector was attached to a Hewlett Packard 34970A multimeter equipped by a 34901A multiplexer module allowing switching between measured channels. The switching frequency was chosen such that a quasireal time measurmenet of all 9 channels was possible, i.e. the sampling frequency of signal from each sensing element was much higher than its sensing response dynamics. Measured values were recorded by a PC via GPIB (General Purpose Interface Bus).

7. RESULTS AND DISCUSSIONS

In this Thesis, preparation of fully inkjet printed gas humidity and alcohol vapours CuO based sensor on a common flexible PET substrate is demonstrated. An original microvave enhanced synthesis of CuO nanostructured particles was developed. The key issue for success is formulation of the ink, its matching to the substrate surface and optimization of its properties with regard to the printing process mainly. Achievement of the good printability is also a non-trivial task. It shall be emphasized also that prepared device cannot be fired at high temperatures to achieve sintering and remove volatilize-able components of the ink due to the limited temperature stability of the polymeric substrate. Moreover, it is expected that the device should be operated at room temperature. Therefore, the main emphasis is put on the fundamental question of the microphysical mechanism of sensing at low temperature. A methodological peculiarity of sensor's resistance measurement had to be addressed too. As a proof of application potential of prepared ink and to prepare samples for study of the sensing mechanism, gas sensors were printed out, characterized and their performance tested.

7.1 CuO particles characterization

In Figure 19, it can be seen that prepared copper oxide nanoparticles have characteristic morphology of chrysanthemum flowers with large surface area which gives the best chance of the material to be sensitive to any electron donating gaseous substance. The size of CuO nanosheets which form the individual petals of the flower-like morphology is about several hundreds nm in length, width of the nanosheets ranges from several tens up to one hundred nm and their thickness can be roughly estimated less than a few tens nm. Superiority of nanostructured sensors has been already demonstrated for nanowires [137] and nanostructured films [138] both experimentally and theoretically. The flower-like morphology is a third candidate. The attachment of individual CuO nanosheets to a common

centre (like petals in the flower) creates large free space between individual nanosheets and avoids collapse this expanded voluminous configuration due to stacking of nanosheets which would occur if exfoliated nanosheets are used. Single nanoshets in disersions tends to assemble spontaneously which is a kind of an agglomeration instability. Such process is then almost unavoidable during drying of the dispersion. [136]
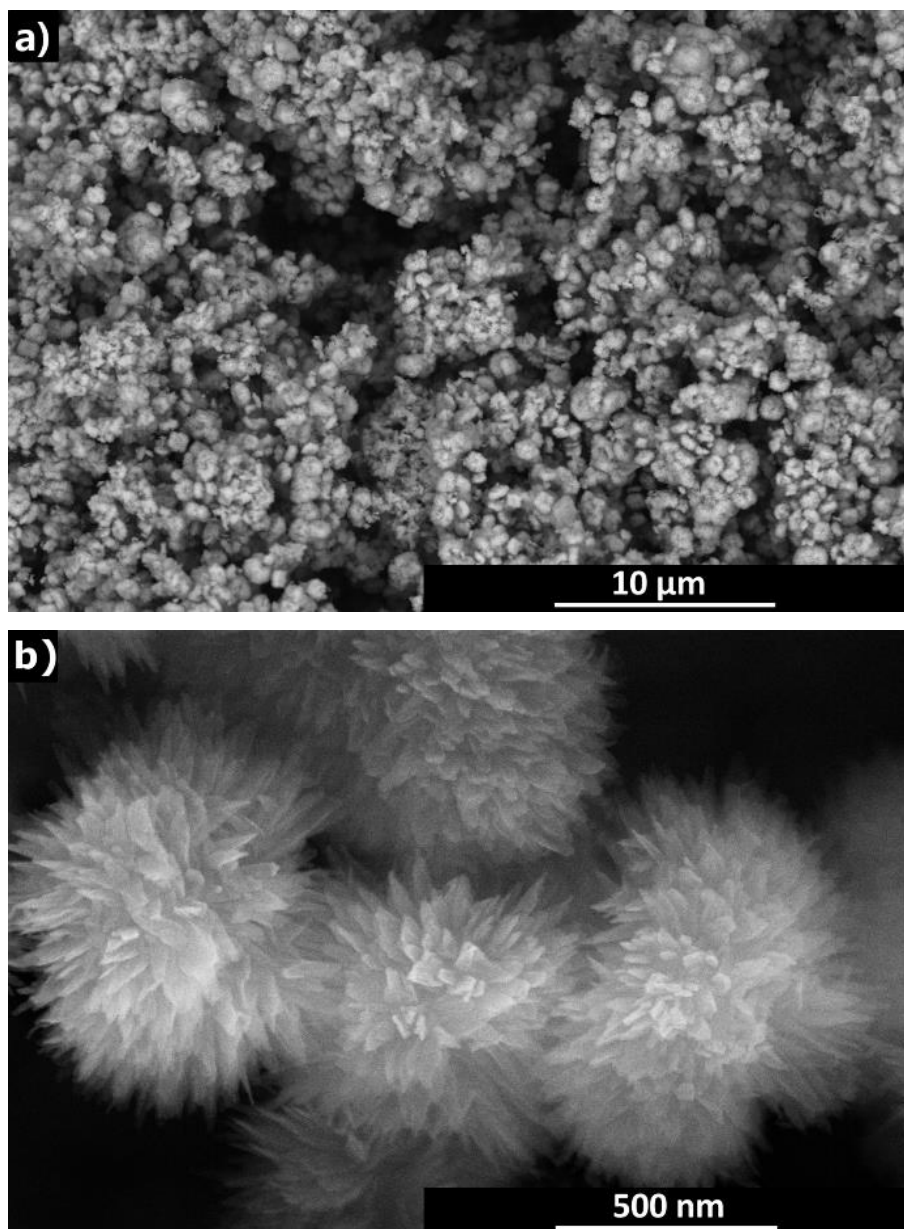

Figure 19 SEM images of CuO nanostructured particles at different magnification. [136]

Results obtained by XRD analysis of prepared powder material are presented in Figure 20. Copper oxide CuO monoclinic phase (C2/c) was confirmed (according to JCPDS No. 01-080-0076) as the prevailing crystalline phase in the material. There are only four peaks of very low intensity in the diffractogram which can be attributed (according to JCPDS No. 01-071-4310) to Cu_2O cubic phase (Pn-3m) manifesting thus presence of trace concentration of this phase in prepared material. All peaks in the diffractogram are clearly indexed. Evident broadness of recorded diffraction lines testifies for nanosize of diffracting crystallites although no further analysis of the data was performed for this sake. [136]
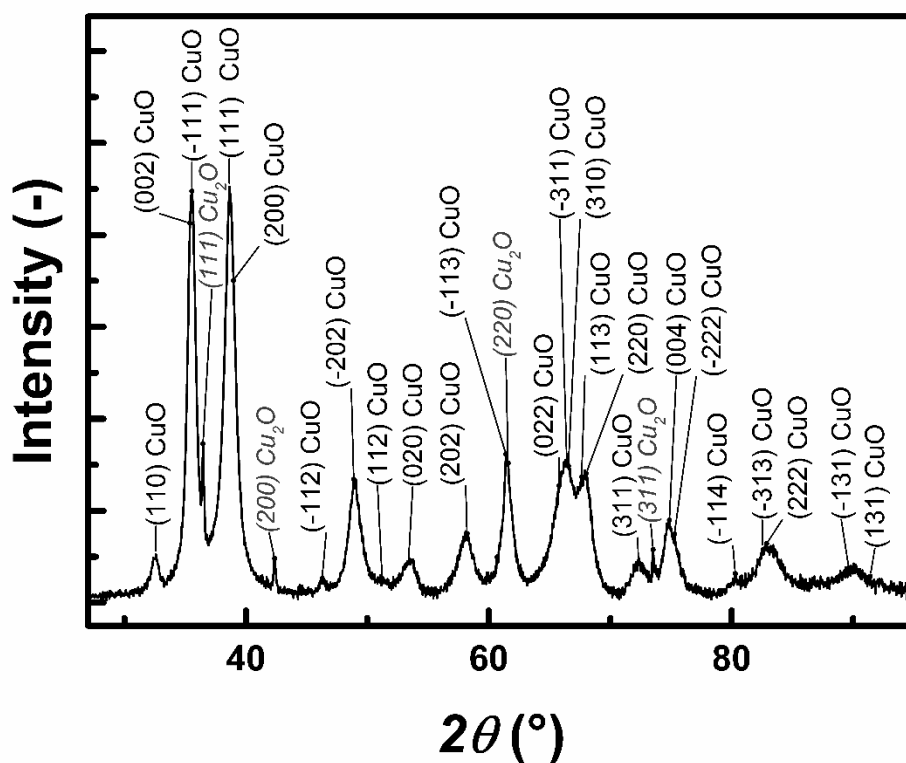
Figure 20 XRD analysis of prepared powder material. [136]

7.2 Ink formulation and characterization

Firstly, it is important to note that prepared inks did not meet the required surface tension in range 28-42 mN/m, viscosity in range 10-12 mPa·s and particle size below than 0.2 μm as suggested by the material printer Dimatix DMP 2800 series producer for optimal use of inks in inkjet printing using original 10 pL printing head. However, according to the producer, viable viscosity range may be extended from 1 mPa·s for water-like fluids up to 30 mPa·s. Similarly, surface tension range may be extended from 20 mN/m up to about 70 mN/m. [33]   [136]

Table 4 shows experimental values of surface tension and viscosity of prepared CuO inks. The dispersions were prepared at various concentrations of the surfactant and dispersant. As can be seen, additives substantially affect the surface tension in the desired way. The addition of surfactant led to the significant decrease in the surface tension of aqueous systems, therefore particularly improves substrate wetting and levelling, while dispersant additives deflocculates particles through the steric stabilization of the particles. These components reduce viscosity, thus the levelling is improved and higher particles loading is possible. Figure 21 illustrates ink sedimentation stability exemplified on aqueous dispersion of CuO with additives and without additives. It is evident that the ink with additives is stable over weeks (and months, photographs not taken) while the dispersion without additives sediment settled within several tens of minutes. The surface tension of the ink plays an important role in the formation of droplets and adhesion to the substrate. The surface tension did not significantly vary between different inks and was around 22 mN/m. This is due to relatively high concentration of additives needed to stabilize the suspensions. However, the surface tension value was found suitable as prepared inks matched to the used substrate and showed good wetting properties as verified by simple laboratory test. Similarly, the density of prepared ink fluids did not vary too. Viscosity was the main parameter varied in dependence on the concentration of solid phase and on the ratio of used surfactant and dispersant additives. [136]

Table 4 Composition, viscosity, surface tension and density of CuO ink and solvent at 25°C. [136]

Ink	Surfactant (wt%)	Dispersant (wt%)	CuO (wt%)	Viscosity (mPa·s)	Surface tension (mN/m)	Density (g·cm^{-3})
Ink 1	21.60	7.20	3.40	(4.66 ± 0.04)	(22.13 ± 0.09)	(1.04±0.04)
Ink 2	14.20	14.20	4.80	(7.13 ± 0.02)	(21.98 ± 0.04)	(1.05±0.06)
Ink 3	13.90	13.90	6.60	(6.53 ± 0.01)	(21.73 ± 0.08)	(1.04±0.03)
Ink 4	7.20	21.60	3.40	(6.59 ± 0.02)	(21.42 ± 0.08)	(1.04±0.07)
Ink 5	12.88	19.32	7.20	(10.54 ± 0.01)	(21.52 ± 0.05)	(1.09±0.04)
Water	0	0	0	(1.00 ± 0.02)	(72.22 ± 0.08)	(0.99±0.01)
CuO + water	0	0	3.00	(1.18 ± 0.02)	(71.56 ± 0.01)	(1.00 ± 0.02)
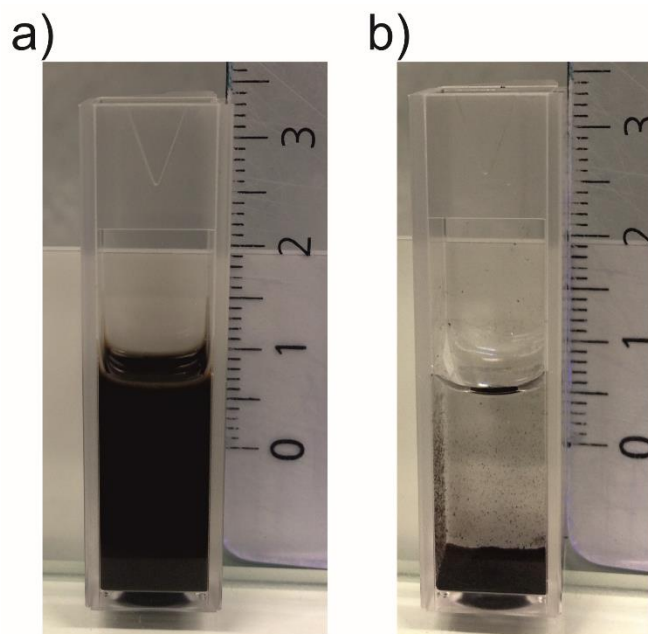
Figure 21 Ink stability of a) aqueous dispersion of CuO with additives after three weeks, and b) aqueous dispersion of CuO without additives after 1 hour. [136]

7.3 Printing process

7.3.1 Preliminary dimensionless criteria analysis

As mentioned in chapter 3.2.3, dimensionless correlations are usefull in development of ink formulation with respect to the process conditions and tool used for printing. The graph in Figure 22 constructed according to McKinley and Renardy [67] is used to discuss specific issues of inks [68] prepared in this work. The quadrangle ABCD defines the region where the particular fluids are printable and single drop formation may be achieved or merging with the satellite can be expected. To remind (see the previous chapter), surface tension in range 28-42 mN/m and viscosity in range 10-12 mPa·s is suggested by the printer producer. I na accordace with Table 4, the density value 1 g·cm^{-3} was chosen for the model. The characteristic length 21.5 μm is used since it is the size of the side of the square shaped orificium of the printing head nozzle and is constant.
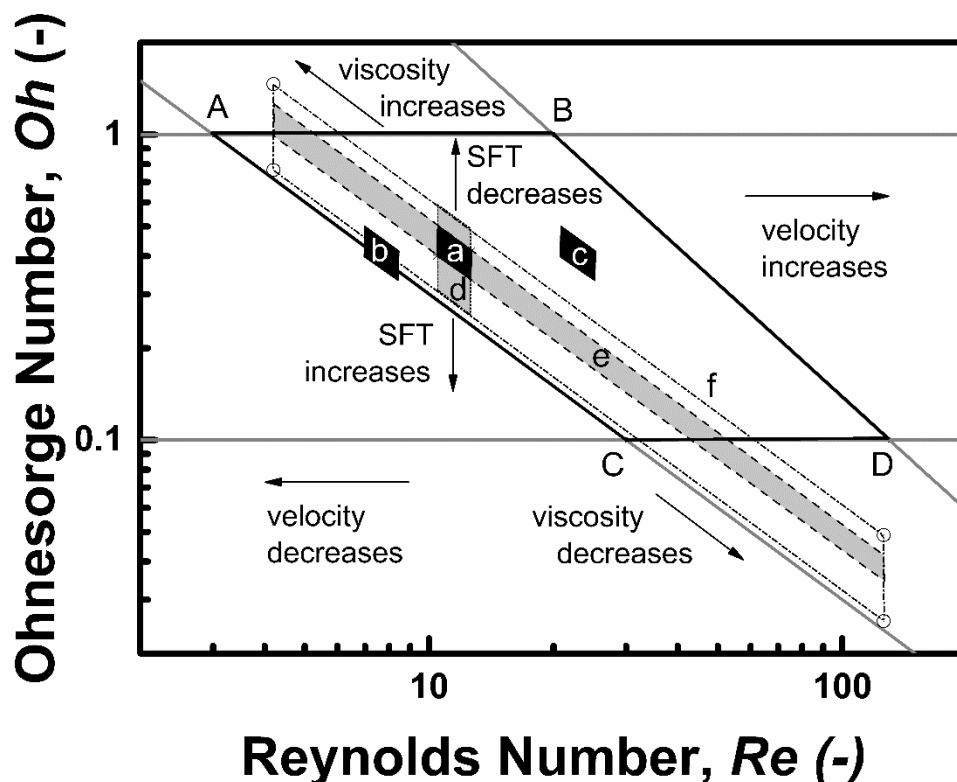
Figure 22 Schematic diagrams showing the operating regime for ink-jet printing according to McKinley and Renardy.

The small black full parallelogram (**a**) near the center of the ABCD area represents optimum printability space as defined by the producer for the Dimatix printer at the jetting velocity 6 m/s. The droplet velocity can be varied by the waveform process control (see the next chapter). The small full black parallelograms (**b**) and (**c**) show the pritability space of Dimatix printer at jetting velocities 4 and 12 m/s, respectively. Slowing the droplet ejection velocity may be necessary to avoid satellite creation although it can be seen in the graph, that the low velocity can result into failure of drop formation due to the lack of mechanical energy. Decrease of the velocity decreases the value of *Re* since the Reynolds number scales with the velocity while the Ohnesorge number does not depend on the velocity at all. On the other hand, increase of the velocity shifts any printing operation point to the right side of the area. If the velocity doubled again up to 24 m/s, the system reaches onset of splashing. Changes of material related variables involved in dimensionless criteria result into typical shifts or extensions of this parameter space also. The directions of these changes are marked by arrows in the graph. As the Reynolds number is independent on the surface tension (surface energy), the increase of surface tension shifts the parameter space border downwards while decrease of surface tension results into the shift upwards. Liquids with the surface tension from 20 up to approximately 70 mN·m^{-1} may be jetted with limited performance. The value about 73 mN·m^{-1} can be accepted as the limit for water. Hence, the the small parallelogram (**a**) is extended into the grey parallelogram (**d**). Increase of the fluid viscosity range from 1 up to 30 mPa·s results into the shift along the top-left to bottom-right diagonal since $Re \sim \eta^{-1}$ and $Oh \sim \eta$ and a slender parallelogram is obtained for this situation denoted as (**e**) with grey filling in the graph. Full extension of the printability span according to both extreme viscosities (1-30 mPa·s) and surface tensions (20-73 mN·m^{-1}) is indicated by the largest quadrangle with circles in its corners and short dash dot sides.

7.3.2 Optimization of printing process

The drops of ink are ejected by voltage-driven deformations of a piezoelectric element integrated into the wall of the channel behind each nozzle. The segments of this action make up a waveform that needs to be optimized for each ink as well as the intended print job.

The waveform, in combination with settings for print height (stand-off), nozzle firing voltage, and cartridge temperature make up a cartridge jetting settings. The print optimization of material printer Dimatix DMP 2800 series is a very important step for acquiring of precise printed motives. A general scheme how the drop generation of used printer is controlled by the waveform is shown in Figure 23. The most important is to create perfect waveform, according to this waveform the printhead or more precisely piezoelectric elements operate. The pulse generated by the piezoelectric element in the second step gives the momentum to the ejected liquid and so the drop velocity is defined, while filling in the first step defines the drop volume. Nominally, it is a 10 pL printing head which was used in presented work. However, actual volume of the drop may be different and was estimated as about 15 pL.
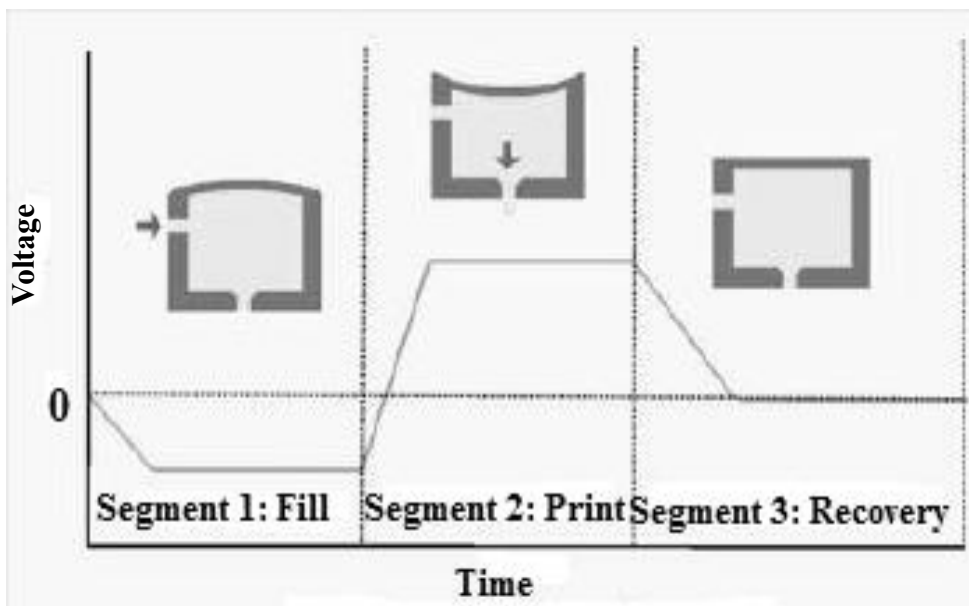
Figure 23 Control of actuation of the piezo-driven nozzle by waveform setting. Adapted from [33].
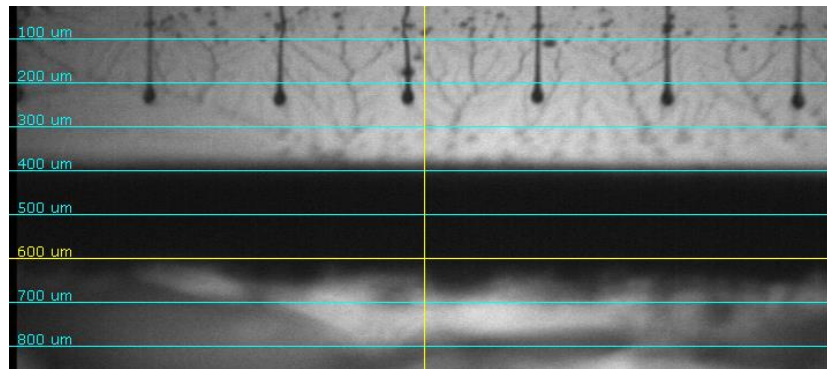
Figure 24 Camera view of CuO ink (Ink 4) drops jetting from a printhead.

According to preliminary considerations velocity about 6 m·s⁻¹ was considered as the first guess. However, these conditions did not yield good printability for any of the prepared inks. Therefore, the conditions were changed according to analysis described in following chapter and finally the velocity of drops was set to 4 m·s⁻¹ to achieve precise drop jetting. As can be seen in the image in Figure 24 captured for CuO Ink 4, jetting of single droplets was uniform with tails but without satellites. The tail was present only at the start of jetting after pinch off. The tail blended into the drop without breakup on a short distance hence the precision of printing was assured and Ink 4 was found as best performing.

Figure 25 An example of a waveform which was used for printing of CuO layers.

Individual nozzles on the printing head may vary to some extent in their properties but uniform drop generation is required to achieve good quality printing using naturally as many nozzles as available on the printing head. On the other

hand, in case of nozzle clogging or any other need, only selected nozzles can be operated while the other are not used. Therefore, independent waveform is set for every nozzle of the printing head in the control software. An example of a waveform is given in Figure 25.

7.3.3 Refinement of the dimensionless criteria analysis

Table 5 summarises values of dimensionless criteria calculated for prepared ink dispersions under conditions of the real printing process, i.e. the velocity 4 m/s and characteristic length 21.5 µm of the printing nozzle.

Table 5. Values of selected dimensionalless criteria for CuO inks, dispersion of CuO in water and water alone at 25°C based on data from previous table using the velocity 4 m/s and characteristic length 21.5 µm. [136]

Ink	Dimensionless criterion				
	Re	*We*	*Oh*	*Z*	*Ca*
Ink 1	18.7	15.8	0.212	4.72	0.84
Ink 2	12.4	16.1	0.324	3.09	1.30
Ink 3	13.4	16.1	0.300	3.34	1.20
Ink 4	13.3	16.3	0.305	3.28	1.23
Ink 5	8.7	17.0	0.475	2.11	1.96
Water	83.2	4.6	0.026	38.75	0.06
CuO + water	71.2	4.7	0.030	32.85	0.07

Figure 26 shows positions of prepared inks in the *Oh* versus *Re* space. Tested inks are represented by five empty circle data points labelled in accordance with Table 5. Points for water and for CuO dispersion in water are displayed too. It must be noted, that the points are aligned along a virtual line (marked by a dot line in the graph), which has the slope -1 representing constant value of $We^{1/2} = 4$

which corresponds to the average value *We* = 16 from Table 5. Actually, the graph can be parametrised by set of $We^{1/2}$ isolines based on the formula

$$Oh = \frac{\sqrt{We}}{Re} \qquad (7.1)$$

These hyperbolic isolines transforms into straight lines with negative slope s using logarithmic axes for plotting *Oh* versus *Re*. Similarity of these lines with diagonal borders of the ABCD area invokes the idea of importance of the *We* number as discussed in [68]. It can be hypothesised that it is due to the primary importance of surface tension among all discussed inkjet characteristics. The formation of ink droplets is the crucial step of printing process and there is only one variable that may work as the source of forces giving the droplet its spherical shape, and it is the surface tension. Indeed, no significant influence of the viscosity was observed, and good printability was achieved by manipulation of the jetting velocity. [136]
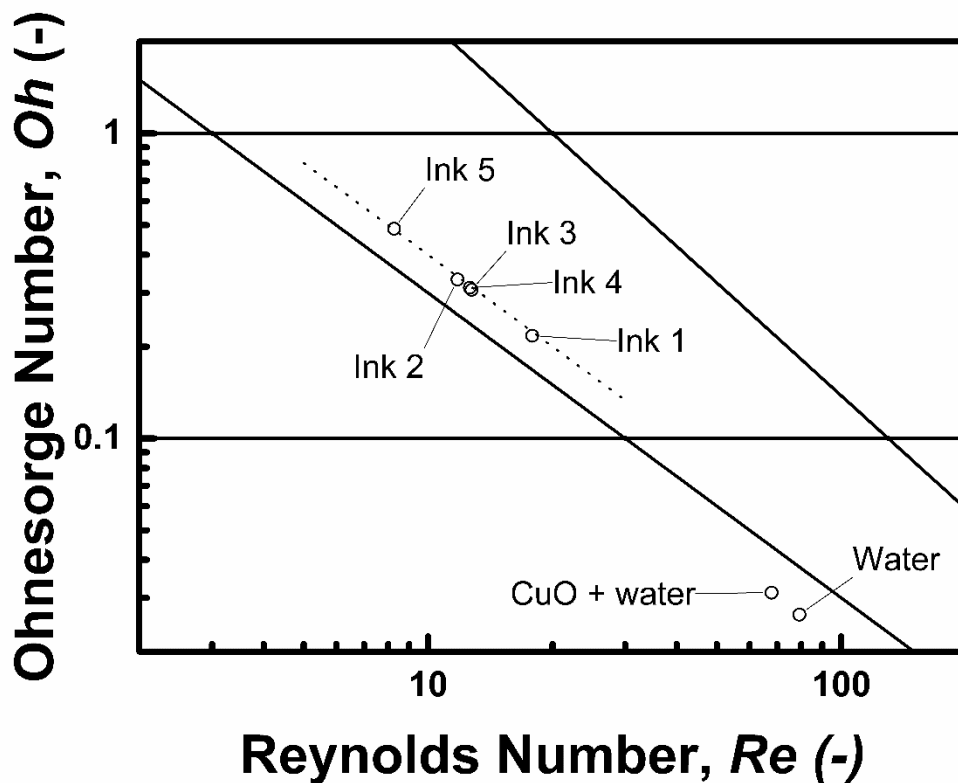
Figure 26 Positions of prepared inks in the *Oh* versus *Re* space.

A central group of inks (Ink 2, 3 and 4) can be found in the centre of the graph. Nevertheless, the Ink 4 performed better than the Ink 3 under otherwise nearly the same conditions which points towards the importance of internal material (structural) parameters of the ink. Most likely, the fluid is viscoelastic to certain extent, and the elasticity contributes to the drop formation also, however deeper analysis in that way is beyond the scope of this work and remains as a challenging issue for eventual successors in the research group. [136]
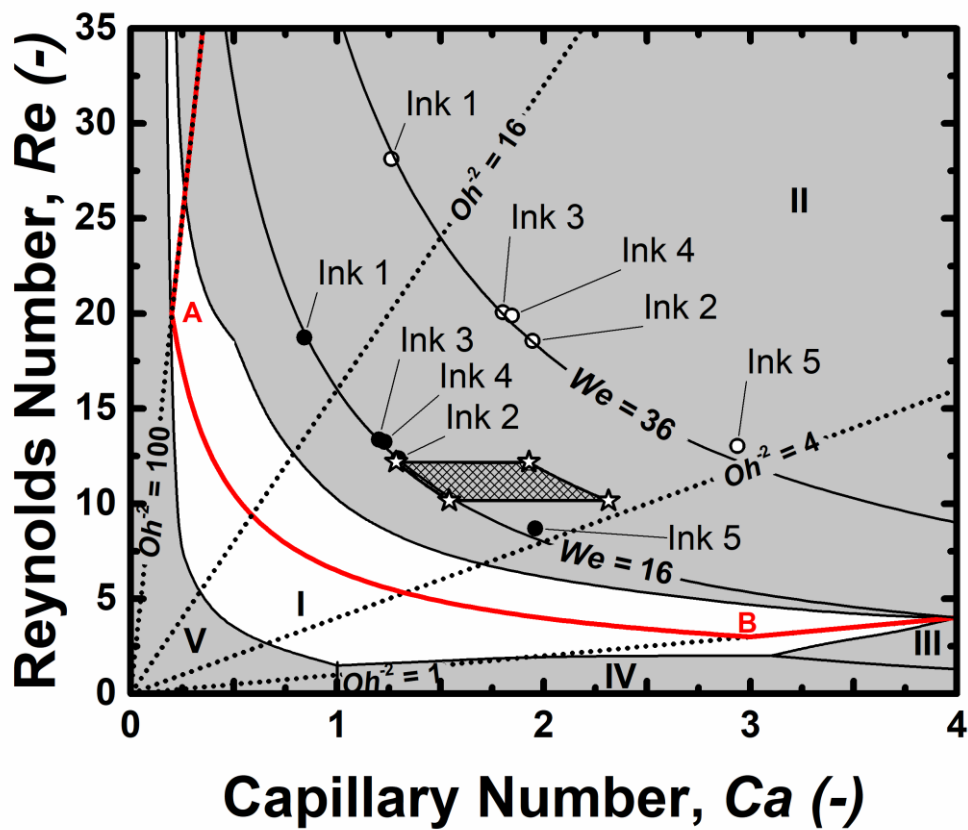
Figure 27 Processing window for the used printer as suggested by its producer using jetting velocity 6 m/s. [46]

Since original Kim&Baek's [56] graph for printability assessment is not fully suitable (see chapter 3.2.3) for systems operating in conditions of larger *We* number, its replotted version may work better [22]. Indeed, the graph in Figure 27 shows processing window (grey patterned field with empty asterisks in its corners) for the used printer as suggested by its producer using jetting velocity 6

m/s. The meaning of printability areas marked by roman numerals from I to V is the same as in the original Kim&Baek's publication [56]. The processing window of the printer falls into the area II in which one or more satellite drops are generated, but they do not recombine with the main drop in case of purely Newtonian fluids. However, the good printability region I can be expanded towards the top right direction for weakly viscoelastic fluids due to the contribution of elasticity which works in the same direction as surface tension and contributes to recombination of the satellites with the main drop. Operating points for all inks (from Ink 1 to Ink 5) at this velocity are shown as empty circles aligned along the Weber number isoline at the value 36. It was not possible to achieve good printability under these conditions. Therefore, the velocity was decreased to 4 m/s which allowed reasonable printing at $We = 16$. Operating point of inks are plotted as full black circles. The Ink 4 was then found as the best performing among others.

7.3.4 Final tuning of the process parameters

The cartridge temperature 30 °C, a substrate temperature 55-60 °C, and voltage 24 V approximately and individually fine-tuned for each nozzle led to optimal jetting conditions. The resolution was adjusted to 1280 dpi which corresponds to drop spacing in size of the half dot diameter. The Ink 4 showed good wetting and adhesion to the substrate. Single drop impact without splashing resulting into a circular dot was experienced.

The printing of interdigitated electrodes by nanosilver ink was controlled by suitable waveform and slightly modified conditions setup too, however it was a commercial ink and as such the optimization of its printing process lacks of scientific interest.

7.4 Analysis of printed patterns – single sensor

The structure of printed Ag layers was analysed microscopically. Figure 28 shows a part of interdigit's surface captured by the optical microscope. The results of SEM observation are shown in Figure 29 in different magnifications.
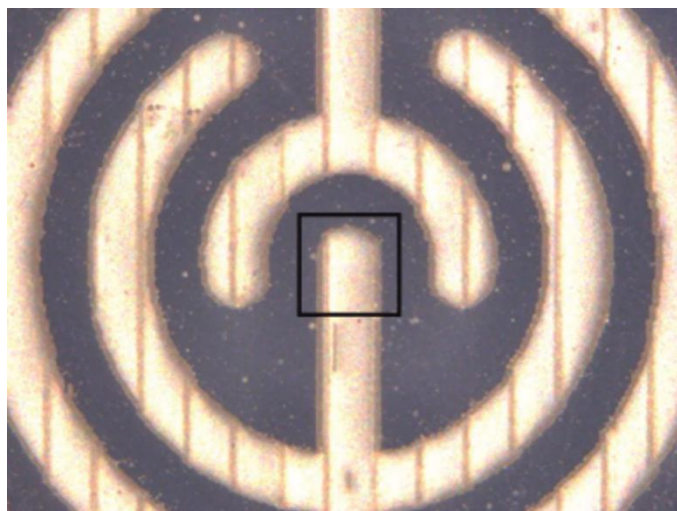

Figure 28 A part of Ag interdigit surface. The black line rectangle in the middle marks area of the interdigit surface used for further SEM analysis. Image captured by the optical microscope. [136]

Dimensions of silver particles are below 100 nm. The printed layer was dried at 80 °C in vacuum in order to achieve better homogeneity of layers and impart good conductivity to electrodes. It can be seen that there are some macropores in size about 1 μm but they are sparsely distributed that it cannot limit conductivity of the printed lines of much bigger dimensions. As seen in the image with the highest magnification, silver particles are densely packed and congruent enough to assure contiguity of the printed material pattern. [136]

Sensitive CuO layer was printed on the top of Ag pattern as Figure 30 shows. As can be seen in Figure 31, the CuO layer is relatively compact and the particles kept their original morphology without being either damaged, lost petals or modified in any other way by the processes of ink making and printing. The hoarfrost look of particles in SEM image can be ascribed to residual surfactant and dispersant. [136]
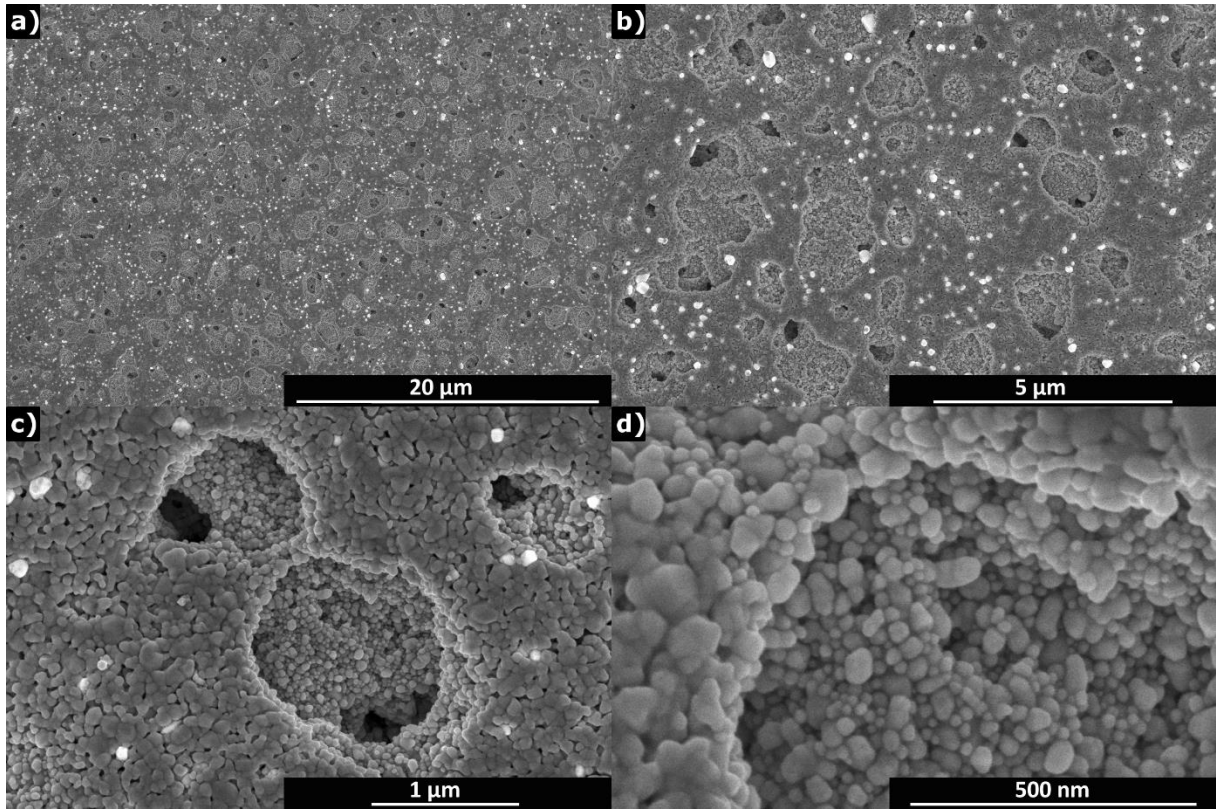
Figure 29 SEM images of printed Ag layers at different magnification. [136]
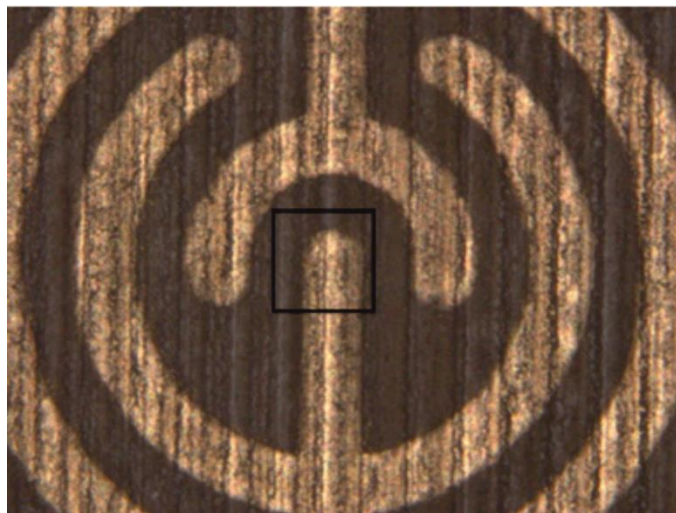
Figure 30 A part of Ag interdigit with CuO layer surface. The black line rectangle in the middle of the interdigit with CuO layer surface shows area for SEM analysis. The image was captured by optical microscopy. [136]
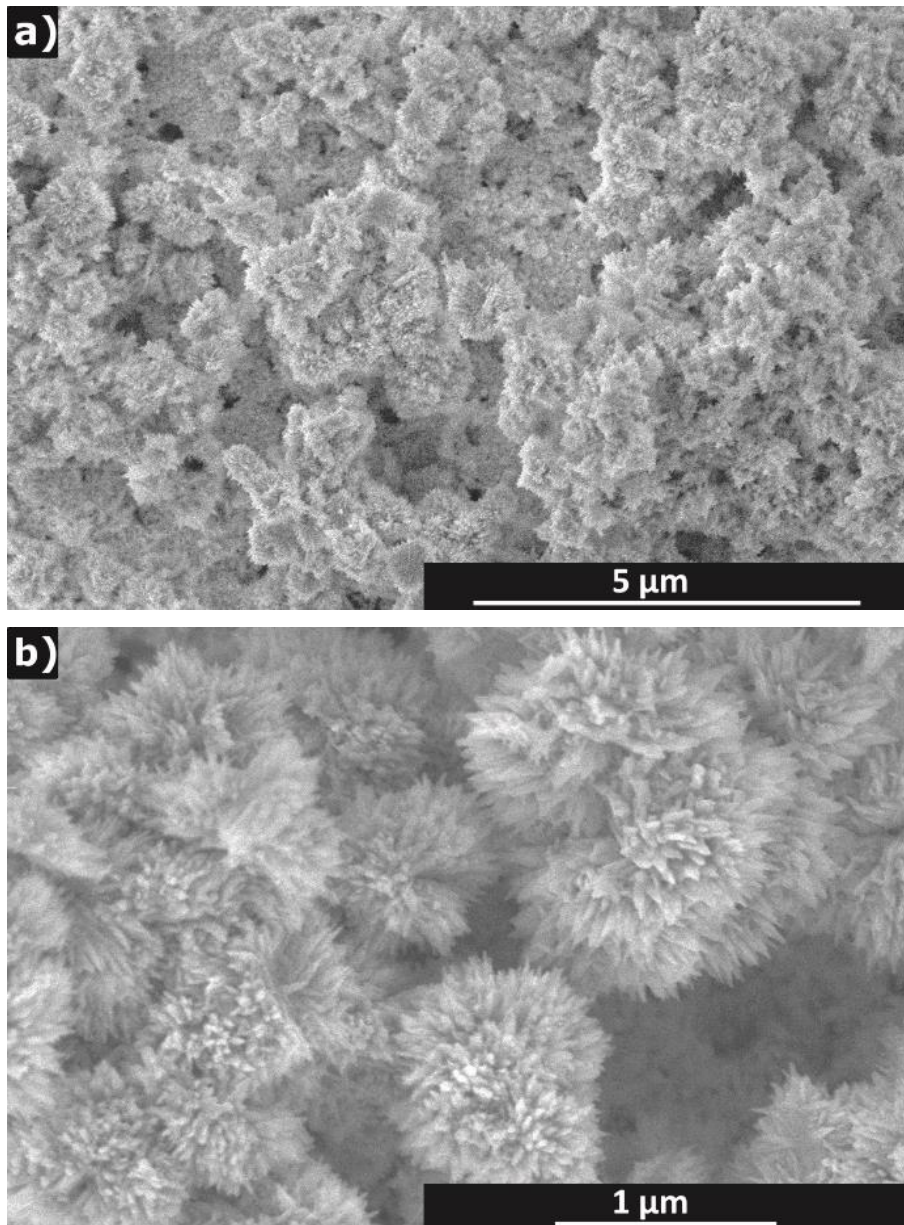
Figure 31 SEM pictures of printed CuO sensitive layer on Ag layers in different resolution.
[136]

The sensing layer was printed five times because the trapping of layers improved the coverage, thickness and homogeneity of CuO layer and reduces relatively the roughness of the layers with respect to the total thickness of the layer. The AFM measurement confirmed the enormous roughness on nanoscale expected according to the observation of synthesized nanostructured CuO microparticles. Typical images of surface topography on nanoscale for single layer and five layers on each other are shown in Figure 32. It is obvious that there is no difference between samples in terms of maximum and minimum height span,

as it was always the last printed layer which was examined and that surface of only several adjacent particles was scanned. On the other hand, average numbers show a difference. The roughness of single CuO layer is 2770 ± 140 nm and of four CuO layers is the roughness 170 ± 70 nm. [136]
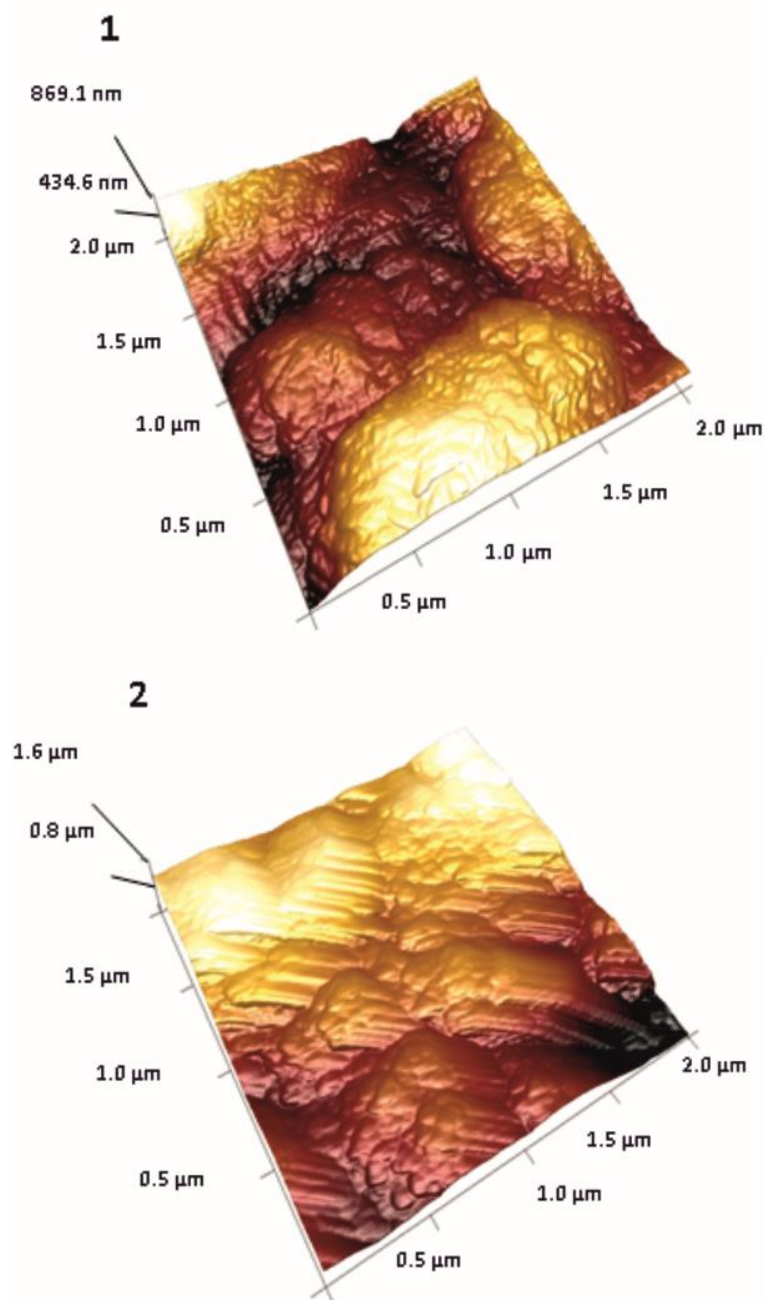
Figure 32 Representative 3D views of peak force mode AFM images of a single CuO layer (1) and four layers on each other (2). Scan area size was 2x2 μm. [136]
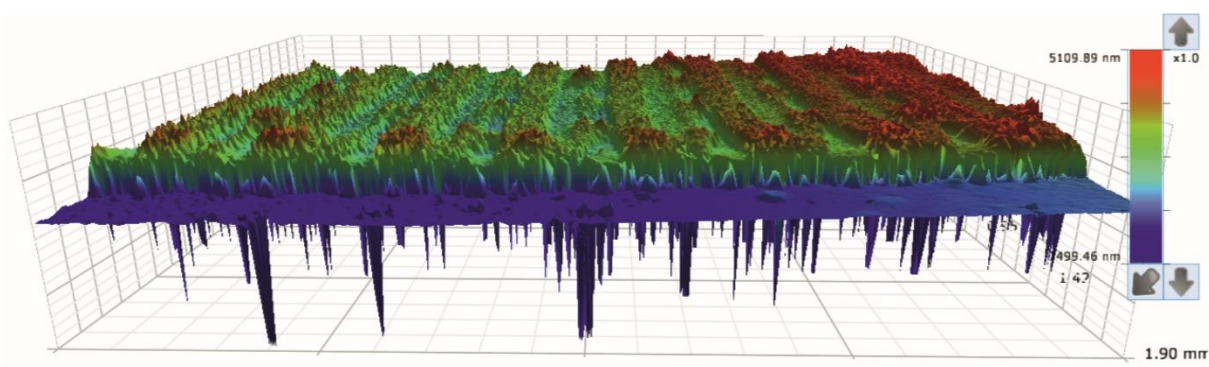
Figure 33 3D topography of printed Ag layers. [136]

Figure 33 shows 3D topography of printed Ag layers. A relatively high roughness of the surface is evident however it must be taken into account that negative peaks in the graph are artefacts only caused by porosity of the printed layers. However, the two layers of silver are enough to assure sufficient electrical properties of the printed electrode motif. The overall impression from the landscape depicted in the graph invokes the view on a potato field. Such morphology is a result of chosen drop spacing and dot size, which results into overlay and coalescence of printed droplets. Since the printing head has 16 nozzles and the resolution was set 1280 dpi, it means that one printed row is 0.3175 mm wide theoretically. The trapping of layers was intentionally shifted by approximately one half of the row width to assure efficient overlay of the material in both directions throughout the printed motive. Indeed, the analysis of printed motive profiles shown in Figure 34 confirmed the periodicity of lines to be 0.32 mm and the shift between lower and upper layer is found to be 40 % of the line width. The upper graph in the figure confirms good continuity of the double layer. The middle graph shows a representative X profile recorded on the sample surface. Positions of height maxima are marked by diamonds symbols. The full symbols belong to one layer and open to the second one with the same periodicity of 0.32 mm and shift 0.13 mm. The lower graph shows an example of Y profile recorded on the ridge of a "hilled row". The total thickness of printed motive varies between 1 and 3 μm. [136]
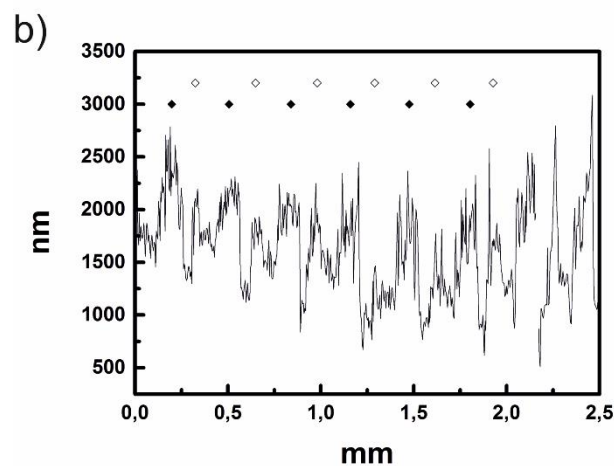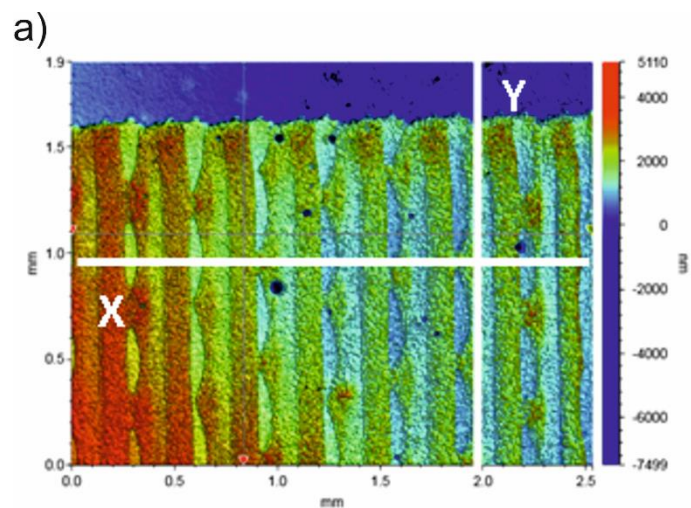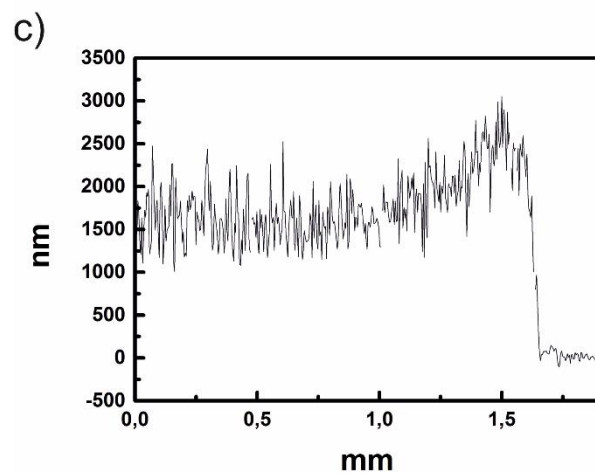
Figure 34 Profile analysis [136]:
a) Top view of printed Ag layers, the same area is shown as in Figure 33;
b) X profile – for symbol explanation see text;
c) Y profile

The printing of the device was finished by five overlays of CuO layers in order to obtain homogeneous sensing layer because the ink had much small content of solid phase than the silver dispersion. Numerous overprinting of the substrate smeared the "potato field" like texture of the substrate and relatively smooth surface envelope reproduced the basic shape of interdigitated electrodes. However, the surface is very rough on small scale due to the enormous CuO layer porosity and morphology of the CuO particles. In fact, this is a suitable morphology for a VOC sensing device. Figure 35 gives an overview of the 3D topography of the final surface of printed sensing device. [136]
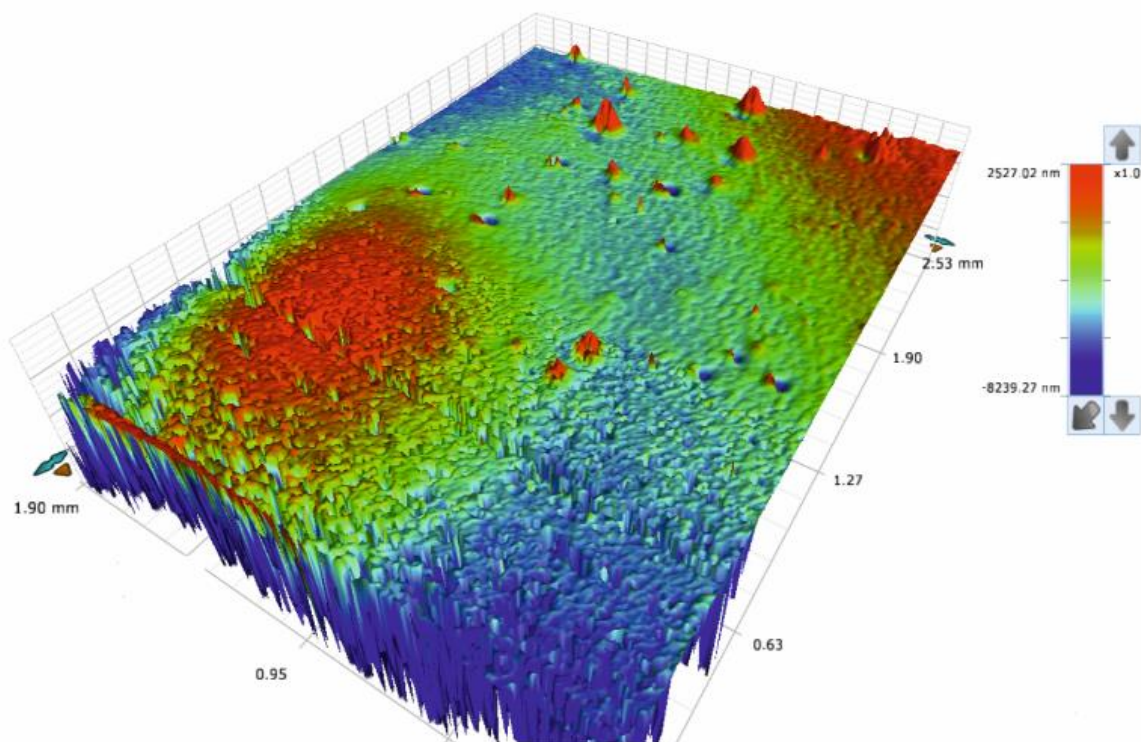

Figure 35 3D topography of printed CuO layers. [136]

7.5 Resistivity of printed layers

Table 6 shows the conductivities of single layer material samples deposited on the original substrate and printed with the aim to characterise the basic material components of the multilayer device. The size of printed square was 2 cm x 2 cm. The resolution and other parameters of the printing process were kept the same as in the real device fabrication. The conductivity of printed thin silver layer is not far from tabulated value 6.3 x 10^7 S/m (1.59 x 10^{-6} Ω·cm) for bulk silver metal [139]. However, the resistivity of printed CuO layer exceeded measurement range of the four-point probe apparatus, designed for measurements of conductive materials.[136]

Table 6 Resistivity of CuO layer and Ag interdigitate was measured with four-point probe technique [136]

Material	Resistivity (Ω·cm)
CuO layer (made from Ink 4)	>10^4
Ag interdigit	(2.4 ± 0.6) x 10^{-7}

7.6 Electrical and sensing properties – single sensor

The response and recovery properties of the sensor were investigated first by using ethanol and water as representative examples targeted gas analytes at temperatures 25°C. Firstly, response of bare interdigitate silver electrode structures was tested. No exposure to any of tested conditions delivered measurable resistance response. In all cases, overload was signalised by the measuring apparatus indicating thus that the resistance of the incomplete device was higher than 40 MΩ which is the maximum range of the used multimeter. Any contribution of the surface of the flexible PET substrate is excluded. [136]
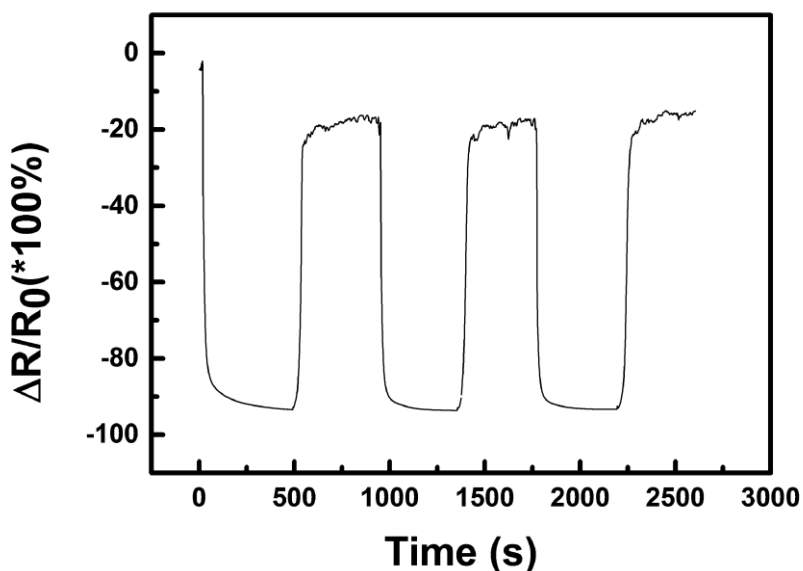
Figure 36 Relative resistance change ($\Delta R/R0$) of the nano-copper oxide sensor within water sensing at 25°C (R – actual resistance value, R0–initial resistance) [136]

Figure 36 shows typical resistance change of the device prepared with the best ink (Ink 4) composition within saturated water vapours sensing test at 25°C. The initial value (at time zero) was measured for the sensor freshly taken out from the storage conditions (stored in a dessicator with RH in the range 20-30 %) and it is the first measurable value below the upper measurement range of the multimeter which is 40 MΩ. Both on- and off-values of resistance show relatively fast saturation and virtually approach constant value after several minutes and the sensor has good reversibility of the signal over several tested complete cycles of sensor testing procedure. However, the recovery of the sensor resistivity was incomplete due to the relative humidity of the air in the laboratory. The sensor was actually cycled between ambient humidity in the laboratory (off state) where RH is normally kept in the range 40-50 % and in saturated vapours (on state) with RH = 100 %. Since the experiment was taking less than one hour, the air humidity in the laboratory was stable enough to cause no baseline drift. It can be said that both the saturation of the sensor in vapours and recovery outside the vapour environment have approximately the same rate. This indicates that the sensing process is reversible with steady base resistance value although more thoroughly

78

performed studies using vapour-gas mixing unit and controlled testing chamber will be necessary for further studies. [136]

The sensing principle of CuO based devices has been numerously reported in [131, 132, 140] and many other references. The sensing mechanism of gas sensors based on p-type semiconductors such as CuO is different from the one of much more frequently utilised and known n-type metal oxides. In the air, oxygen molecules are adsorbed onto the CuO surface forming oxygen ions by trapping electrons which causes bending of energy band upwards at the surface. Wang et al. [141] This results in an accumulation of holes at the CuO particle surface while the trapped electrons leave holes following the mechanism [138, 141, 142]:

$$O_2 \leftrightarrow O_2^- + 1hole \tag{7.2}$$
$$\tfrac{1}{2} O_2 \leftrightarrow O^{2-} + VacancyCu^{2+} + 2hole \tag{7.3}$$

Adsorbed molecular oxygen (O_2) can be ionised preferentially to molecular O_2^- at temperatures below 200 °C and to atomic O^- and O^{2-} predominantly at temperatures higher than 200 °C. [136]

When the surface is exposed to water vapour, the double ionized oxygen (Equation 7.4) reacts with H^+ coming from the dissociation of water vapour to form OH^- as the below equation [143]:

$$H^+ + O^{2-} \leftrightarrow OH^- \tag{7.4}$$

This reaction leads to release of the trapped electrons and neutralize the holes in p-type CuO. Moreover, it can be generalized to any reducing species (such as NH_3 or alcohols etc.) that can be oxidized and release a negative charge (electron). This consequently decreases the concentration of holes and thus increases the resistance in the surface layer of CuO. Meanwhile, the number of oxygen ions O^-, O^{2-} and O_2^{2-} absorbed on the surface of CuO is also reduced, which leads to the

decrease in the magnitude of the negative quasi-gate resulting in further decrease in conductivity. [84, 140] As a result, we will observe a monotonic increase in resistance with the increase of relative humidity if CuO sensor is operated as usually at high temperatures. [136]

Nevertheless, it can be clearly seen in Figure 36 that the resistance of the sensor decreases with increasing humidity which is in opposite to previously described behaviour. It is generally known, that the sensing response is largely influenced by device operating temperature due to the temperature dependence of adsorption-desorption kinetics as well as reaction rates and equilibriums occurring on the sensing material surface. [144, 145] Ceramic and semiconductor sensors are operated usually at higher temperatures of several hundreds of centigrees which assures the surface cleanliness while precise keeping constant temperature provides the sensor response stability. Fully printed sensor on common plastic (PET polymer) substrate cannot be either prepared or operated at such high temperatures and the above described microphysical mechanism can be hardly the main one in action. At the laboratory temperature, molecular forms of adsorbed oxygen prevail over atomic ions as well the equilibrium in Equation 7.4 should be shifted to the left side of the reaction which means that reactants in are strongly favoured over the product. Moreover, the sensing layer consists not only of pure CuO nanoparticles interacting with gaseous species, but contains surfactant and dispersing agent in non-negligible amounts. The primary physical p-type semiconductor surface reaction principle is most likely overbalanced by other mechanism(s) in such complex system. [136]

To analyse the other possible mechanisms, morphology the active layer shall be considered first. As shown by SEM, AFM and profilometric study, the layer has sponge-like structure with pore dimensions varying from nano- to micrometers. The porous structure is developed on two morphological levels. To begin with single particle, it must be reminded that each chrysanthemum-like nanostructured particle has its internal porous structure as shown in Figure 19.

The anchoring of CuO nanosheets to a common centre in the flower creates large free space between individual petals. Moreover, this expanded configuration of petals is stable and avoids collapse of the voluminous structure due to stacking of nanosheets which would occur if exfoliated nanosheets are used that can spontaneously assemble during drying of the ink dispersion. Preservation of the flower-like assemblies in finished layers is documented in Figure 31. Higher hierarchical level of porous morphology is created by deposition of the ink and assembling of nanostructured CuO "flowers" into a thin film by its drying. The contiguity of single printed layer is too low causing its resistance practically immeasurable (see section 3.3 ad the first paragraph of this section), therefore, four additional layers needed to be trapped on the primary one to obtain applicable film which was manifested by significant decrease of its roughness. Resistance of such printed motif was then suitable over tested range of parameters. [136]

Humidity can not only be adsorbed on the solid surface, but may capillary condense in the microporous structure and dissolve the residual additives. A report on porous systems with high porosity hence possibly poor contact between particles and operated at room temperature [146] described similar behaviour to our system. An otherwise very authoritative review [84] left the occurrence of such contradictory behaviour uncommented. The conductivity is increased by moisture condensation and possibly by increase of ionic conductivity. According to [81], the conductivity is increased by moisture condensation inside the pores due to both electron transfer and proton transfer mechanisms and possibly by increase of ionic conductivity if some soluble ionic species are available in the material. Since the portion of solid residuals from the additives in the ink formulation should be relatively high, their effect on sensor sensitivity and sensing behavior cannot be neglected. The surfactant (BYK® 348) is a non-ionic compound polyether-modified siloxane which is not expected to contribute directly to the conduction mechanism. Formation of hydrogen bonds with the oxygen atoms in this polymer would most likely impede the proton transfer

mechanism. On the other hand, the polymeric part of the dispersant (DISPERBYK® 190) is a high molecular weight block co-polymer with carboxyl groups that have high affinity to the surface of the nanostructured CuO particles. The adsorbed ionic groups on the semiconductor surface can affect the surface electron transport (tunnelling effect), moreover the proton transfer mechanism may be influenced by hydrolytic equilibrium as well as by the involvement of carboxylic groups in hydrogen bond formation too. It can be expected, that some carboxylic groups in the DISPERBYK co-polymer are neutralised and that the polyelectrolyte based humidity response contributes to the sensing mechanism also. According to our opinion, it is reasonable to expect that it is not only moisture which can influence the sensing layer properties by capillary condensation. Any solvent that is miscible with original ink composition, like alcohols, which we tested too, can contribute to conductivity increase if condensed inside the porous structure due to interactions with chemisorbed and physisorbed layers of water. [136]

It must be noted, that the method of the sensing device resistance measurement may have impact on measured result itself. Usually, an affordable and simple digital multimeter can be used for efficient measurements of higher values of resistance similarly to the case presented in this Thesis. Such practical apparatus employs two wire method which is suitable for measuring values above 100 Ω up to several tens of MΩ, when high accuracy is not required. The principle is as follows. A test current is forced through the measured device and the multimeter measures voltage at its terminals. The test current is commonly measured as a voltage drop on an internal standard resistor of known resistance inside the multimeter. Change of the internal resistor can be used for choice of resistance measuring ranges on the multimeter. Important fact is, that the applied voltage changes with the resistance of the measured sample (device) which may result into nonlinearity of its response if the sensing device is not of purely ohmic character. [136]
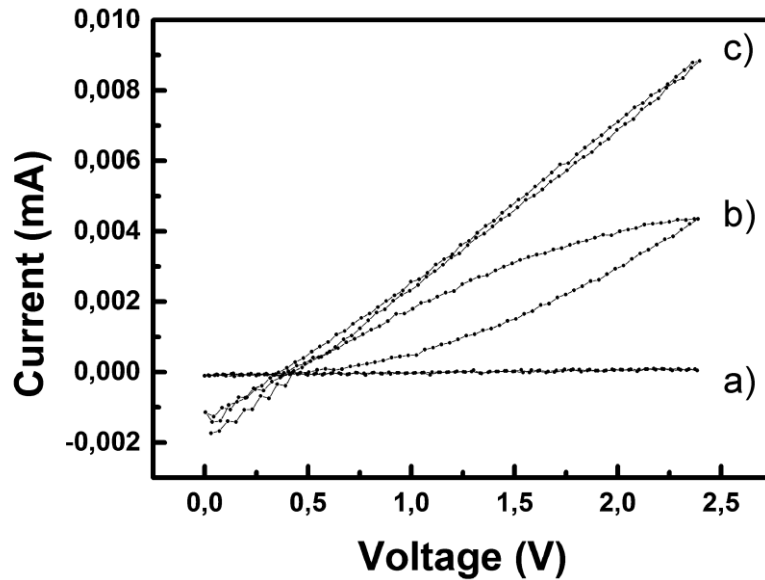
Figure 37 I-V characteristics of CuO sensors measured at 25°C in water vapours, a) outside from vapours b) hysteresis and c) stabilized. [136]

In order to investigate this issue, the current-voltage (I-V) characteristics were recorded. Figure 37 shows I–V characteristics of a sample measured at 25°C under three different stages of the testing cycle. Recording of each curve (i.e. from 0 V up to 2.5 V and back down to 0 V) took 60 s. Curve a) was recorded for the sensor stabilized in the air atmosphere. As can be expected, the resistance of the device is high (calculated from the slope cca 13 MΩ) and there is no hysteresis observed. The second curve b) was recorded for the device after being inserted into the saturated vapour i.e. before the signal saturation. Changing of the resistance value is manifested in a well-developed hysteresis showing continuous decrease of the resistance of the device. The last curve c) was recorded for the device being equilibrated for five minutes in the saturated vapours. Resistance of the device is obviously stabilized at a constant value and is about 0.2 MΩ (calculated from the slope). The cross-section of the I-V curve with the x axis was always at about 0.35 V. It must be reminded that the used electrical source was asymmetric (actually not grounded hence floating) and the I-V characteristics were the same regardless to the polarity of the device connection. Indeed, the device is of symmetric design, however, the (0.35 ± 0.02) V offset developed

83

always in the same manner and vanished after the device was taken out from the vapour environment. The value 0.34 V is standard reduction potential at 25 °C for following reaction:

$$Cu^{2+}(aq) + 2 e^{-} \rightarrow Cu(s) \tag{7.5}$$

As a reasonable explanation can be suggested that an electrochemical cell was temporarily developed each time, when the device was exposed to higher voltage by reduction of small amount of copper from CuO in vapour environment which created liquid electrolyte environment by condensation in the pores of the sensing layer enabling thus the redox reaction. The Cu phase must be highly dispersed with large specific surface, if created, and oxidized due to oxygen in air immediately after being removed from the vapour environment and disconnected. Thus we observed the same behaviour in all tests taking the device into the testing chamber and out changing wire connections from time to time. This may have implications towards linearity of the sensor's response in some specific electrical connections (using higher voltage than the reduction potential for resistance measurement). [136]
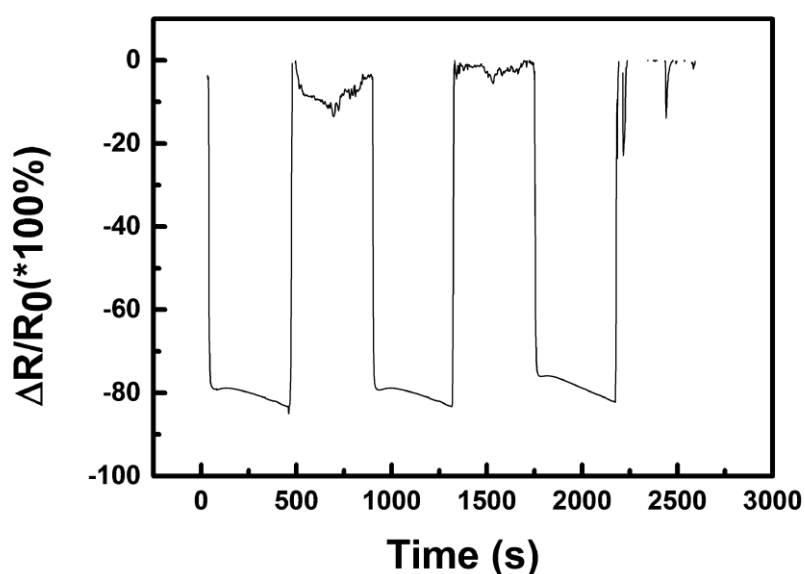
Figure 38 Relative resistance change ($\Delta R/R0$) of the sensor in ethanol sensing at 25°C. [136]

Similar sets of data were recorded for ethanol and methanol. Also in this case, each experiment was taking less than one hour, so the air humidity in the laboratory was stable enough to cause no baseline drift, so observed resistance changes can be ascribed solely to sensing of alcohol vapours, although the general level of the sensor's response shall be influenced by the humidity as well. Further studies will be necessary to analyse simultaneous effect of moisture and alcohol vapours on the response of the sensor. The record of three cycles for ethanol (see Figure 38) showed roughly similar behaviour to water, but both the saturation of the sensor after insertion into vapours and its recovery after taking out is much faster than in case of water. Moreover, the recovery to initial value reaches the resistance limit for used multimeter as seen by cut data at 0 % level. Such situations can make the use of the sensor impracticable. A more detailed inspection of the graph in Figure 38 revealed that the saturation of the signal is reached quite fast possibly due to easier adsorption (diffusion or dissolution?) of ethanol into the active layer but moreover the saturation is quickly overbalanced by another process which results into a continuous steady (linear) decrease of resistance unlike a simple exponential saturation observed for water. Both observations can be explained by relatively slow replacement of adsorbed moisture in the sensing CuO layer by alcohol molecules since partial pressure of water in saturated vapours over absolute ethanol is certainly much lower than in the ambient air in the laboratory. Measured I-V characteristics for ethanol shown in Figure 39 are again roughly similar to those recorded for water. Measured I-V characteristics for ethanol shown in Figure 39 are again roughly similar to those recorded for water. Three characteristic curves a) for sensor outside vapours, b) with hysteresis, and c) with the slope approx. 0.7 MΩ at more or less equilibrated state were recorded. Interestingly, the voltage offset is shifted slightly to higher values up to (0.42 ± 0.05) V. It can be hypothesised, that besides copper reduction, oxidation of ethanol to acetaldehyde can be a simultaneously occurring process

which could contribute to the observed linear decrease of the sensor's resistivity when exposed to vapours of ethanol. [136]
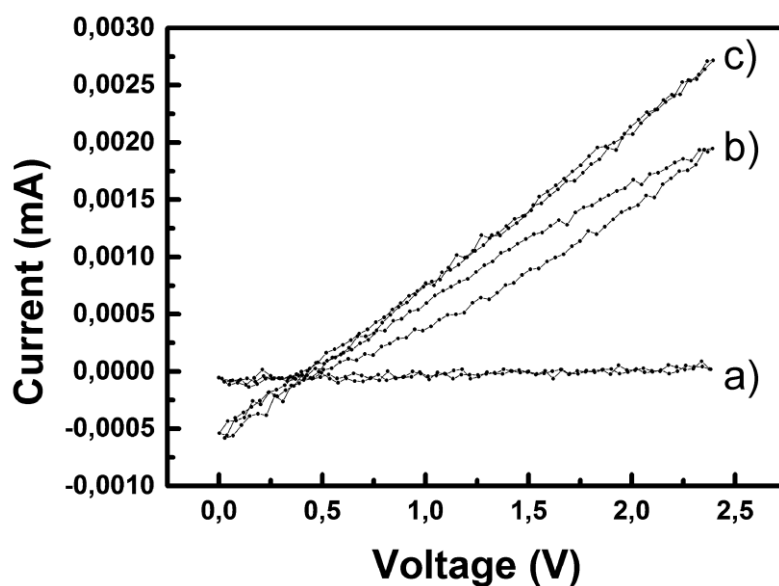

Figure 39 I-V characteristics of CuO sensors measured at 25°C in ethanol vapours, a) outside from vapours, b) hysteresis and c) stabilized. [136]

Methanol was another investigated organic volatile liquid. It can be seen on the three cycles recorded for the sensor insertion into and taking out of saturated vapours of methanol (see Figure 40) that the Relative resistance change reaches nearly down to -100 % which corresponds to decrease of resistance to several tens of kΩ. While the resistance decrease after insertion of the sensor into methanol vapours seems to be much faster than in case of water, the recovery of the sensor is significantly slower and even slowed more at -40% which may indicate that two processes are manifested in recorded curve. [136]

A record of I-V characteristics for the sensor in methanol vapours is shown in Figure 41. The measurement was started before insertion of the sensor into vapours environment and then continued cycle by cycle up to nearly saturated state with the slope approx. 0.05 MΩ. In total the record took 7 minutes. [136]
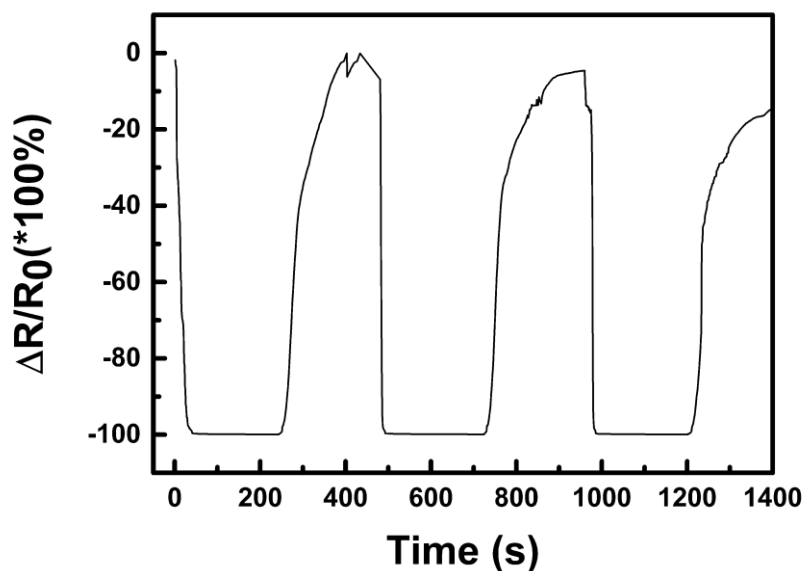
Figure 40 Relative resistance change (ΔR/R0) of the nano-copper oxide sensor within methanol sensing at 25°C. [136]

According to that, it can be said that the resistance measurement did not show the saturation kinetics optimally because of the linear (percentual) scale and that there is a continuing decrease to lower resistances similarly as in the case of ethanol but the process is either of much larger extent or much faster. It might be, that some product of this processes are generated and accumulated in the sensor and that this is that what is manifested during the sensor recovery on the dry air atmosphere also. A notable characteristic is the voltage offset (0.46 ± 0.03) V again. The potential necessary for simple oxidation of a primary alcohol to the corresponding aldehyde (formaldehyde in case of methanol) might be estimated to + (0.1-0.2) V which coincides with the increase of the voltage offset in comparison with that observed for moisture exposure. It can be expected that methanol has similar high affinity to the dried materials present in the active sensing layer as ethanol, but it has higher diffusion coefficient and eventual reactivity. It should be also mentioned, that methanol is the most volatile among tested compounds and has the highest absolute partial pressure of its saturated vapours among already tested liquids (i.e. higher than ethanol which again has higher partial pressure than water vapours). Based on presented data only, it

87

cannot be distinguished which processes exactly took place in the sensor, however it can be said that the sensing mechanism is not the one typical for p-type semiconductors at higher temperatures but most likely that it is primarily based on adsorption and condensation of the volatile compounds and accomplished by subsequent electrochemical reactions. [136]
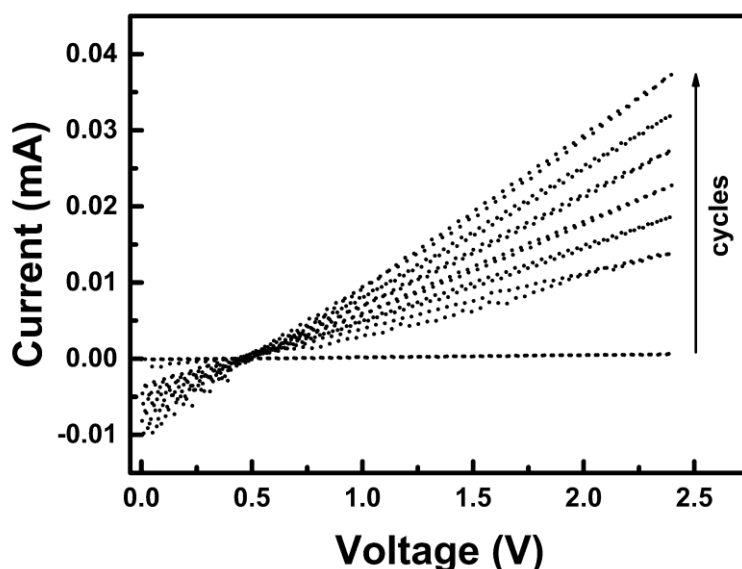

Figure 41 I-V characteristics of CuO sensors measured at 25°C in methanol vapours. The arrow shows sequence of cycles. [136]

To generalize the main lesson taken from the presented experimental results, it can be noted that the impossibility of polymer flexible substrate solution/dispersion processed sensors to be fired and operated at high temperatures results into requirement of the use of only low temperature processes in their fabrication. Any additive used in ink preparation that cannot be removed by annealing at relatively low temperatures even with the help of vacuum resides in the prepared layers and affects its properties. Moreover, it can influence the sensing mechanism as well. The low operation temperature may also invoke another principally different sensing mechanism than that which is expectable according to the experience with the sensing material in standard high temperature sensor applications. Thus, formulation of inks and smart engineering of the

fabrication process in order to circumvent these limitations represents the greatest challenge in this field nowadays. It was demonstrated in this case, that such task can be successfully accomplished. [136]

7.7 Sensor matrix

The final objective of this Thesis is preparation of a sensor field to demonstrate the capability of printing process. Therefore, a flexible device comprising matrix arrangement of 9 interdigits with sensing function was designed. This matrix element contained nine interdigits of the same kind as the individual ones described in previous sections. The device was printed in the same manner as the single devices, i.e. with the aid of the Dimatix laboratory printer using low temperature processes. The function of the device was demonstrated on its response to alcohol vapours. [147]

7.7.1 Design and preparation of the sensor matrix

Design of the sensor matrix included multiplication of the single interdigit motif described in the chapters above, arrangement of single devices into a 3 x 3 field and their wiring with a series of conductive paths. Motifs for printing were created in a format supporting vector graphics, which was then exported into a bitmap file, suitable as input for the Dimatix 2800 Series printer. In order to test the best condition, the resolution of bitmaps was 1000 and 1270 dpi. The latter one was successfully used for overprinting of the sensor matrix. [147] The final motif design of conductive paths joining the electrical circuit together is shown in Figure 42. The two black squares, one in the upper left corner and another one in the lower right corner, serve as registration marks to assure precise material placing during multiple production steps. They also serve as crop marks for final trimming of prepared sensor field. Each element of the sensor field can be assigned by a pair of numbers (X,Y) where X is the row number and Y is the column number. The numbering coordinates is such, that the element in left upper position in Figure 42 is (1,1).
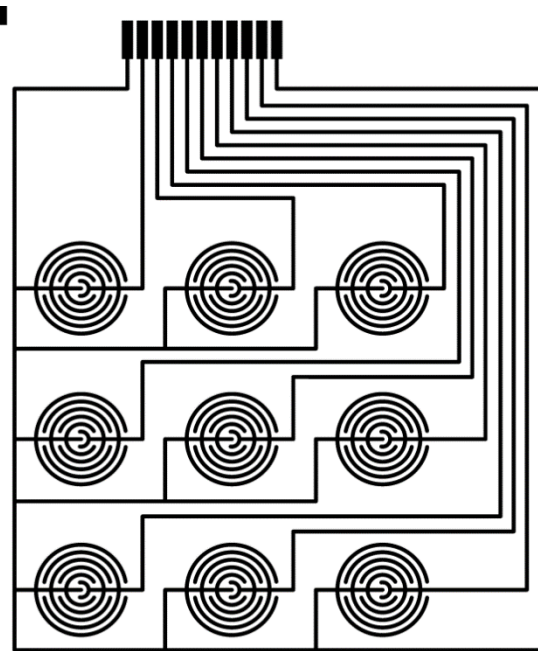
Figure 42 Motif of conductive paths. Courtesy Petr Měrka, [147]

At first, it was necessary to choose a final size of matrix element. There was no need of miniaturization at this stage of the research. Based on the dimensions of the connector for conductive connection between the matrix element and the interconnecting element of the multiplexer (a female FFC/FPC connector DS1020-04-22BRT1, CONNFLY), male output contact elements were designed. The width of the contacts was chosen 1.4 mm and length 5 mm. The distance between contacts was set 0.58 mm. The width of the array of 11 contacts is 21.2 mm. Compliance with all of these dimensions is necessary so that the male output contacts array accurately alignes with the contacts in the female connector. The outer contacts (1st and 11th) were used as a common cathode (- polarity). The nine contacts from the 2nd to the 10th were used as individual anodes (+ polarity) The next step was to create a design of nine interdigits, arranged in a matrix array (3x3). Distance between centers of interdigits was set the same horizontally and vertically to 20 mm. Diameter of interdigits is 13 mm. The motif developed for single sensor device was simply copied and joined by the conductive paths.

90

The motif for printing sensitive layers was simple. It was designed so that each single conductive interdigit motive was exactly overprinted by a disc from CuO ink assuring the disc overlap the motive sufficiently. Figure 43 shows this simple geometry.
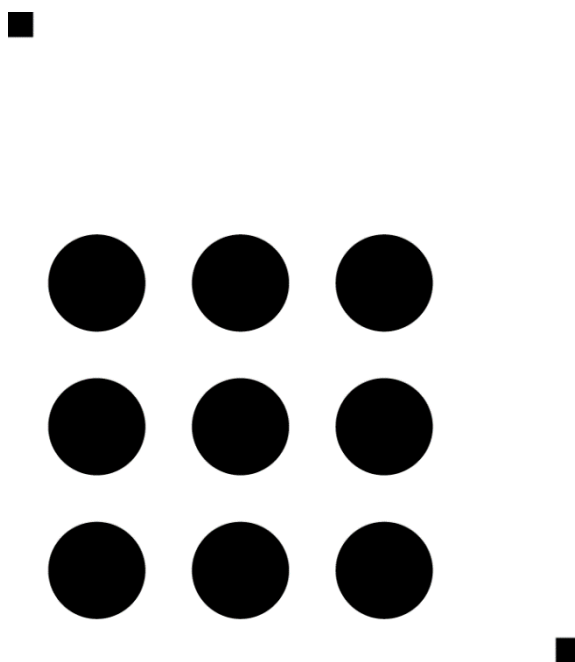

Figure 43 Motif of sensitive layer. Courtesy Petr Měrka, [147]

The same sequence of printing and postreatment steps as in the case of single sensor specimens was used for preparation of the sensor field. In order to utilize the full capacity of the printer, prepared motifs were replicated and printed on A4 substrate sheets in the arrangement shown on Figure 44.
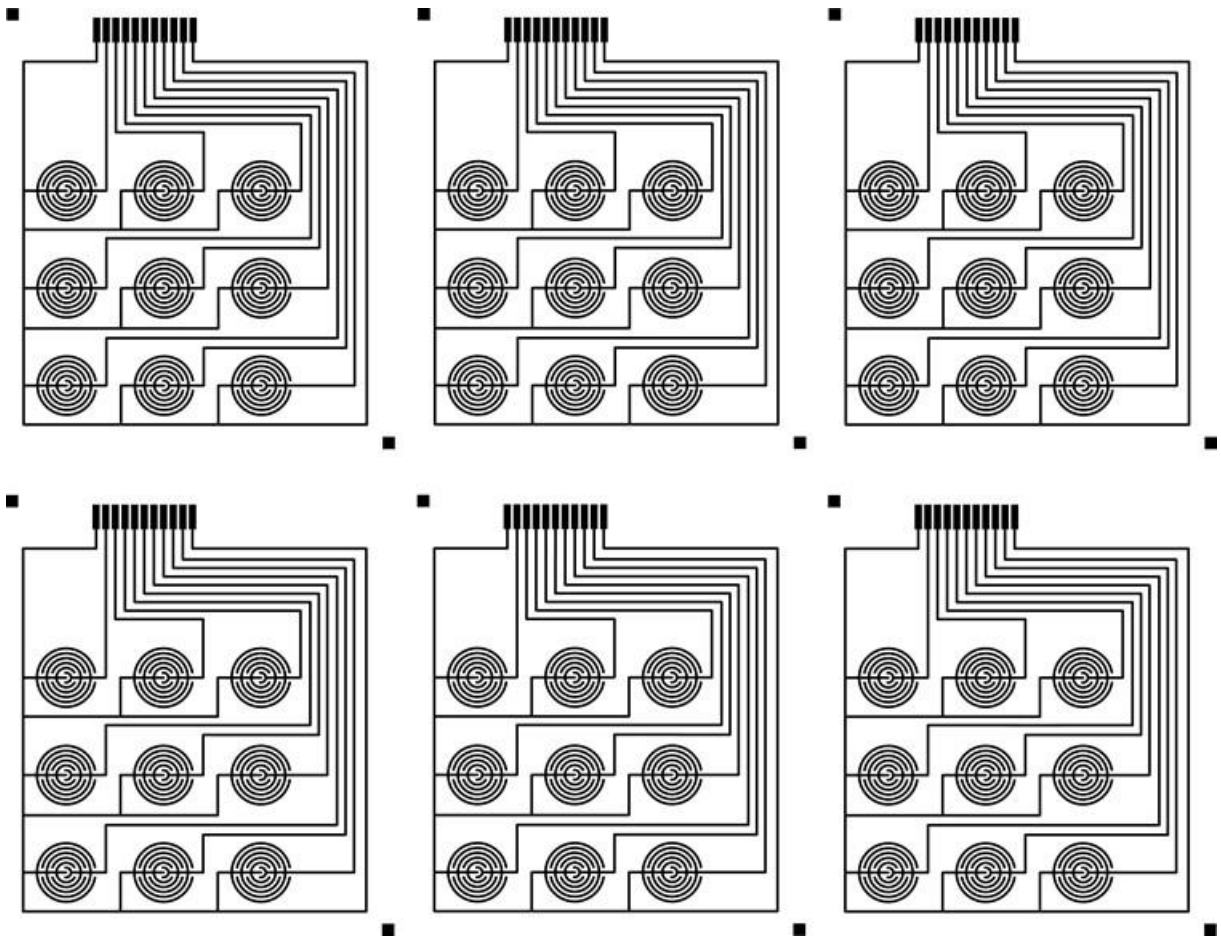
Figure 44 Motifs for A4 substrate size printing. Courtesy Petr Měrka, [147]

7.7.2   Response of the matrix to alcohol vapours

The data gathered in [147] were further processed and analysed. The adsorption of alcohol vapour molecules causes sharp decrease of the electrical resistance and their desorption causes rapid increase of resistance as in the case of single sensing devices. However, the sensor field shows reproducibility of the effect. The response of the sensor field to a sequence of four exposures to saturated ethanol vapours is shown in Figure 45. Seven matrix elements worked as expected manifesting almost identical behaviour. However, the element (3,1) exceeded the measurement range in both directins, i.e. its resistance was too high at ambient atmosphere and too low in the saturate vapours of ethanol. This could be possibly improved if a multimeter with broader resistance range is utilized. The element

(3,3) showed incomplete relaxation after first vapour exposure followed by regular behaviour, yet on narrower scale of resistances. Such phenomena can be explained by virtual insertion of a parallel constant resistance to the interdigit structure. In reality, this might be caused by some damage of the printed motif and partial shortcutting.
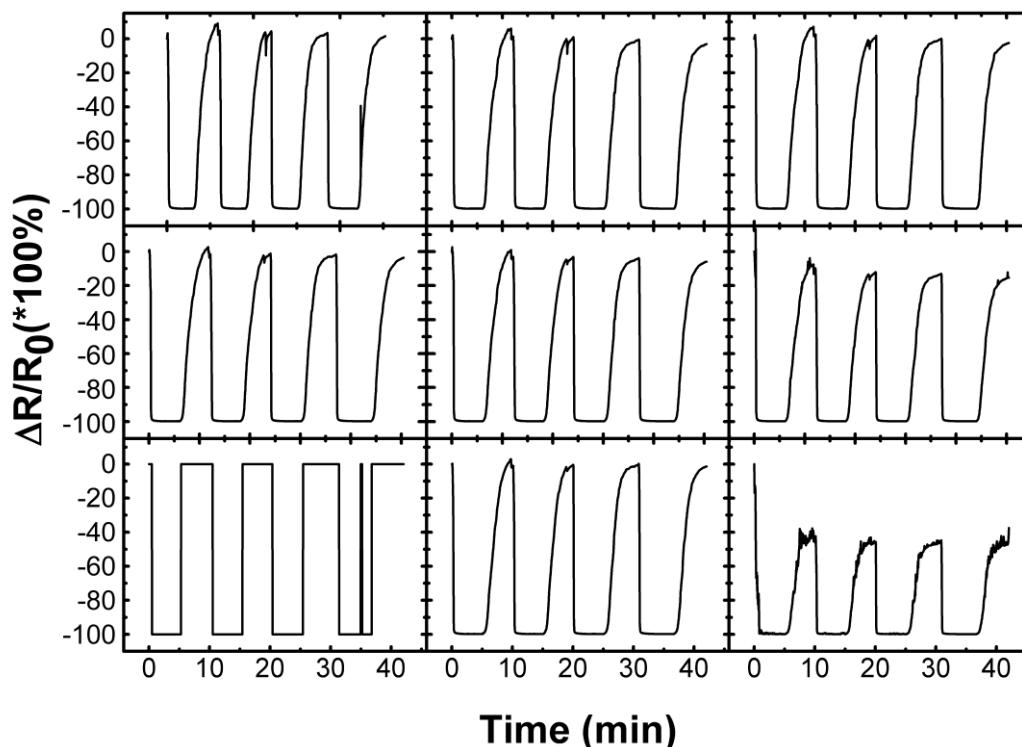

Figure 45 The response of the sensor field to a sequence of four exposures to saturated ethanol vapours

Similar behaviour was observed when the same sensor field was four times exposed to methanol vapours. As seen in Figure 46 The first two rows of the matrix responded perfectly, while the sensor element (3,1) seemed to be out of range and the respons of the sensor element (3,2) becomes to be noisy. On the other hand, the sensor element (3,3) was rescaled to its *off* resitance value and standard behavioiur was observed. Due to smaller resistance range between *on* and *off* states, the noise is much mire manifested than in case of the first six sensor elements.
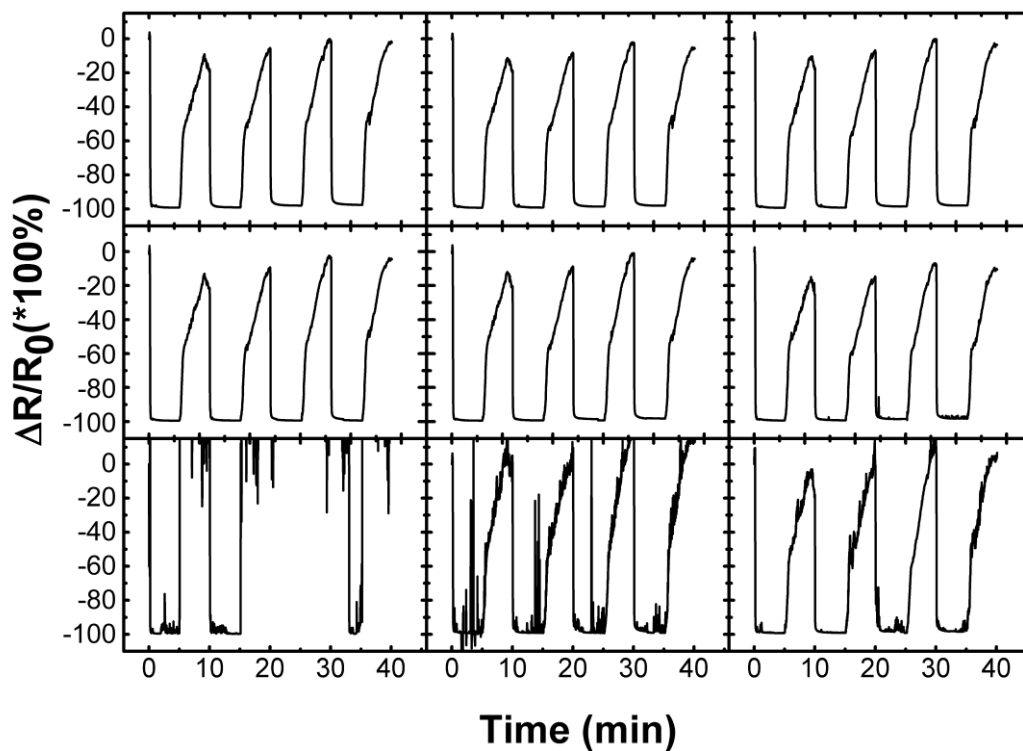
Figure 46 The response of the sensor field to a sequence of four exposures to saturated methanol vapours

The series of sensor field demonstration tests was finished by its exposure to isopropanol vapours, see Figure 47. Since the change of resistance in most of cases was surprisingly higher at the sensor elements' recovery and surpassed initial resistance values recoded for them at ambient atmosphere, the results are plotted just as a the ratio of the instantaneous value of the resistance R versus the initial resistance value R_0. The trend of increase of the *off* resistance value is most pronounced for the sensor element (1,1) while the other six elements (1,2; 1,3; 2,1; 2,2; 2,3; 3,2) show this behaviour in a less pronounced manner. The sensor elements (3,1 and 3,3) show shortcutting, moreover the element (3,1) was damaged totally after two cyclesses. Nevertheless, even in this case, the resinstance change curves have specific shapes of adsorption/desorption with clear on/off effect.

94
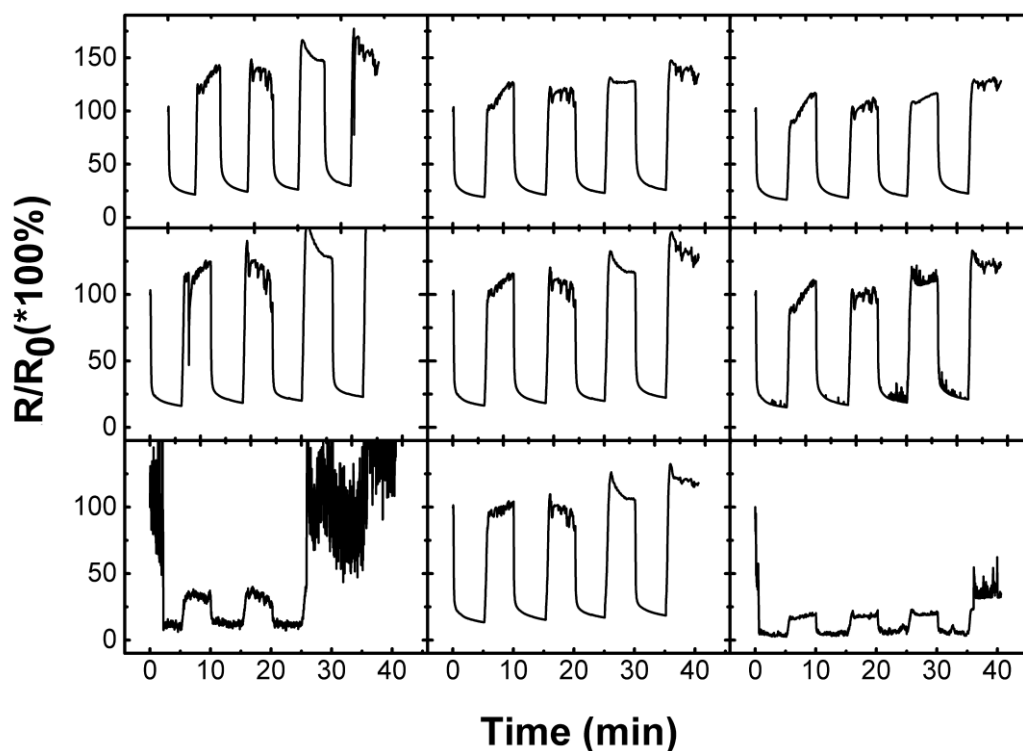
Figure 47 The response of the sensor field to a sequence of four exposures to saturated isopropanol vapours.

To summarize, the potential of preparation of fully printed sensing devices in form of a matrix field on flexible PET substrate was demonstrated and its function with respect to sensing of alcohol vapours (ethanol, methanol, and isopropanol) was confirmed. However, many practical issues are left unsolved, among them selectivity of sensors and their life time represent the most topical challenges. To draw future research directions, suggested improvements in both fileds have to be achieved by the use of low temperature process. The selectivity might be improved by printing integration of different sensing elements into the matrix field, while the resistance of the printed devices against surrounding conditions could be improved by encapsulation of all passive areas.

8. CONCLUSIONS

A series of inkjet inks was prepared from copper (II) oxide nanoparticles synthesized by MW enhanced solvothermal technique. The phase structure of prepared powder materials was verified by XRD technique. Only trace amount of Cu_2O were found in the otherwise prevailing CuO phase. The morphology of prepared particles resembled shape of chrysanthemum flowers of sub-micrometric size. Anchoring of CuO nanosheets to a common centre like petals in the flower creates large free space between individual nanosheets. Moreover, this expanded configuration of petals is stable and avoids collapse of the voluminous structure due to stacking of nanosheets which would occur if exfoliated nanosheets are used and spontaneously assemble during drying of the ink dispersion. This type morphology of constituing blocks of final sensing layer is suitable for gas sensing purposes.

The particles were dispersed in water with the aid of mixture of two surface active compounds (Byk 348 and Disperbyk 190) in different ratio keeping constant final volume of the dispersion. Dispersions stable over three weeks were prepared. It was found that addition of a mixture of the dispersant and the stabilizer affects the viscosity of inks more than the content of copper (II) oxide itself. On the other hand, the surface tension of all inkjet inks was around 22 $mN \cdot m^{-1}$ which means that the surface tension of the aqueous dispersion of CuO was reduced more than three times. The viscosity of prepared ink dispersions varied between 4.6 and 10.5 mPa·s. Since the material parameters, namely surface tension, viscosity and density of prepared inks are not sufficient for analysis of their printability, the tool and process parameters were taken into consideration as well. The hydrodynamic diameter of the printing nozzle is the main parameter related to the printer and liquid ejection velocity is the main processing parameter, while temperature is considered as external condition. In order to find optimum composition and printing conditions, the printablity of inks was analysed in terms

of dimensionless criteria. The single criterion approach based on the vast majority of the literature was found insuficient, therefore various two criterial printability assessment approaches were discussed and finaly the McKinley & Renardy's map of printability regimes in *Oh* vs. *Re* was revived. This approach was chosen since it utilizes the whole material-tool-process parameter triade and in contrast to other approaches it handles the parametric space within logarithmic coordinates allowing thus investigate and cover a large span of variables influencing the printing process. On the general level, the processing window suggested by the printer producers was analysed with regard to the possibility of good printability achievement. Then, the analytical framework was used in optimization of the inks and printing process development.

While conductive paths and interdigit electrodes were printed from commercially available silver inks in a standard way, the printing of active layer from original ink compositions was necessary to optimize. It was possible to achieve good printability with CuO ink drop ejection velocity about 4 m·s^{-1}. First, single thin films were printed to characterize their basic properties, then the CuO active layers was deposited on the electrode patterns to make sensing devices. The trapping of four layers on the primary layer of the CuO improved significantly the homogeneity of the surface as confirmed by the AFM and optical profilometry. The fabrication of sensing device fully printed on a flexible polymer substrate was finished by postreatment in a vacuum oven. All processing steps were performed at low temperature limited by the PET substrate stability.

Possible applicability of nanostructured copper (II) oxide films for the methanol, ethanol, and humidity sensing was demonstrated and the sensing mechanism was studied. The operating temperature for sensing was 25 ̊ C. Good sensitivity and response reversibility of the CuO film based sensor was proven although no significant differences in selectivity to used alcohols and water were observed. According to the obtained results, the presence of the surfactant and the dispersant remaining in the sensing CuO layer affects its final properties as well

as the sensing mechanism. The mechanism typical for p-type of semiconductors was not observed due to the low temperature operation of the sensor material. A mechanism involving most likely capillary condensation of moisture or vapours in the porous structure of the active layer followed by electrochemical reactions was proposed. An offset about 0.35 V in I-V characteristics of the sensors points towards electrochemical reaction involving reduction of CuO to Cu^0. Also oxidation of primary alcohols to corresponding aldehydes can be hypothesised as plausible process influencing the sensing mechanism. Hysteresis was in I-V curves recorded during changes of stimulus concentration as well. Regardless to what is the possible source of sensor's response nonlinearity, it seems that more attention should be paid to the method of resistance measurement itself, namely keeping the voltage applied to the sensor smaller than eventual critical values. [136]

Besides single sensor specimens, the sensor field in form of a 3 x 3 matrix of single device elements was printed as well. Its function was demonstrated by cyclic exposure to saturated vapours of alcohols, namely ethanol, methanol and isopropanol. Most of the elements showed sufficient reproducibility of the measurements. The selectivity and resistance of printed devices against external conditions remain as the most serious challenges for further research and development.

9. CLOSING REMARKS

9.1 Contribution to science and practice

This work contributed to science and practice not only by the accompplishement of the aim of the Thesis which is the development of the fully inkjet printed gas and humidity CuO based sensor on flexible PET polymer substrate but also by all the partial tasks that had to be researched and developed towards the achievement of the main aim:

- A facile microwave assisted solvothermal method of synthesis of the nanostructured CuO with flower-like morphology suitable for gas sensing was developed.

- Ink formulation and optimization was performed exemplifying good selection of suitable surfactants and stabilizers in order to achieve stable dispersion with suitable surface tension and viscosity.

- Reviving of the McKinley & Renardy's approach to printability regime assessment and good printability parameters evaluation which included a general analysis of the processing window for used printer. Presented printability analysis framework was used specifically for the laboratory material printer Dimatix DMP 2800 series, however it is applicable to any inkjet printer in a general manner. Similarly, the analysis of ink composition printability empfasizing the Weber number represents a lesson that may be easily adopted to other situations.

- Strong and weak sides of the sensor fabrication at low temperature were demonstrated and discussed.

- Low temperature sensing mechanism was partially addressed although it partially remains also a question open for further studies. If understood well, it will have implications to further changes in the design of the sensing device.

- Advantages and disadvantages of the resistance measurements with common multimeters were discussed and their consideration resulted into measurements of Volt-Ampere characteristics for each device and analyte application since a sensing device does not necessarily have to be an ohmic element at all.

- Finally, demonstration of the integration of the sensing devices into a sensor field entirely prepred by the inkjet printing confirmed potential of this technology. On the other hand, future challenges have become evident due to some drawbacks of the prepared specimens.

9.2 Ongoing research and future prospective

The research in the field of the printed polymer electronics does not stop with accomplishement of the aim of this Thesis. Our Group of Multifuctional nanomaterials continues in the research of material properties oriented namely on the understanding structure-property relationship in the active sensing layer materials focusing on the sensing mechanisms under low temperature operation. Understanding the mechanism will have impact on the design of the devices which are structures with size-scale dependent properties. With respect to obtained general knowledge, the method of synthesis of nanostructured semiconductor materials are further developed with the ultimate goal of tailoring desired structure, morphology and function.

With regard to the specific sensors presented in this Thesis, the future research and development will be focused both on the more detailed studies of the sensing mechanism as well as on the issue of the resistance of printed devices against deterioration by external conditions.

REFERENCES

1. KREBS, F.C. Fabrication and Processing of Polymer Solar Cells: A Review of Printing and Coating Techniques. *Solar Energy Materials and Solar Cells*, APR, 2009, vol. 93, no. 4. pp. 394-412 ISSN 0927-0248. DOI 10.1016/j.solmat.2008.10.004.

2. PUDAS, M., HAGBERG, J. and LEPPAVUORI, S. Printing Parameters and Ink Components Affecting Ultra-Fine-Line Gravure-Offset Printing for Electronics Applications. *Journal of the European Ceramic Society*, SEP, 2004, vol. 24, no. 10-11. pp. 2943-2950 ISSN 0955-2219. DOI 10.1016/j.jeurceramsoc.2003.11.011.

3. BURMANN, P., ZORNOZA, B., TELLEZ, C. and CORONAS, J. Mixed Matrix Membranes Comprising MOFs and Porous Silicate Fillers Prepared Via Spin Coating for Gas Separation. *Chemical Engineering Science*, APR 7, 2014, vol. 107. pp. 66-75 ISSN 0009-2509. DOI 10.1016/j.ces.2013.12.001.

4. CREGAN, V. and O'BRIEN, S.B.G. Extended Asymptotic Solutions to the Spin-Coating Model with Small Evaporation. *Applied Mathematics and Computation*, OCT 15, 2013, vol. 223. pp. 76-87 ISSN 0096-3003. DOI 10.1016/j.amc.2013.07.071.

5. HERRERA, M.A., MATHEW, A.P. and OKSMAN, K. Gas Permeability and Selectivity of Cellulose Nanocrystals Films (Layers) Deposited by Spin Coating. *Carbohydrate Polymers*, NOV 4, 2014, vol. 112. pp. 494-501 ISSN 0144-8617. DOI 10.1016/j.carbpol.2014.06.036.

6. WANG, X., et al. A Sol-Gel Dip/Spin Coating Method to Prepare Titanium Oxide Films. *Thin Solid Films*, DEC 2, 2013, vol. 548. pp. 34-39 ISSN 0040-6090. DOI 10.1016/j.tsf.2013.08.056.

7. ITO, S. Printable Solar Cells. *Wiley Interdisciplinary Reviews-Energy and Environment*, JAN-FEB, 2015, vol. 4, no. 1. pp. 51-73 ISSN 2041-8396. DOI 10.1002/wene.112.

8. STEIRER, K.X., et al. Ultrasonic Spray Deposition for Production of Organic Solar Cells. *Solar Energy Materials and Solar Cells*, APR, 2009, vol. 93, no. 4. pp. 447-453 ISSN 0927-0248. DOI 10.1016/j.solmat.2008.10.026.

9. PUDAS, M., HAGBERG, J. and LEPPAVUORI, S. Gravure Offset Printing of Polymer Inks for Conductors. *Progress in Organic Coatings*, MAY, 2004, vol. 49, no. 4. pp. 324-335 ISSN 0300-9440. DOI 10.1016/j.porgcoat.2003.09.013.

10. GHADIRI, F., AHMED, D.H., SUNG, H.J. and SHIRANI, E. Non-Newtonian Ink Transfer in Gravure-Offset Printing. *International Journal of Heat and Fluid Flow*, FEB, 2011, vol. 32, no. 1. pp. 308-317 ISSN 0142-727X. DOI 10.1016/j.ijheatfluidflow.2010.09.004.

11. SANKARAN, A.K. and ROTHSTEIN, J.P. Effect of Viscoelasticity on Liquid Transfer during Gravure Printing. *Journal of Non-Newtonian Fluid Mechanics*, MAY, 2012, vol. 175. pp. 64-75 ISSN 0377-0257. DOI 10.1016/j.jnnfm.2012.03.011.

12. DODDS, S., CARVALHO, M.d.S. and KUMAR, S. Stretching and Slipping of Liquid Bridges Near Plates and Cavities. *Physics of Fluids*, SEP, 2009, vol. 21, no. 9. pp. 092103 ISSN 1070-6631. DOI 10.1063/1.3212963.

13. AHN, S.H. and GUO, L.J. Large-Area Roll-to-Roll and Roll-to-Plate Nanoimprint Lithography: A Step Toward High-Throughput Application of Continuous Nanoimprinting. *Acs Nano*, AUG, 2009, vol. 3, no. 8. pp. 2304-2310 ISSN 1936-0851. DOI 10.1021/nn9003633.

14. Ho Anh Duc Nguyen, et al. An Approach for Controlling Printed Line-Width in High Resolution Roll-to-Roll Gravure Printing. *Journal of Micromechanics and Microengineering*, SEP, 2013, vol. 23, no. 9. pp. 095010 ISSN 0960-1317. DOI 10.1088/0960-1317/23/9/095010.

15. DEGANELLO, D., CHERRY, J.A., GETHIN, D.T. and CLAYPOLE, T.C. Patterning of Micro-Scale Conductive Networks using Reel-to-Reel Flexographic Printing. *Thin Solid Films*, AUG 31, 2010, vol. 518, no. 21. pp. 6113-6116 ISSN 0040-6090. DOI 10.1016/j.tsf.2010.05.125.

16. ZOLEK-TRYZNOWSKA, Z. and IZDEBSKA, J. Flexographic Printing Ink Modified with Hyperbranched Polymers: Boltorn (TM) P500 and Boltorn (TM) P1000. *Dyes and Pigments*, FEB, 2013, vol. 96, no. 2. pp. 602-608 ISSN 0143-7208. DOI 10.1016/j.dyepig.2012.10.003.

17. DILFER, S., HOFFMANN, R.C. and DOERSAM, E. Characteristics of Flexographic Printed Indium-Zinc-Oxide Thin Films as an Active Semiconductor Layer in Thin Film Field-Effect Transistors. *Applied Surface Science*, NOV 30, 2014, vol. 320. pp. 634-642 ISSN 0169-4332. DOI 10.1016/j.apsusc.2014.09.106.

18. KUO, H., et al. Preparation of the Working Electrode of Dye-Sensitized Solar Cells: Effects of Screen Printing Parameters. *Journal of the Taiwan Institute of Chemical Engineers*, SEP, 2014, vol. 45, no. 5. pp. 2340-2345 ISSN 1876-1070. DOI 10.1016/j.jtice.2014.06.004.

19. YEN, Y., FANG, T. and LIN, Y. Optimization of Screen-Printing Parameters of SN9000 Ink for Pinholes using Taguchi Method in Chip on Film Packaging. *Robotics and Computer-Integrated Manufacturing*, JUN, 2011, vol. 27, no. 3. pp. 531-537 ISSN 0736-5845. DOI 10.1016/j.rcim.2010.09.008.

20. FADDOUL, R., REVERDY-BRUAS, N. and BLAYO, A. Formulation and Screen Printing of Water Based Conductive Flake Silver Pastes Onto Green Ceramic Tapes for Electronic Applications. *Materials Science and Engineering B-Advanced Functional Solid-State Materials*, AUG 1, 2012, vol. 177, no. 13. pp. 1053-1066 ISSN 0921-5107. DOI 10.1016/j.mseb.2012.05.015.

21. LEACH, R.H. *The Printing Ink Manual.* 5th ed. London ; New York: Blueprint, 1993. ISBN 0948905816.

22. SULY, P., et al. Poly(Vinyl Alcohol): Formulation of a Polymer Ink for the Patterning of Substrates with a Drop-on-Demand Inkjet Printer. *Materiali in Tehnologije*, 2017, 2017, vol. 51, no. 1. pp. 41-48 ISSN 1580-2949.

23. CALVERT, P. Inkjet Printing for Materials and Devices. *Chemistry of Materials*, OCT, 2001, vol. 13, no. 10. pp. 3299-3305 ISSN 0897-4756. DOI 10.1021/cm0101632.

24. XU, Q., et al. Template-Induced Fabrication of Nanopatterned Polymeric Films by Inkjet Printing. *Applied Surface Science*, SEP 15, 2014, vol. 313. pp. 237-242 ISSN 0169-4332. DOI 10.1016/j.apsusc.2014.05.190.

25. ESPOSITO, V., et al. Fabrication of Thin Yttria-Stabilized-Zirconia Dense Electrolyte Layers by Inkjet Printing for High Performing Solid Oxide Fuel Cells. *Journal of Power Sources*, JAN 1, 2015, vol. 273. pp. 89-95 ISSN 0378-7753. DOI 10.1016/j.jpowsour.2014.09.085.

26. CASTREJON-PITA, J.R., et al. Future, Opportunities and Challenges of Inkjet Technologies. *Atomization and Sprays*, 2013, vol. 23, no. 6. pp. 541-565 ISSN 1044-5110.

27. DERBY, B. Inkjet Printing of Functional and Structural Materials: Fluid Property Requirements, Feature Stability, and Resolution. *Annual Review of Materials Research, Vol 40*, 2010, vol. 40. pp. 395-414 ISSN 1531-7331; 978-0-8243-1740-9. DOI 10.1146/annurev-matsci-070909-104502.

28. MCLLROY, C., HARLEN, O.G. and MORRISON, N.F. Modelling the Jetting of Dilute Polymer Solutions in Drop-on-Demand Inkjet Printing. *Journal of Non-Newtonian Fluid Mechanics*, NOV, 2013, vol. 201. pp. 17-28 ISSN 0377-0257. DOI 10.1016/j.jnnfm.2013.05.007.

29. ORLANDINI, J.O., et al. Development and Characterization of a Thermal Inkjet-Based Aerosol Generator for Micro-Volume Sample Introduction in Analytical Atomic Spectrometry. *Journal of Analytical Atomic Spectrometry*, 2011, vol. 26, no. 9. pp. 1781-1789 ISSN 0267-9477. DOI 10.1039/c1ja10015g.

30. MAGDASSI, S. *The Chemistry of Inkjet Inks.* Singapore ; Hackensack, NJ: World Scientific, 2010. ISBN 9789812818218.

31. VIJAYA, M.S. *Piezoelectric Materials and Devices : Applications in Engineering and Medical Sciences.* Boca Raton, Fla.; London: CRC; Taylor & Francis distributor, 2013. ISBN 9781439887868.

32. *Inkjet-Based Micromanufacturing.* J.G. KORVINK, P.J. SMITH and D. SHIN eds., Weinheim: Wiley-VCH, 2012. ISBN 9783527319046.

33. Anonymous. *FUJIFILM Dimatix Materials Printer DMP-2800 Series User Manual.* User Manual ed. U.S.A.: FUJIFILM Dimatix, Inc., 2010.

34. SAUNDERS, R.E., GOUGH, J.E. and DERBY, B. Delivery of Human Fibroblast Cells by Piezoelectric Drop-on-Demand Inkjet Printing. *Biomaterials*, JAN, 2008, vol. 29, no. 2. pp. 193-203 ISSN 0142-9612. DOI 10.1016/j.biomatei-ials.2007.09.032.

35. KIM, J.Y., et al. Inkjet-Printed Multicolor Arrays of Highly Luminescent Nanocrystal-Based Nanocomposites. *Small*, MAY 4, 2009, vol. 5, no. 9. pp. 1051-1057 ISSN 1613-6810. DOI 10.1002/smll.200801315.

36. DERBY, B. Inkjet Printing Ceramics: From Drops to Solid. *Journal of the European Ceramic Society*, NOV, 2011, vol. 31, no. 14. pp. 2543-2550 ISSN 0955-2219. DOI 10.1016/j.jeurceramsoc.2011.01.016.

37. SOUSA, S., et al. Interactions of Ink Colourants with Chemically Modified Paper Surfaces Concerning Inkjet Print Improvement. *Materials Chemistry and Physics*, MAY 15, 2013, vol. 139, no. 2-3. pp. 877-884 ISSN 0254-0584. DOI 10.1016/j.matchemphys.2013.02.048.

38. MIELONEN, K., et al. Inkjet Ink Spreading on Polyelectrolyte Multilayers Deposited on Pigment Coated Paper. *Journal of Colloid and Interface Science*, JAN 15, 2015, vol. 438. pp. 179-190 ISSN 0021-9797. DOI 10.1016/j.jcis.2014.09.077.

39. TITTERINGTON, D.R., BUI, L.V., HIRSCHY, L.M. and FRAME, H.R. *Indirect Printing Process for Applying Selective Phase Change Ink Compositions to Substrates.* 1994 ProQuest Technology Collection.

40. BANNING, J.H., BUI, L.V., KING, C.R. and TITTERINGTON, D.R. *Phase Change Ink Formulation using a Urethane Isocyanate-Derived Resin and a Urethane Isocyanate-Derived Wax.* 1998 ProQuest Technology Collection.

41. BROWN, B.J., et al. *Solvent-Based Inkjet Ink Formulations.* 2014 ProQuest Technology Collection.

42. PAPAIACOVOU, I., GALLINO, Z., BALBINDER, D.H. and SLEP, D. *Solvent-Based Dye Sublimation Ink Composition.* 2012 ProQuest Technology Collection.

43. EL-MOLLA, M.M. Synthesis of Polyurethane Acrylate Oligomers as Aqueous UV-Curable Binder for Inks of Ink Jet in Textile Printing and Pigment Dyeing. *Dyes and Pigments*, 2007, 2007, vol. 74, no. 2. pp. 371-379 ISSN 0143-7208. DOI 10.1016/j.dyepig.2006.02.021.

44. ZHAI, D., et al. Water-Based Ultraviolet Curable Conductive Inkjet Ink Containing Silver Nano-Colloids for Flexible Electronics. *Colloids and Surfaces A-Physicochemical and Engineering Aspects*, MAY 5 2013, 2013, vol. 424. pp. 1-9 ISSN 0927-7757. DOI 10.1016/j.colsurfa.2013.01.055.

45. MIRSCHEL, G., et al. In-Line Monitoring of Printing Processes in an Offset Printing Press by NIR Spectroscopy: Correlation between the Conversion and the Content of Extractable Acrylate in UV-Cured Printing Inks. *Progress in*

Organic Coatings, NOV 2014, 2014, vol. 77, no. 11. pp. 1682-1687 ISSN 0300-9440. DOI 10.1016/j.porgcoat.2014.05.012.

46. ŠULY, P. *Study of Poly(Vinyl alcohol) Solution for Inkjet Printing.* Ph.D. Thesis. ed. Zlin: Tomas Bata University in Zlin, 2017.

47. SOCHI, T. Non-Newtonian Flow in Porous Media. *Polymer*, OCT 15, 2010, vol. 51, no. 22. pp. 5007-5023 ISSN 0032-3861. DOI 10.1016/j.polymer.2010.07.047.

48. SOCHI, T. and BLUNT, M.J. Pore-Scale Network Modeling of Ellis and Herschel-Bulkley Fluids. *Journal of Petroleum Science and Engineering*, FEB, 2008, vol. 60, no. 2. pp. 105-124 ISSN 0920-4105. DOI 10.1016/j.petrol.2007.05.009.

49. SPERLING, L.H. *Introduction to Physical Polymer Science.* 4th ed. New York ; Chichester: Wiley, 2006. ISBN 047170606X.

50. KRONBERG, B., HOLMBERG, K. and LINDMAN, B. *Surface Chemistry of Surfactants and Polymers.* Wiley, 2014. ISBN 9781119961246.

51. BARNES, H.A., HUTTON, J.F. and WALTERS, K. *An Introduction to Rheology.* Elsevier, 1989. ISBN 0444871403.

52. WANG, X., CARR, W.W., BUCKNALL, D.G. and MORRIS, J.F. High-Shear-Rate Capillary Viscometer for Inkjet Inks. *Review of Scientific Instruments*, JUN, 2010, vol. 81, no. 6. pp. 065106 ISSN 0034-6748. DOI 10.1063/1.3449478.

53. EBERHART, J. Surface Tension of Binary Liquid Mixtures. *Journal of Physical Chemistry*, 1966, vol. 70, no. 4. pp. 1183-& ISSN 0022-3654. DOI 10.1021/j100876a035.

54. VARGAFTIK, N., VOLKOV, B. and VOLJAK, L. International Tables of the Surface-Tension of Water. *Journal of Physical and Chemical Reference Data*, 1983, vol. 12, no. 3. pp. 817-820 ISSN 0047-2689. DOI 10.1063/1.555688.

55. STAMM, M. Polymer Surface and Interface Characterization Techniques. *In Polymer surfaces and interfaces: characterization, modification and applications.* M. STAMM ed., 1st ed. Berlin: Springer, 2008., pp. 324 ISBN 9783540738640.

56. KIM, E. and BAEK, J. Numerical Study on the Effects of Non-Dimensional Parameters on Drop-on-Demand Droplet Formation Dynamics and Printability Range in the Up-Scaled Model. *Physics of Fluids*, AUG, 2012, vol. 24, no. 8. pp. 082103 ISSN 1070-6631. DOI 10.1063/1.4742913.

57. DONG, H., CARR, W.W. and MORRIS, J.F. An Experimental Study of Drop-on-Demand Drop Formation. *Physics of Fluids*, JUL, 2006, vol. 18, no. 7. pp. 072102 ISSN 1070-6631. DOI 10.1063/1.2217929.

58. MORRISON, N.F. and HARLEN, O.G. Viscoelasticity in Inkjet Printing. *Rheologica Acta*, JUN, 2010, vol. 49, no. 6. pp. 619-632 ISSN 0035-4511. DOI 10.1007/s00397-009-0419-z.

59. RAYLEIGH, L. On the Instability of Jets. *Proceedings of the London Mathematical Society*, 1878, vol. 1, no. 1. pp. 4-13.

60. HARTMAN, R., et al. Jet Break-Up in Electrohydrodynamic Atomization in the Cone-Jet Mode. *Journal of Aerosol Science*, JAN, 2000, vol. 31, no. 1. pp. 65-95 ISSN 0021-8502. DOI 10.1016/S0021-8502(99)00034-8.

61. JANG, D., KIM, D. and MOON, J. Influence of Fluid Physical Properties on Ink-Jet Printability. *Langmuir*, MAR 3, 2009, vol. 25, no. 5. pp. 2629-2635 ISSN 0743-7463. DOI 10.1021/la900059m.

62. JERRARD, H.G. and MCNEILL, D.B. *A Dictionary of Scientific Units: Including Dimensionless Numbers and Scales.* 6th ed. London ; New York: Chapman & Hall, 1992. ISBN 0412467208.

63. KUNEŠ, J. and KUNEŠ, J. *Dimensionless Physical Quantities in Science and Engineering.* London ; Waltham, MA: Elsevier, 2012. ISBN 9780124160132.

64. FROMM, J. Numerical-Calculation of the Fluid-Dynamics of Drop-on-Demand Jets. *Ibm Journal of Research and Development*, 1984, vol. 28, no. 3. pp. 322-333 ISSN 0018-8646. DOI 10.1147/rd.283.0322.

65. REIS, N. and DERBY, B. Ink Jet Deposition of Ceramic Suspensions: Modelling and Experiments of Droplet Formation. *Solid Freeform and Additive Fabrication-2000*, 2000, vol. 625. pp. 117-122 ISSN 0272-9172; 1-55899-533-1. DOI 10.1557/PROC-625-117.

66. CLASEN, C., PHILLIPS, P.M., PALANGETIC, L. and VERMANT, J. Dispensing of Rheologically Complex Fluids: The Map of Misery. *AIChE Journal*, OCT, 2012, vol. 58, no. 10. pp. 3242-3255 ISSN 0001-1541. DOI 10.1002/aic.13704.

67. MCKINLEY, G.H. and RENARDY, M. Wolfgang Von Ohnesorge. *Physics of Fluids*, DEC, 2011, vol. 23, no. 12. pp. 127101 ISSN 1070-6631. DOI 10.1063/1.3663616.

68. MASLIK, J., et al. Water-Based Indium Tin Oxide Nanoparticle Ink for Printed Toluene Vapours Sensor Operating at Room Temperature. *Sensors*, OCT, 2018, vol. 18, no. 10. pp. 3246 ISSN 1424-8220. DOI 10.3390/s18103246.

69. HUTCHINGS, I.M. and MARTIN, G. *Inkjet Technology for Digital Fabrication.* Chichester, West Sussex, United Kingdom: Wiley, 2013. ISBN 9780470681985.

70. SCHMIDT, G. and MALWITZ, M.M. Properties of Polymer-Nanoparticle Composites. *Current Opinion in Colloid & Interface Science*, MAR 2003, 2003,

vol. 8, no. 1. pp. 103-108 ISSN 1359-0294. DOI 10.1016/S1359-0294(03)00008-6.

71. FRADEN, J. *Handbook of Modern Sensors: Physics, Designs, and Applications.* 4th ed. New York: Springer, 2010. ISBN 9781441964656.

72. KALANTAR-ZADEH, K. *Sensors: An Introductory Course.* New York: Springer, 2013. ISBN 9781461450511.

73. JANATA, J. *Principles of Chemical Sensors.* Dordrecht ; New York: Springer, 2009. ISBN 9780387699301.

74. *Sensor Technology Handbook.* J.S. WILSON ed., Amsterdam ; Boston: Elsevier, 2005. ISBN 0750677295.

75. HASSAN, M.A., KAMARUDIN, S.K., LOH, K.S. and DAUD, W.R.W. Sensors for Direct Methanol Fuel Cells. *Renewable & Sustainable Energy Reviews*, DEC, 2014, vol. 40. pp. 1060-1069 ISSN 1364-0321. DOI 10.1016/j.rser.2014.07.067.

76. GANGOPADHYAY, T.K., et al. Detection of Chemicals using a Novel Fiber-Optic Sensor Element Built in Fiber Loop Ring-Resonators. *Sensors and Actuators B-Chemical*, JAN, 2015, vol. 206. pp. 327-335 ISSN 0925-4005. DOI 10.1016/j.snb.2014.09.024.

77. HARRAZ, F.A. Porous Silicon Chemical Sensors and Biosensors: A Review. *Sensors and Actuators B-Chemical*, OCT, 2014, vol. 202. pp. 897-912 ISSN 0925-4005. DOI 10.1016/j.snb.2014.06.048.

78. BARRERO MORENO, J.M. and F. ROSSI, M.W. *Review* on the Application of (Bio)Chemical Sensors for Air Monitoring of Volatile Organic Compounds. *EU Publications*, 2003 Ispra (VA) Italy, vol. 22, no. Chemical industry ISSN 1018-5593.

79. LLOBET, E. Gas Sensors using Carbon Nanomaterials: A Review. *Sensors and Actuators B-Chemical*, MAR 31, 2013, vol. 179. pp. 32-45 ISSN 0925-4005. DOI 10.1016/j.snb.2012.11.014.

80. HULANICKI, A., GLAB, S. and INGMAN, F. Chemical Sensors Definitions and Classification. *Pure and Applied Chemistry*, SEP, 1991, vol. 63, no. 9. pp. 1247-1250 ISSN 0033-4545. DOI 10.1351/pac199163091247.

81. CHEN, Z. and LU, C. Humidity Sensors: A Review of Materials and Mechanisms. *Sensor Letters*, DEC, 2005, vol. 3, no. 4. pp. 274-295 ISSN 1546-198X. DOI 10.1166/sl.2005.045.

82. KHAN, S., LORENZELLI, L. and DAHIYA, R.S. Technologies for Printing Sensors and Electronics Over Large Flexible Substrates: A Review. *Ieee Sensors Journal*, JUN, 2015, vol. 15, no. 6. pp. 3164-3185 ISSN 1530-437X. DOI 10.1109/JSEN.2014.2375203.

83. PRUDENZIATI, M. and HORMADALY, J. *Printed Films: Materials Science and Applications in Sensors, Electronics and Photonics*. Cambridge, UK ; Philadelphia: Woodhead Publishing, 2012. ISBN 9781845699888.

84. ZHANG, Q., et al. CuO Nanostructures: Synthesis, Characterization, Growth Mechanisms, Fundamental Properties, and Applications. *Progress in Materials Science*, MAR 2014, 2014, vol. 60. pp. 208-337 ISSN 0079-6425. DOI 10.1016/j.pmatsci.2013.09.003.

85. ANANDAN, S. and YANG, S. Emergent Methods to Synthesize and Characterize Semiconductor CuO Nanoparticles with various Morphologies - an Overview. *Journal of Experimental Nanoscience*, 2007, vol. 2, no. 1. pp. 23-56 ISSN 1745-8080. DOI 10.1080/17458080601094421.

86. LIU, Y., et al. Anion-Controlled Construction of CuO Honeycombs and Flowerlike Assemblies on Copper Foils. *Crystal Growth & Design*, MAR, 2007, vol. 7, no. 3. pp. 467-470 ISSN 1528-7483. DOI 10.1021/cg060480r.

87. VASEEM, M., UMAR, A., KIM, S.H. and HAHN, Y. Low-Temperature Synthesis of Flower-Shaped CuO Nanostructures by Solution Process: Formation Mechanism and Structural Properties. *Journal of Physical Chemistry C*, APR 17, 2008, vol. 112, no. 15. pp. 5729-5735 ISSN 1932-7447. DOI 10.1021/jp710358j.

88. MACDONALD, A. Superconductivity - Copper Oxides Get Charged Up. *Nature*, NOV 22, 2001, vol. 414, no. 6862. pp. 409-410 ISSN 0028-0836.

89. R. JANA, et al. *Direct Observation of Re-Entrant Multiferroic CuO at High Pressures.* , 2015 Available from: https://arxiv.org/ftp/arxiv/papers/1508/1508.02874.pdf.

90. XIA, Y., et al. One-Dimensional Nanostructures: Synthesis, Characterization, and Applications. *Advanced Materials*, MAR 4, 2003, vol. 15, no. 5. pp. 353-389 ISSN 0935-9648. DOI 10.1002/adma.200390087.

91. FILIPIC, G. and CVELBAR, U. Copper Oxide Nanowires: A Review of Growth. *Nanotechnology*, MAY 17, 2012, vol. 23, no. 19. pp. 194001 ISSN 0957-4484. DOI 10.1088/0957-4484/23/19/194001.

92. SINGH, D.P. and ALI, N. Synthesis of TiO2 and CuO Nanotubes and Nanowires. *Science of Advanced Materials*, SEP, 2010, vol. 2, no. 3. pp. 295-335 ISSN 1947-2935. DOI 10.1166/sam.2010.1095.

93. RAHMAN, M.M., et al. A Comprehensive Review of Glucose Biosensors Based on Nanostructured Metal-Oxides. *Sensors*, MAY, 2010, vol. 10, no. 5. pp. 4855-4886 ISSN 1424-8220. DOI 10.3390/s100504855.

94. KISLYUK, V.V. and DIMITRIEV, O.P. Nanorods and Nanotubes for Solar Cells. *Journal of Nanoscience and Nanotechnology*, JAN, 2008, vol. 8, no. 1. pp. 131-148 ISSN 1533-4880. DOI 10.1166/jnn.2008.N16.

95. CHOI, K.J. and JANG, H.W. One-Dimensional Oxide Nanostructures as Gas-Sensing Materials: Review and Issues. *Sensors*, APR, 2010, vol. 10, no. 4. pp. 4083-4099 ISSN 1424-8220. DOI 10.3390/s100404083.

96. Zhou Ling, et al. A New Hybrid Optimization of Reactive Optimization and Voltage Stability. *2010 Asia-Pacific Power and Energy Engineering Conference (Appeec)*, 2010 ISSN 2157-4839; 978-1-4244-4813-5.

97. WANG, S., ZHANG, M. and ZHANG, W. Yolk-Shell Catalyst of Single Au Nanoparticle Encapsulated within Hollow Mesoporous Silica Microspheres. *Acs Catalysis*, MAR, 2011, vol. 1, no. 3. pp. 207-211 ISSN 2155-5435. DOI 10.1021/cs1000762.

98. ROSSI, C., et al. Nanoenergetic Materials for MEMS: A Review. *Journal of Microelectromechanical Systems*, AUG, 2007, vol. 16, no. 4. pp. 919-931 ISSN 1057-7157. DOI 10.1109/JMEMS.2007.893519.

99. ZHU, Y., et al. Large-Scale Synthesis and Field Emission Properties of Vertically Oriented CuO Nanowire Films. *Nanotechnology*, JAN, 2005, vol. 16, no. 1. pp. 88-92 ISSN 0957-4484. DOI 10.1088/0957-4484/16/1/018.

100. ZHANG, X., et al. High-Power and High-Energy-Density Flexible Pseudocapacitor Electrodes made from Porous CuO Nanobelts and Single-Walled Carbon Nanotubes. *Acs Nano*, MAR, 2011, vol. 5, no. 3. pp. 2013-2019 ISSN 1936-0851. DOI 10.1021/nn1030719.

101. ALI, I. New Generation Adsorbents for Water Treatment. *Chemical Reviews*, OCT, 2012, vol. 112, no. 10. pp. 5073-5091 ISSN 0009-2665. DOI 10.1021/cr300133d.

102. YU, X., et al. Novel 3D Hierarchical Cotton-Candy-Like CuO: Surfactant-Free Solvothermal Synthesis and Application in as(III) Removal. *Acs Applied Materials & Interfaces*, APR, 2012, vol. 4, no. 4. pp. 1954-1962 ISSN 1944-8244. DOI 10.1021/am201663d.

103. LIU, J., JIANG, X., NISHIYAMA, H. and KATO, N. Exact Throughput Capacity Under Power Control in Mobile Ad Hoc Networks. *2012 Proceedings Ieee Infocom*, 2012. pp. 1-9 ISSN 978-1-4673-0775-8.

104. KUMAR, R., DIAMANT, Y. and GEDANKEN, A. Sonochemical Synthesis and Characterization of Nanometer-Size Transition Metal Oxides from Metal Acetates. *Chemistry of Materials*, AUG, 2000, vol. 12, no. 8. pp. 2301-2305 ISSN 0897-4756. DOI 10.1021/cm000166z.

105. ZHANG, X., et al. Different CuO Nanostructures: Synthesis, Characterization, and Applications for Glucose Sensors. *Journal of Physical Chemistry C*, OCT 30, 2008, vol. 112, no. 43. pp. 16845-16849 ISSN 1932-7447. DOI 10.1021/jp806985k.

106. XU, L., et al. Novel Urchin-Like CuO Synthesized by a Facile Reflux Method with Efficient Olefin Epoxidation Catalytic Performance. *Chemistry of*

Materials, APR 14, 2009, vol. 21, no. 7. pp. 1253-1259 ISSN 0897-4756. DOI 10.1021/cm802915m.

107. ZHOU, K., WANG, R., XU, B. and LI, Y. Synthesis, Characterization and Catalytic Properties of CuO Nanocrystals with various Shapes. *Nanotechnology*, AUG 14, 2006, vol. 17, no. 15. pp. 3939-3943 ISSN 0957-4484. DOI 10.1088/0957-4484/17/15/055.

108. ZHOU, K. and LI, Y. Catalysis Based on Nanocrystals with Well-Defined Facets. *Angewandte Chemie-International Edition*, 2012, vol. 51, no. 3. pp. 602-613 ISSN 1433-7851. DOI 10.1002/anie.201102619.

109. PARK, J., et al. Synthesis of Monodisperse Spherical Nanocrystals. *Angewandte Chemie-International Edition*, 2007, vol. 46, no. 25. pp. 4630-4660 ISSN 1433-7851. DOI 10.1002/anie.200603148.

110. DEVAN, R.S., PATIL, R.A., LIN, J. and MA, Y. One-Dimensional Metal-Oxide Nanostructures: Recent Developments in Synthesis, Characterization, and Applications. *Advanced Functional Materials*, AUG 21, 2012, vol. 22, no. 16. pp. 3326-3370 ISSN 1616-301X. DOI 10.1002/adfm.201201008.

111. WANG, X. and LI, Y. Solution-Based Routes to Transition-Metal Oxide One-Dimensional Nanostructures. *Pure and Applied Chemistry*, JAN, 2006, vol. 78, no. 1. pp. 45-64 ISSN 0033-4545. DOI 10.1351/pac200678010045.

112. WANG, D., XIE, T. and LI, Y. Nanocrystals: Solution-Based Synthesis and Applications as Nanocatalysts. *Nano Research*, JAN, 2009, vol. 2, no. 1. pp. 30-46 ISSN 1998-0124. DOI 10.1007/s12274-009-9007-x.

113. ZHUANG, Z., PENG, Q. and LI, Y. Controlled Synthesis of Semiconductor Nanostructures in the Liquid Phase. *Chemical Society Reviews*, 2011, vol. 40, no. 11. pp. 5492-5513 ISSN 0306-0012. DOI 10.1039/c1cs15095b.

114. ZHAO, Y., et al. Room Temperature Synthesis of 2D CuO Nanoleaves in Aqueous Solution. *Nanotechnology*, MAR 18, 2011, vol. 22, no. 11. pp. 115604 ISSN 0957-4484. DOI 10.1088/0957-4484/22/11/115604.

115. WU, D., ZHANG, Q. and TAO, M. LSDA+U Study of Cupric Oxide: Electronic Structure and Native Point Defects. *Physical Review B*, JUN, 2006, vol. 73, no. 23. pp. 235206 ISSN 1098-0121. DOI 10.1103/PhysRevB.73.235206.

116. BOURNE, L., YU, P., ZETTL, A. and COHEN, M. High-Pressure Electrical-Conductivity Measurements in the Copper Oxides. *Physical Review B*, DEC 1, 1989, vol. 40, no. 16. pp. 10973-10976 ISSN 0163-1829. DOI 10.1103/PhysRevB.40.10973.

117. GRIONI, M., et al. Unoccupied Electronic States of Cuo - an Oxygen 1s X-Ray-Absorption Spectroscopy Investigation. *Physical Review B*, MAR 15, 1989,

vol. 39, no. 8. pp. 4886-4890 ISSN 1098-0121. DOI 10.1103/PhysRevB.39.4886.

118. SINGH, I. and BEDI, R.K. Studies and Correlation among the Structural, Electrical and Gas Response Properties of Aerosol Spray Deposited Self Assembled Nanocrystalline CuO. *Applied Surface Science*, JUN 15, 2011, vol. 257, no. 17. pp. 7592-7599 ISSN 0169-4332. DOI 10.1016/j.apsusc.2011.03.133.

119. BANERJEE, A., KUNDOO, S. and CHATTOPADHYAY, K. Synthesis and Characterization of P-Type Transparent Conducting CuAlO2 Thin Film by DC Sputtering. *Thin Solid Films*, SEP 1, 2003, vol. 440, no. 1-2. pp. 5-10 ISSN 0040-6090. DOI 10.1016/S0040-6090(03)00817-4.

120. MEYER, B.K., et al. Binary Copper Oxide Semiconductors: From Materials Towards Devices. *Physica Status Solidi B-Basic Solid State Physics*, AUG, 2012, vol. 249, no. 8. pp. 1487-1509 ISSN 0370-1972. DOI 10.1002/pssb.201248128.

121. HSIEH, J.H., et al. Opto-Electronic Properties of Sputter-Deposited Cu2O Films Treated with Rapid Thermal Annealing. *Thin Solid Films*, JUN 30, 2008, vol. 516, no. 16. pp. 5449-5453 ISSN 0040-6090. DOI 10.1016/j.tsf.2007.07.097.

122. SERIN, T., YILDIZ, A., SAHIN, S.H. and SERIN, N. Extraction of Important Electrical Parameters of CuO. *Physica B-Condensed Matter*, FEB 1, 2011, vol. 406, no. 3. pp. 575-578 ISSN 0921-4526. DOI 10.1016/j.physb.2010.11.044.

123. SERIN, T., YILDIZ, A., SAHIN, S.H. and SERIN, N. Multiphonon Hopping of Carriers in CuO Thin Films. *Physica B-Condensed Matter*, OCT 1, 2011, vol. 406, no. 19. pp. 3551-3555 ISSN 0921-4526. DOI 10.1016/j.physb.2011.06.021.

124. ZHENG, H., et al. Nanostructured Tungsten Oxide - Properties, Synthesis, and Applications. *Advanced Functional Materials*, JUN 21, 2011, vol. 21, no. 12. pp. 2175-2196 ISSN 1616-301X. DOI 10.1002/adfm.201002477.

125. KEIS, K., et al. Nanostructured ZnO Electrodes for Dye-Sensitized Solar Cell Applications. *Journal of Photochemistry and Photobiology A-Chemistry*, MAY 31, 2002, vol. 148, no. 1-3. pp. 57-64 ISSN 1010-6030. DOI 10.1016/S1010-6030(02)00039-4.

126. POTYRAILO, R.A., SURMAN, C., NAGRAJ, N. and BURNS, A. Materials and Transducers Toward Selective Wireless Gas Sensing. *Chemical Reviews*, NOV, 2011, vol. 111, no. 11. pp. 7315-7354 ISSN 0009-2665. DOI 10.1021/cr2000477.

127. WANG, C., et al. Metal Oxide Gas Sensors: Sensitivity and Influencing Factors. *Sensors*, MAR, 2010, vol. 10, no. 3. pp. 2088-2106 ISSN 1424-8220. DOI 10.3390/s100302088.

128. JIMENEZ-CADENA, G., RIU, J. and RIUS, F.X. Gas Sensors Based on Nanostructured Materials. *Analyst*, 2007, vol. 132, no. 11. pp. 1083-1099 ISSN 0003-2654. DOI 10.1039/b704562j.

129. LEE, J. Gas Sensors using Hierarchical and Hollow Oxide Nanostructures: Overview. *Sensors and Actuators B-Chemical*, JUN 18, 2009, vol. 140, no. 1. pp. 319-336 ISSN 0925-4005. DOI 10.1016/j.snb.2009.04.026.

130. ZHU, G., et al. Facile Fabrication and Enhanced Sensing Properties of Hierarchically Porous CuO Architectures. *Acs Applied Materials & Interfaces*, FEB, 2012, vol. 4, no. 2. pp. 744-751 ISSN 1944-8244. DOI 10.1021/am2013882.

131. HANSEN, B.J., et al. Transport, Analyte Detection, and Opto-Electronic Response of P-Type CuO Nanowires. *Journal of Physical Chemistry C*, FEB 18, 2010, vol. 114, no. 6. pp. 2440-2447 ISSN 1932-7447. DOI 10.1021/jp908850j.

132. KIM, H., et al. H2S Gas Sensing Properties of Bare and Pd-Functionalized CuO Nanorods. *Sensors and Actuators B-Chemical*, JAN 3, 2012, vol. 161, no. 1. pp. 594-599 ISSN 0925-4005. DOI 10.1016/j.snb.2011.11.006.

133. HSUEH, H.T., et al. CuO Nanowire-Based Humidity Sensors Prepared on Glass Substrate. *Sensors and Actuators B-Chemical*, AUG 2011, 2011, vol. 156, no. 2. pp. 906-911 ISSN 0925-4005. DOI 10.1016/j.snb.2011.03.004.

134. HONG, J., LI, J. and NI, Y. Urchin-Like CuO Microspheres: Synthesis, Characterization, and Properties. *Journal of Alloys and Compounds*, JUL 29, 2009, vol. 481, no. 1-2. pp. 610-615 ISSN 0925-8388. DOI 10.1016/j.jallcom.2009.03.043.

135. MIRZAEI, A. and NERI, G. Microwave-Assisted Synthesis of Metal Oxide Nanostructures for Gas Sensing Application: A Review. *Sensors and Actuators B-Chemical*, DEC, 2016, vol. 237. pp. 749-775 ISSN 0925-4005. DOI 10.1016/j.snb.2016.06.114.

136. KRCMAR, P., et al.
Fully Inkjet-Printed CuO Sensor on Flexible Polymer Substrate for Alcohol Vapours and Humidity Sensing at Room Temperature . *Sensors*, 2019, submitted ISSN 1234-5678.

137. LUPAN, O., et al. Influence of CuO Nanostructures Morphology on Hydrogen Gas Sensing Performances. *Microelectronic Engineering*, OCT 1, 2016, vol. 164. pp. 63-70 ISSN 0167-9317. DOI 10.1016/j.mee.2016.07.008.

138. CRETU, V., et al. Synthesis, Characterization and DFT Studies of Zinc-Doped Copper Oxide Nanocrystals for Gas Sensing Applications. *Journal of Materials Chemistry A*, 2016, vol. 4, no. 17. pp. 6527-6539 ISSN 2050-7488. DOI 10.1039/c6ta01355d.

139. A.M. HELMENISTINE. *Table of Electrical Resistivity and Conductivity.* ThoughtCo. Sep. 24, 2018, 2018.

140. HSUEH, H.T., et al. CuO Nanowire-Based Humidity Sensors Prepared on Glass Substrate. *Sensors and Actuators B-Chemical*, AUG 2011, 2011, vol. 156, no. 2. pp. 906-911 ISSN 0925-4005. DOI 10.1016/j.snb.2011.03.004.

141. WANG, C., et al. Surface Accumulation Conduction Controlled Sensing Characteristic of P-Type CuO Nanorods Induced by Oxygen Adsorption. *Nanotechnology*, APR 11, 2007, vol. 18, no. 14. pp. 145506 ISSN 0957-4484. DOI 10.1088/0957-4484/18/14/145506.

142. LI, D., HU, J., WU, R. and LU, J.G. Conductometric Chemical Sensor Based on Individual CuO Nanowires. *Nanotechnology*, DEC 3, 2010, vol. 21, no. 48. pp. 485502 ISSN 0957-4484. DOI 10.1088/0957-4484/21/48/485502.

143. CHAUHAN, P., ANNAPOORNI, S. and TRIKHA, S. Humidity-Sensing Properties of Nanocrystalline Haematite Thin Films Prepared by Sol-Gel Processing. *Thin Solid Films*, JUN 1, 1999, vol. 346, no. 1-2. pp. 266-268 ISSN 0040-6090. DOI 10.1016/S0040-6090(98)01771-4.

144. PITOIS, A., PILENGA, A., PFRANG, A. and TSOTRIDIS, G. Temperature-Dependent CO Desorption Kinetics on Supported Gold Nanoparticles: Relevance to Clean Hydrogen Production and Fuel Cell Systems. *International Journal of Hydrogen Energy*, APR, 2011, vol. 36, no. 7. pp. 4375-4385 ISSN 0360-3199. DOI 10.1016/j.ijhydene.2010.12.123.

145. TANVIR, N.B., YURCHENKO, O., LAUBENDER, E. and URBAN, G. Investigation of Low Temperature Effects on Work Function Based CO2 Gas Sensing of Nanoparticulate CuO Films. *Sensors and Actuators B-Chemical*, AUG, 2017, vol. 247. pp. 968-974 ISSN 0925-4005. DOI 10.1016/j.snb.2017.11.020.

146. XU, J., et al. Synthesis, Field Emission and Humidity Sensing Characteristics of Honeycomb-Like CuO. *Journal of Physics D-Applied Physics*, APR 7, 2009, vol. 42, no. 7. pp. 075417 ISSN 0022-3727. DOI 10.1088/0022-3727/42/7/075417.

147. MĚRKA, P. *Matrix Element for Sensors Printed on Flexible Substrate.* MSc. Thesis ed. Zlin: Tomas Bata University in Zlin, 2015.

LIST OF FIGURES

LIST OF TABLES

LIST OF ABBREVIATIONS

3D	three-dimensional
AFM	atomic force microscopy
CB	conduction band
CIJ	Continuous inkjet
CMC	Critical micelle concentration
DOD	Drop-on-Demand
DPI	Dots per inch
EM	energetic material
GPIB	General Purpose Interface Bus
ITO	Indium tin oxide
MO	Metal oxide
MSD	Minimum stand-off distance
MW	microwave
LIB	lithium-ion batterie
LSDA	local spin-density approximation
PC	Polycarbonate
PCB	Printed circuit boards
PE	Polyethylene
PES	Polyester
PET	Poly(ethylene terephthalate)
PI	Polyimide
PIJ	Piezoelectric inkjet
PP	Polypropylene
PS	Polystyren
PTFE	Polytetrafluoroethylene
PVC	Polyvinylchlorid
PZE	Piezoelectric element

RFID	Radio-frequency identification
SEM	scanning electron microscope
SFT	Surface tension
TIJ	Thermal inkjet
UV	Ultraviolet
VB	valence band
VOC	Volatile organic compound
XRD	X-ray diffraction

LIST OF SYMBOLS

A	Preexponential factor
B	Sensitivity
E_a	Activation energy
R	Universal gas constant
R	*electrical resistence*
$R0$	*initial resistance*
U	*voltage*
I	*electrical current*
T	Thermodynamic temperature
S	*Electrical conductivity*
S	Response electrical signal
s	Stimulus
wt%	percentage by mass
τ	Shear stress
η	Shear viscosity
$\dot{\gamma}$	Shear rate
r	radius

ρ	Density
σ	Surface tension
τ_d	Time constant
τ_0	Yield stress
v	Velocity
n	Flow behaviour index
λ	wavelenght

LIST OF UNITS

°C	degree Celsius
A	ampere
cm	centimeter
eV	electronvolt
g	gram
$g \cdot cm^{-3}$	gram per reciprocal cubic centimeter
h	hour
kPa	kilopascal
m/s	meter per reciprocal second
min	minute
mm	milimeter
ml	mililiter
mN/m	milliNewtons per meter

mPa·s	milliPascal second
nm	nanometer
Pa	Pascal
pL	picoliter
S/m	siemens per meter
s^{-1}	reciprocal second
Ω	Ohm
Ω·cm	Ohm centimeter
$Ω^{-1}$	reciprocal Ohm
kΩ	kiloOhm
MΩ	megaOhm
V	volt
μm	micrometer

LIST OF DIMENSIONLESS NUMBERS

Ca	Capillary number
La	Laplace number
Oh	Ohnesorge number
Re	Reynolds number
Su	Suratman number
We	Weber number
Z	*Z* number, reciprocal Ohnesorge number

LIST OF PUBLICATIONS AND OTHER OUTPUTS

Articles available in WoS

1. P. Suly, P. Krcmar, J. Maslik, P. Urbanek, I. Kuritka, Poly(vinyl Alcohol): Formulation of a Polymer Ink for the Patterning of Substrates with a Drop-On-Demand Inkjet Printer, Materiali in Tehnologije. 51 (2017) 41-48.

2. J. Matyas, L. Munster, R. Olejnik, K. Vlcek, P. Slobodian, P. Krcmar, P. Urbanek, I. Kuritka, Antenna of silver nanoparticles mounted on a flexible polymer substrate constructed using inkjet print technology, Japanese Journal of Applied Physics. 55 (2016) 02BB13.

3. J. Maslik, I. Kuritka, P. Urbanek, P. Krcmar, P. Suly, M. Masar, M. Machovsky, Water-Based Indium Tin Oxide Nanoparticle Ink for Printed Toluene Vapours Sensor Operating at Room Temperature, Sensors. 18 (2018) 3246.

Conference proceedings in WoS

4. P. Urbanek, I. Kuritka, P. Krcmar, J. Maslik, J. Bartos, Polysilanes Thin Films Doped by Coumarin, Nanocon 2012, 4th International Conference. (2012) 391-394.

5. P. Krcmar, P. Urbanek, I. Kuritka, J. Maslik, J. Bartos, The Effect of the Exalite Dopant on Photoluminescence of Poly[methylphenylsilane] in Thin Films, Nanocon 2012, 4th International Conference. (2012) 832-835.

6. J. Matyas, R. Olejnik, P. Slobodian, L. Munster, P. Krcmar, A. Steininger, Multiband Antenna made of Flexible Polymer Substrate Printed with Silver Nanoparticles using Inkjet Print Technology - a Feasibility Study, Nanocon 2015: 7th International Conference on Nanomaterials - Research & Application. (2015) 377-381.

Other conference proceedings

7. Petr Krčmář, Pavel Urbánek, Ivo Kuřitka. The influence of the substrate surface on deposition of thin layers from PEDOT:PSS. In Plastko 2012 Conference proceedings, 2012 ISBN 978-80-7554-137-7

8. Petr Krčmář, Pavel Urbánek, Ivo Kuřitka, Jan Mašlík and Pavol Šuly (2014), The preparation and characterization of CuO inkjet inks for gas

sensors. Lopec 2014 7th International Exhibition and Conference for the Printed Electronics Industry – Conference proceedings

9. Jan Mašlík, Pavel Urbánek, Ivo Kuřitka, Petr Krčmář, Pavol Šuly and Michal Machovský (2014), The preparation and characterization of ITO ink for gas sensing. Lopec 2014 7th International Exhibition and Conference for the Printed Electronics Industry – Conference proceedings

10. Jan Maslik, Pavel Urbanek, Ivo Kuritka, Petr Krcmar; Surface Modification of ITO coated PET foil for material printing. Conference contribution for Eurodisplay 2013 ISSN: 2168-0159

11. Pavel Urbanek, Ivo Kuritka, Petr Krcmar , Jan Maslik; Optoelectronic properties of MEH-PPV thin films influenced by their thickness. Conference contribution for Eurodisplay 2013 ISSN: 2168-0159

12. Pavel Urbánek, Ivo Kuřitka, and Petr Krčmář. 2011. The Influence of ZnO content on optoelectronic properties of films from MEH-PPV/ZnO composite. In Proceedings of the 13th WSEAS international conference on Mathematical and computational methods in science and engineering (MACMESE'11), Metin Demiralp, Zoran Bojkovic, and Angela Repanovici (Eds.). World Scientific and Engineering Academy and Society (WSEAS), Stevens Point, Wisconsin, USA, 411-414, ISBN: 978-1-61804-046-6.

Patents and patent applications

13. Active layer for electroluminescent foils. Ivo Kuřitka, Pavel Urbánek, Petr Krčmář, Mráček Jakub. ID 304387-Patent

14. Inorganic ink for material printing applications, comprises copper oxide nanoparticles, polymeric dispersant and rest of water. Krčmář, P, Kuřitka, I, Mašlík J, Šuly P, Urbánek P. ID 307435-Patent

Utility models

15. Inorganic ink based on nanoparticles, intended especially for material printing. Ivo Kuřitka, Pavel Urbánek, Petr Krčmář, Jan Mašlík, Pavol Šuly. ID 26391- Utility model

16. Polymeric ink for material printing. Ivo Kuřitka, Pavel Urbánek, Petr Krčmář, Jan Mašlík. ID 26729-Utility model

17. Active layer for electroluminescent foils. Ivo Kuřitka, Pavel Urbánek, Petr Krčmář, Mráček Jakub. ID 25048-Utility model

Proofs of concept

18. Printed flexible sensor for gas detection. Ivo Kuřitka, Pavel Urbánek, Petr Krčmář, Jan Mašlík. ID 43871727-Proof of concept

19. Printed flexible thermo sensor. Ivo Kuřitka, Pavel Urbánek, Petr Krčmář, Jan Mašlík. ID 43871728- Proof of concept

CURRICULUM VITAE

Name: Petr Krčmář

Date of birth: 1986, August 03

Place of birth: Zlín, Czech Republic

Permanent address: Sadová 1027, Valašsské Klobouky 766 01

Nationality: Czech

Affilation: Centre of Polymer Systems, Tomas Bata University in Zlin, trida T. G. Masaryka 5678, 760 01 Zlin, Czech Republic

Phone: (+420)-57-603-8128

Email: pkrcmar@ft.utb.cz

Employment: 2015-2018: ZÁLESÍ a.s., Uherskobrodská 119, 763 26 Luhačovice

Education: 2011-to date: Faculty of technology, Tomas Bata University in Zlin, Czech Republic, Ph.D. studies at the Polymer Centre in Chemistry and Materials Technology, Technology of Macromolecular compounds.

2009-2011: Faculty of technology, Tomas Bata University in Zlin, Czech Republic, Master´s degree Ing. (MSc.) in Chemistry and Materials Technology, Polymer Engineering.

2006-2009: Faculty of technology, Tomas Bata University in Zlin, Czech Republic, Bachelor´s degree Bc. (BSc.) in Chemistry and Materials Technology.

Projects: FR-TI3/424 *The electroluminescence foils for safety interior lighting* – Member of the project team

IGA/FT/2014/006 *The modification of polymer substrates and new materials for inkjet printing of sensors* - member of research team

IGA/FT/2013/025 *The material printing of polymeric and inorganic inks for advanced applications* - member of research team

IGA/FT/2012/025 *The modified polymeric materials for a thin layers* - member of research team

Petr Krčmář

Fully inkjet printed gas and humidity CuO sensor on flexible polymer substrate

Senzor plynů a vlhkosti na bázi CuO připravený výhradně inkoustovým tiskem na ohebném polymerním substrátu

Doctoral Thesis